Hydraulically Controlled Magnetic Bougienage for Correction of Long-gap Esophageal Atresia

by

Minkyun Noh

Submitted to the Department of Mechanical Engineering
in partial fulfillment of the requirements for the degree of

Master of Science in Mechanical Engineering

at the

MASSACHUSETTS INSTITUTE OF TECHNOLOGY

June 2014

Author .....
Department of Mechanical Engineering
May 9, 2014

Certified by .....
David L. Trumper
Professor of Mechanical Engineering
Thesis Supervisor

Accepted by .....
David E. Hardt
Chairman, Department Committee on Graduate Students

Hydraulically Controlled Magnetic Bougienage for Correction of Long-gap Esophageal Atresia

by

Minkyun Noh

Submitted to the Department of Mechanical Engineering
on May 9, 2014, in partial fulfillment of the
requirements for the degree of
Master of Science in Mechanical Engineering

Abstract

About one in 4000 babies [11] in the United States is born with their esophageal disconnected and separated by a gap, which is called esophageal atresia. Esophageal atresia with a relatively short gap can be directly corrected with surgery, whereas babies with a relatively long gap requires a treatment over several weeks to stretch the esophageal pouches. In this thesis, we have designed and developed a hydraulically controlled bougienage system as a case study for correction of long-gap esophageal atresia. We insert two magnetic bougies into the esophageal pouches and applying stretching force. The key idea is to employ the magnetic force between the two bougies. The bougie is designed based on a piston mechanism, which consists of a barrel and a magnetic plunger. The plunger has a through hole in the center, so that we can push water into the piston to extend the barrel. A catheter is connected to the bougie to transfer the water. Also, the catheter is driven using a friction drive placed near the mouth, which adjusts the neutral gap size between the two magnets. A syringe pump pushes water through the catheter to extend the tip of the bougie. Therefore, the system can stretch the esophageal pouch without changing the gap size between the two magnets, which helps to apply the stretching force in a controllable manner. The piston mechanism also enables measurement of the stretching force while the bougienage is being performed. A prototype bougienage system is built and integrated on a test bench, in which surgical rubber tubing is used as a mock-up of the esophagus. We have experimentally demonstrated that the prototype bougienage system can stretch the mock-up by a desired amount of force. Also, we have shown that the bougie can reliably measure the stretching force when the O-ring friction is compensated with dither. This bench level experiment shows promising results and forms the basis for further efforts towards utilization in patients.

Thesis Supervisor: David L. Trumper
Title: Professor of Mechanical Engineering

Acknowledgments

I would like to thank Professor David Trumper for his guidance during my master program. I still remember the very first research meeting with him, where he emphasized the importance of visualizing mathematical equations for a design engineer. The lesson has had a great impact on my learning and research. In every meeting with him, I was able to learn something new from his physical intuition and experience in technical details. I am happy that I have worked with such a nice advisor. I also thank Dr. David Mooney at Boston Children's Hospital. He is always wearing a big smile on his face. He has been so supportive during this research, and also very approachable via e-mails. Learning a different point of view for the same issue was a valuable experience for me.

I would like to thank my lab mates for their support. Jun Young Yoon has helped me a lot since I first came here MIT. Without his help, I was not able to settle down here Precision Motion Control Lab. Ian MacKenzie is a big boss of our lab. He introduced me RCA technical journals, which will help me to study a new topic for my Ph.D program. Roberto Meléndez and Lei Zhou are my battle buddies who joined this lab together with me. We took several courses together, and I really enjoyed the discussion on the subjects. Roberto is such an energetic man who makes our lab happier. I really enjoyed sailing following Capt. Roberto in last summer. Lei Zhou is such a kind lady and so approachable. I was fortunate to have her as a TA for 2.14/2.140. It is hard to imagine that I was a TA without her help. Joe Church is an inborn engineer, who enjoys to collect old historical engineering objects, such as a *Spirule* to sketch a root locus. I really enjoyed general discussions on control theory as we ran the 2.14/2.140 labs together this semester. Phillip Daniel is such an energetic man and he loves challenges. He built a coil winder for our lab, which definitely will help us to build different types of motors.

I would like to thank the alumni of our lab whom I have spent time together. Mohammad Imani Nejad is such an experienced engineer who loves nuts and bolts. He is so experienced that I learned a lot of engineering skill from him. Darya Amin-Shahidi

is so knowledgeable. He was an instructor of 2.737 in 2013 Spring, where I learned a variety of subjects by building a macro scale AFM he designed and developed. Zhen Sun helped me a lot to settle down in the first year here at MIT. I also should thank Laura Zaganjori for her kind support for everything that I need in the lab.

Dr. Piet Van Rens at Settels van Amelsvoort introduced me the idea of rolling diaphragm seal, which will be a good candidate to design a new bougie for the future research. I would like to thank FerroTech for the ferrofluid samples, and Senior Aerospace Metal Bellows for the edge-welded bellows sample. Special thanks to Heejin Ahn for being here at MIT with me. She also helped me to review this thesis, and gave a lot of comments and feedbacks. I am happy to study with such a beautiful lady.

Finally and most importantly, I dedicate this thesis to my parents in Korea. I really appreciate their endless love and support, which enabled me to explore what I like to do. Also, I would like to thank my brother and sister-in-law for their support for my parents. I am looking forward to see my dear nephew and niece in this summer.

Contents

1 Introduction **17**

1.1 Thesis Overview 18

1.2 Prior Art 19

2 Long-gap Esophageal Atresia **25**

2.1 Background 25

2.2 Design Requirements 28

2.3 Summary 31

3 Hydraulically Controlled Magnetic Bougienage **33**

3.1 Strategy 33

3.1.1 Bougienage with Permanent Magnets 36

3.1.2 Bougienage with Pushing Mechanism 40

3.1.3 Bougienage with Tip Extension Modulation 43

3.2 Design Concepts 49

3.2.1 Piston 49

3.2.2 Bellows 58

3.2.3 Balloon 59

3.3 Concept Decision 60

3.4 Summary 61

4 Modules and Components Design **63**

4.1 Magnetic Bougie 64

4.1.1 Barrel . . . 66
4.1.2 Magnetic Plunger . . . 67
4.1.3 Magnetic Force Analysis . . . 71
4.2 Friction Drive . . . 72
4.2.1 Brushless DC Motor . . . 74
4.2.2 Driving Wheel . . . 75
4.2.3 Idler Wheel . . . 77
4.3 Summary . . . 80

5 System Integration and Control **81**
5.1 Test Bench Setup . . . 82
5.1.1 Esophageal Mock-up . . . 82
5.1.2 Friction Drive . . . 85
5.1.3 Syringe Pump . . . 87
5.2 Control Design . . . 88
5.2.1 Brushless DC Motor Control . . . 90
5.2.2 Stepper Motor Control . . . 91
5.3 Summary . . . 100

6 Experimental Results **101**
6.1 O-ring Friction . . . 101
6.2 Bougienage Test . . . 106
6.2.1 Bougienage Test Result ($\xi_0 = 10$ mm) . . . 106
6.2.2 Bougienage Test Result ($\xi_0 = 5$ mm) . . . 115
6.3 Ferrofluid Seal Test . . . 121
6.3.1 Friction Test . . . 122
6.3.2 Sealing Pressure Test . . . 124
6.4 Summary . . . 125

7 Conclusions and Suggestions for Future Work **127**

List of Figures

1-1 A schematic of the hydraulically controlled magnetic bougienage system. 18

1-2 Rehbein and Schweder's method taken from [22]. 20

1-3 Foker process taken from [3]. 21

2-1 Types of esophageal atresia (A-D), and tracheoesophageal fistula without esophageal atresia (E). The figure is taken from [2, p. 817]. 26

3-1 Bougienage with ferromagnetic steel bougies taken from [8]. An external coil generating magnetic field is not shown in the figure. 34

3-2 An electromagnet used by Takayasu et al. at MIT Plasma Science and Fusion Center [24]. Used to characterize the magnetic force for esophageal bougienage. Two ferromagnetic steel bougies are placed in the middle of the air path. Active water cooling (11 L/min) is required when the coil draws a maximum current of 800 A. 35

3-3 Magnetic force between two permanent cylindrical magnets. 36

3-4 Esophageal bougienage with permanent magnets. The two esophageal pouches have a neutral gap of ξ_0 without a magnet in the proximal pouch (left). With a magnet in the proximal pouch, the gap size reduces from ξ_0 to ξ due to the magnetic force F_m stretching the proximal esophageal pouch (right). Static equilibrium is assumed in this figure. 38

3-5 Magnetic bougienage with a pulling cable. Here, K_e is the stiffness of the esophageal pouch and K_s is the stiffness of the supporting structure. Magnetic force F_m is always larger than esophageal stretching force F_e. The bougienage can be accomplished by gradually releasing the magnet with a cable. Cable tension F_t is the distance between the two curves at a given gap size ξ. 39

3-6 Magnetic bougienage with a pushing rod. The magnetic force F_m) intersects the esophageal stretching force F_e twice at ξ_1 and ξ_2. Here ξ_1 is a stable equilibrium point and ξ_2 is an unstable equilibrium point. To push the magnet further from ξ_1 to ξ, a pushing mechanism is required to apply a compressive force F_c. 41

3-7 Force transition from the compression (left) to the tension (right) around the unstable equilibrium point ξ_2. The magnet could take a step change in position δ due to the clearance between the rod and the mouthpiece. The mouthpiece is required to carry the reaction force from the catheter and to provide a lateral guiding force to prevent the catheter from buckling. 43

3-8 Magnetic bougienage with a piston mechanism. Modulating the tip extension d shifts the magnetic force curve in the ξ coordinate. The blue dashed line is the original magnetic force F_m, and the blue solid line is the shifted magnetic force F'_m. 44

3-9 Force curve of bougienage with the tip extension $d = 0$. 46

3-10 Force curve of bougienage in a mode with the stretch induced by the piston. 47

3-11 Force curve of bougienage with decreased initial gap of 17 mm, versus original 20 mm. 47

3-12 Force curve of bougienage with tip displacement = 3.3 mm. 48

3-13 Piston seal with a gap of tight clearance. 50

3-14 Flow between parallel plates: Poiseuille flow. 51

3-15 Piston seal with surface tension of water. 52

3-16 Piston seal with O-rings. 53
3-17 Piston seal with mercury concept, inspired by [30]. 54
3-18 Piston seal with a ferrofluid. 55
3-19 Ferrofluid seal for a rotary shaft taken from [23]. 56
3-20 Piston seal with a rolling rubber diaphragm. 57
3-21 Edge-wedged Bellows (left) and electroformed bellows (right). 58
3-22 A magnetic bougie with a hydraulically controlled balloon developed by the previous MIT student team [18]. 60

4-1 A schematic of the hydraulically controlled magnetic bougienage and two key modules: magnetic bougie and friction drive. 63
4-2 A cross-sectional view of the hydraulically controlled magnetic bougie. 65
4-3 Barrels fabricated from polypropylene syringes. 66
4-4 Two ways to fabricate the barrels. 67
4-5 An aluminum mold to fabricate the barrel by thermoforming. 68
4-6 Magnetic Plunger: (a) the prototype and (b) 3D model. 69
4-7 Stainless steel tubing. The right end is turned with a lathe to fit the ring type magnets inner diameter. Tube provides structural support as well as a fluid connection from the plunger to the catheter. 70
4-8 O-ring gland design. A is the gland depth, B is the groove width, C is the diametrical clearance, and D is the groove depth. The outer diameter of the spacer OD_s determines A and D. 71
4-9 Attractive force between two permanent magnets. The green curve is the result of the simple model (3.6), the blue curve is the FEA result with FEMM software, and the red circles are measured data. 72
4-10 Friction Drive: (a) the prototype and (b) 3D model. 73
4-11 Cross sectional view of the driving wheel. The red arrows denote a compressive force flow through the rubber drum to the motor shaft. . 76
4-12 A propeller adapter manufactured by Hyperion, which is used as a shaft for the driving wheel. 77

4-13 Top view of the idler wheel. 78

4-14 Contact patches on the catheter surface. 78

4-15 The force flow from the compression spring to the driving wheel. . . . 79

5-1 Overview of the bench setup. 81

5-2 A mock-up of an esophageal pouch: (a) overview and (b) the end closing. 82

5-3 (a) A kitchen scale purchased from EatSmart and (b) a bending beam load cell taken from the kitchen scale. 83

5-4 An instrumentation amplifier circuit for a load cell. The amplifier gain is set to 5000 with $R_g = 10\ \Omega$. 84

5-5 Measured esophageal mock-up tension-elongation curve. 84

5-6 (a) An overview of the friction drive integration and (b) a sample mouthpiece. 85

5-7 A cross-sectional view of the esophageal mock-up and mouthpiece. Note that the mouthpiece does not contact the stainless steel tube which supports the esophageal mock-up tubing. 86

5-8 An overview of the test setup for the magnetic bougienage. 86

5-9 Syringe pump: (a) an overview and (b) stepper motor inside the chassis. 88

5-10 Control architecture for the magnetic bougienage system. 89

5-11 CompactRIO real-time target manufactured by National Instuments. 89

5-12 (a) A brushless DC motor mounted in the friction drive and (b) the EPOS2 controller board for the motor. 90

5-13 Brushless DC motor position control architecture. 91

5-14 (a) Stepper motor in the syringe pump and (b) the driver board for the stepper motor. 91

5-15 Stepper motor controller architecture. 92

5-16 A trapezoidal velocity profile and the associate position profile. 93

5-17 A phase plot for the design of a trapezoidal motor angular position trajectory generator. Variables x_1 and x_2 are position error and angular velocity, respectively. Red curve (A) shows a trajectory with initial position error x_a and initial velocity $x_2 = 0$. Blue curve (B) shows a more general initial condition. 94

5-18 Example 1 with $\mathbf{x_a} = (0, -200)$. Velocity is in units of pulse/sec. Position is in units of pulse. 97

5-19 Example 2 with $\mathbf{x_b} = (50, 50)$. Velocity is in units of pulse/sec. Position is in units of pulse. 98

5-20 Pulse generator implementation using LabVIEW. 99

6-1 The test bench set up for O-ring friction measurement. 102

6-2 O-ring friction for different amplitudes of sinusoidal displacement. . . 103

6-3 Dithering test for and to compensate the O-ring friction. 104

6-4 Residual force due to the O-ring friction after applying a bougie push. 105

6-5 O-ring friction is compensated with dither. 105

6-6 The setup for bougienage test. Distance ξ_0 is the neutral gap size of the esophageal mock-up, d_0 is the tip extension of the bougie, and x_0 is the distance between the magnetic plunger and the other magnet mounted on the load cell. 107

6-7 Sinusoidal bougienage ($\xi_0 = 10$ mm and $d_0 = 5$ mm). Top trace is without dither. Bottom trace is with dither. 109

6-8 Step bougienage ($\xi_0 = 10$ mm and $d_0 = 5$ mm). Top trace is without dither. Bottom trace is with dither. 110

6-9 Sinusoidal bougienage ($\xi_0 = 10$ mm and $d_0 = 10$ mm). Top trace is without dither. Bottom trace is with dither. 113

6-10 Step bougienage ($\xi_0 = 10$ mm and $d_0 = 10$ mm). Top trace is without dither. Bottom trace is with dither. 114

6-11 Step bougienage ($\xi_0 = 5$ mm and $d_0 = 5$ mm). Note runaway force and ultimate contact at about 87 seconds, due to slipping of the friction drive. 115
6-12 The magnetic bougie sticks to the other magnet: (a) before sticking and (b) after sticking. Compliance of the catheter tubing and syringe rubber plunger tip allows magnet motions which can runaway at small gaps. 116
6-13 Sinusoidal bougienage ($\xi_0 = 5$ mm and $d_0 = 10$ mm). Top trace is without dither. Bottom trace is with dither. 119
6-14 Step bougienage ($\xi_0 = 5$ mm and $d_0 = 10$ mm). Top trace is without dither. Bottom trace is with dither. 120
6-15 Ferrofluid seal: (a) a ferrofluid is applied on the magnetic plunger and (b) the plunger is inserted into the barrel. Note that the ferrofluid wets plunger barrel, as seen by brown film. 121
6-16 Setup to test the friction of a ferrofluid seal. The pressure sensor is not shown in the figure. 122
6-17 Sinusoidal beougienage with the ferrofluid seal (top) and the O-ring seal (bottom). 123
6-18 Sealing performance of the ferrofluid seal with sylinder fill of air. Note seal failure at a force of about 2 N. 124

List of Tables

4.1 Permanent Magnet Specification 68
4.2 Brushless DC Motor Specifications. 74
4.3 Motor Gearhead Specifications. 74

6.1 Specifications of ferrofluid samples from FerroTech. 122

Chapter 1

Introduction

About one in 4000 babies in the United States is born with their esophagus disconnected and separated by a gap, which is called esophageal atresia [11]. Esophageal atresia with a relatively short gap, for example 2-3 cm, can be directly corrected by surgical connection, which is called primary anastomosis. However, esophageal atresia with a relatively long gap, larger than 3 cm, requires treatment over the course of weeks to elongate the esophageal pouch so that it can grow to a sufficient length for surgery. The standard method for long-gap esophageal atresia is the Foker process [4, 3]. This method works for esophageal atresia with different sizes of gaps, but requires multiple thoracotomies[1] and continuous anesthesia for several weeks.

In this thesis, we design and develop a hydraulically controlled magnetic bougie[2] to propose a new bougienage[3] method for minimally invasive correction of esophageal atresia. The main idea is to utilize the magnetic force between two permanent magnets to stretch the esophageal pouches, thereby stimulating the tissue to grow. Also, a hydraulic piston mechanism is implemented on the magnet to apply the stretching force in a controllable manner while also enabling measurement of the stretching force.

[1] Surgical incision of the chest wall.
[2] A cylindrical instrument inserted into a tubular organ for a medical treatment.
[3] The procedure of stretching or dilating tubal organs with a bougie or bougies.

1.1 Thesis Overview

A schematic in Figure 1-1 helps to understand the basic idea of the hydraulically controlled magnetic bougienage system in relation to the anatomy of a baby with esophageal atresia. The esophagus is disconnected and separated into two halves, where the upper one is called the proximal esophageal pouch and the lower one is called the distal esophageal pouch. A bougie is inserted into each of the esophageal pouches to stretch them, thereby stimulating the tissue to grow. The bougie in the proximal esophageal pouch is inserted via the mouth, and the other bougie in the distal esophageal pouch is inserted via gastrostomy[4].

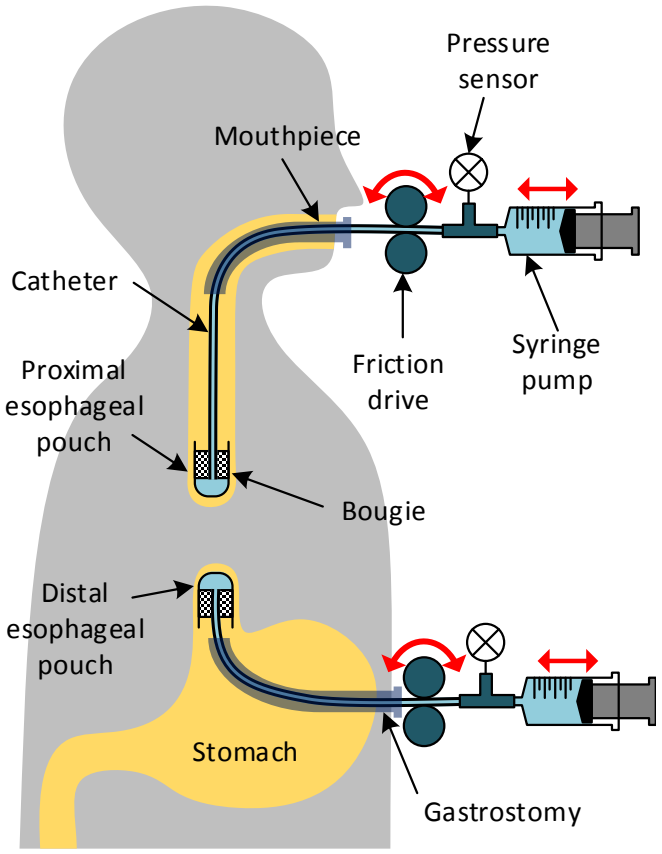

Figure 1-1: A schematic of the hydraulically controlled magnetic bougienage system.

The bougie is designed based on a piston mechanism, which consists of a plunger made of a ring type permanent magnet and a barrel. The magnetic plunger is connected to a syringe pump via a catheter. The syringe pump can extend the tip of the

[4]Creating an artificial external opening into stomach for nutritional support.

bougie by injecting water through the catheter and into the barrel. The hydrostatic pressure in the catheter is measured with an external pressure sensor to estimate the bougienage force, or the tip force that the bougie exerts on the esophageal pouch. The friction drive feeds the catheter back and forth to adjust the distance between the two magnets. The magnetic force helps the bougies to stretch the esophageal pouches in alignment. By modulating the friction drive and the hydraulic piston, we can regulate the bougienage force around the desired value.

This thesis is organized as follows: The rest of this chapter summarizes prior art of correction methods for esophageal atresia. Chapter 2 describes background knowledge to help the reader understand esophageal atresia and the design issues. Also, this chapter defines the problem for the research specifically before moving into the design step. Chapter 3 develops design concepts for a bougienage strategy using permanent magnets for correcting long-gap esophageal atresia, and proposes a variety of configurations based on the magnetic bougie idea. Among the generated concepts, we have chosen a hydraulic piston mechanism and O-ring seal to carry forward into the detailed design. Chapter 4 discusses the design details of modules and components. The design details of two modules, magnetic bougie and friction drive, as well as the considerations during the design process are discussed. Chapter 5 explains how the modules and components are integrated on a test bench, and how the control system is implemented for the system to achieve a desired goal. Chapter 6 describes experimental results to demonstrate the proposed bougienage method. Also, two different piston seal mechanisms, O-ring and ferrofluid, are experimentally compared to exemplify an alternative bougie design for future research. This thesis finishes with Chapter 7, in which we make conclusions and describe some suggestions for future research.

1.2 Prior Art

Esophageal atresia with a relatively short gap, for example 2-3 cm, can be corrected with suturing the two esophageal pouches together via surgery, which is called primary

anastomosis. However, an immediate primary anastomosis cannot be performed for long-gap esophageal atresia due to the limited extension of esophageal pouches.

Colon esophageal replacement [1] had been performed in 1960s-1970s for long-gap esophageal atresia. However, there had been observed long-term side-effects, such as dilatation, kinking, and passage impediments [22], which led surgeons to explore alternative surgical methods.

Howard and Myers [9] introduced a method of applying mechanical stimulation to grow esophageal pouches. They inserted a mercury-loaded bougie into the upper esophageal pouch and pressed down the bottom intermittently for about 10 minutes. The bougienage continued for a month, and they were able to proximate the two pouches to perform a primary anastomosis.

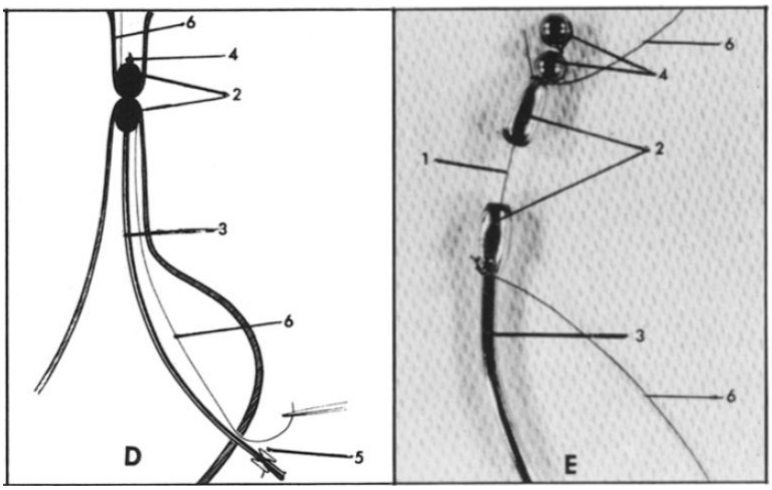

Figure 1-2: Rehbein and Schweder's method taken from [22].

Rehbein and Schweder [22] followed the bougienage method proposed by Howard and Myers, which led them to achieve satisfactory primary anastomosis for some cases of long-gap esophageal atresia. However, there were some other cases in which primary anastomosis was impossible, and therefore they developed a device shown in Figure 1-2 to perform anastomosis in a different way. Here, a thread goes through the two esophageal pouches and two silver olives are introduced along the thread into each pouch. They are in alignment due to the thread. Small metal balls fixed on the thread supports the upper silver olive, and the lower one is pushed with a metal

tube. Two silver olives crush the esophageal tissue between them, thereby creating a channel.

The standard surgical method for correcting long-gap esophageal atresia is the Foker process [4, 3]. The basic idea is to place a suture at the tip of each of the esophageal pouches and apply tension to stretch them. Figure 1-3 taken from [3] helps to understand the process. Here, esophageal pouches are brought out via incisions on the chest wall, and sutures are placed at the tip of each of the pouches to apply tension. The other end of the threads is stitched on the skin surface to make the tread taut. To increase the tension, a small piece of plastic tubing can be placed under the taut thread as a bolster. The detailed step by step process is described in Section 2.1. The induced stress stimulates the tissue, and therefore the esophageal pouches grow gradually. When the esophageal pouches grow by sufficient length such that the gap size between them is small, another surgery is performed to join the two pouches together, which is called primary anastomosis. The operation takes 2-5 weeks depending on the gap size, and babies are continuously anesthetized during the process. The Foker process works for different sizes of gaps, and currently used as

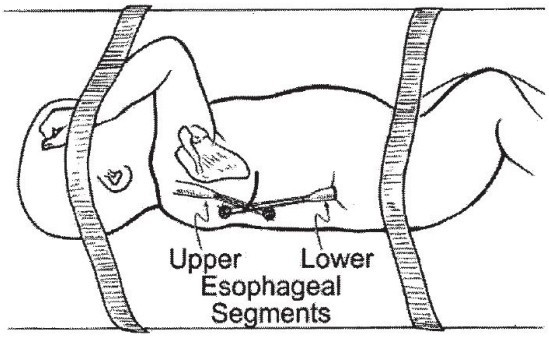

Figure 1-3: Foker process taken from [3].

the standard method for correcting esophageal atresia at Boston Children's Hospital [11]. However, the multiple instances of surgeries and the continuous anesthesia is a harsh condition for newborn babies. Also, the tissue where the traction suture is placed is frequently torn off due to the stress concentration, which makes it difficult to grow the esophageal pouches long enough for primary anastomosis.

There have been attempts to develop bougienage methods using magnetic forces.

Hendren and Hale [8, 6] explored electromagnetic bougienage for esophageal atresia. They placed magnetically-permeable metal bougies into the two esophageal pouches, and applied an magnetic field to pull the bougies together to elongate the pouches. This bougienage method made possible delayed primary anastomosis of the esophageal ends, although needed to be complemented by a surgery for the anastomosis.

Takayasu and Montgomery [24, 25] continued to explore the idea of electromagnetic bougienage. They developed a donut shaped electromagnet to generate a magnetic field, and tested different shapes of metal bougies to characterize bougienage forces. Mongomery's paper on magnetic forces for medical application [17] gives an engineering background for their approach. Their approach is discussed in more detail in Section 3.1.

Zaritzky et al. [32] demonstrated a method of magnetic compression anastomosis for esophageal atresia with a relatively short gap, for example smaller than 3 cm. Such a small gap is a good candidate for primary anastomosis, but their method can in principle lead to non-invasive anastomosis. The basic idea is to utilize the magnetic force between two permanent magnets: two permanent magnets are inserted into esophageal pouches, and then the magnetic force stretches the pouches to grow. When the two magnets stick to each other after a sufficient amount of esophageal growth, the large magnetic force squeezes the esophageal tissue between the two magnets, so that the tissue dies out (necrosis) and the wall tissue grows up naturally to join the two esophageal ends together. This is called magnetic compression anastomosis. The concept of magnetic compression anastomosis is also demonstrated by Jamshidi et al. [10] for the small intestine of a pig.

Vogel et al. [28] introduced a methoed of hydrostatic stretch-induced growth facilitating for long-gap esophageal atresia. Here, a balloon catheter is inserted into the distal esophageal pouch to perform bougienage by dilating the balloon.

A team of MIT students supervised by Prof. David Trumper and Dr. David Mooney at Boston Children's Hospital developed a hydraulically controlled magnetic bougie with a rubber balloon [18] as shown in Figure 3-22. Here, a balloon is attached

at the head of a magnet and a rigid outer casing surrounds the balloon to constrain it to expand in the axial direction only. The idea of combining a permanent magnet and a hydraulic mechanism to develop a new type of bougie showed promise, and inspired me to explore further this topic in this thesis.

Chapter 2

Long-gap Esophageal Atresia

This chapter provides basic background information on esophageal atresia, which we have studied either from articles or from meetings and personal conversations with Dr. David Mooney, Dr. Russell Jennings and other medical doctors. This chapter also clarifies the goals of the research, and summarizes the design requirements for the device.

2.1 Background

The esophagus is a tubular organ that connects the mouth and the stomach. The esophageal wall is very stretchable and is almost fully collapsed when it is empty. The inner wall is slippery because of the saliva from the mouth. The wall is a multi-layered structure, which consists of mucosa, submucosa, circular muscle, and longitudinal muscle from inside to outside. For more detailed background on the biomechanics of the esophagus, we recommend to read [5].

Esophageal atresia is a rare anatomical defect found in infants. It frequently accompanies a tracheoesophageal fistula, which is an abnormal branch between the trachea and the esophagus. Based on the anatomical relation to the tracheoesophageal fistula, esophageal atresia can be categorized into four types as shown in Figure 2-1, which is taken from [2, p. 817]. Notice that type E does not have esophageal atresia.

In type A, the upper and lower segments of the esophagus end in pouches, without

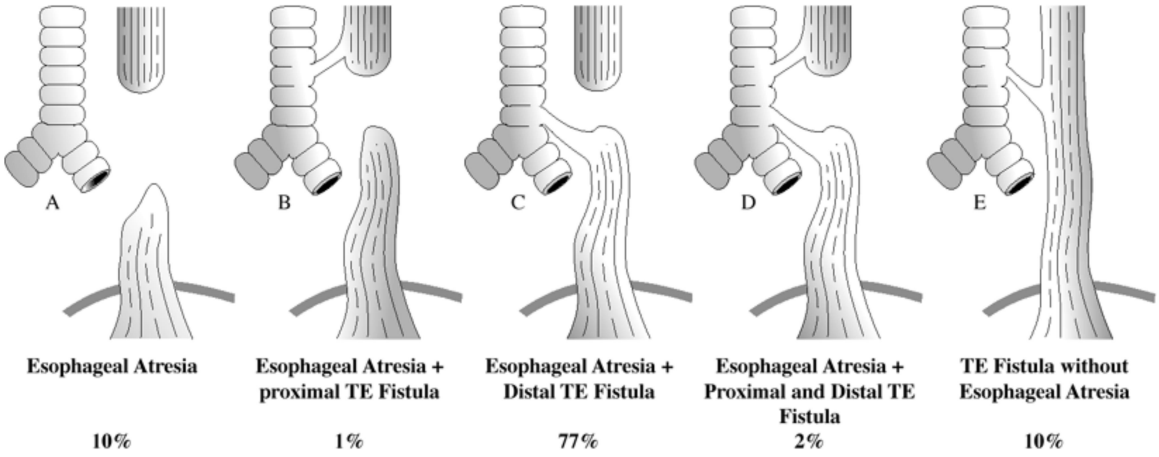

Figure 2-1: Types of esophageal atresia (A-D), and tracheoesophageal fistula without esophageal atresia (E). The figure is taken from [2, p. 817].

connecting to the trachea. In type B, the lower segment ends in a blind pouch, whereas the upper segment is connected to the trachea via a tracheoesophageal fistula. In type C, the upper segment ends in a blind pouch, whereas the lower segment is connected to the trachea via a tracheoesophageal fistula. This is the most common type. In type D, the tracheoesophageal fistula is present on both upper and lower segments.

Most cases of esophageal atresia have a short gap, for example 2-3 cm, between the two esophageal segments. This case of esophageal atresia can be directly corrected by surgical connection, or primary anastomosis. The tracheoesophageal fistula is removed during the operation if it exists. However, long gap esophageal atresia, in which the gap size is larger than 3 cm, is hard to correct via an immediate primary anastomosis, because the esophageal segments do not have sufficient length for joining. In this case, doctors perform treatment over the course of weeks to elongate the esophageal pouch so that it can grow by a sufficient length for surgery. Dr. David Mooney, whom I have worked with for this project, said the longest gap he has seen at Boston Children's Hospital is about 6 cm on newborn babies, and 10 cm on older child babies. He mentioned that some old babies are frequently readmitted to Boston Children's Hospital from other hospitals. The inner diameter of the proximal pouch is about 8-12 mm, and the inner diameter of the distal pouch is about 4-8 mm. He said the proximal pouch is typically more spacious than distal pouch.

The Foker process is the standard operation for long-gap esophageal atresia performed at Boston Children's Hospital. Below is an excerpt from [11], a web publication of Dr. Russell Jennings, which explains the Foker process step by step.

1. The surgeon places around four or five sutures on the upper and lower ends of your child's esophagus. These are tiny stitches that connect the two ends.
2. The tension on the sutures is increased bit by bit, causing each end of the esophagus to grow about one to two millimeters each day - just like a muscle grows when you exercise it. The surgeon applies the proper amount of tension to the ends of the esophagus to create just enough growth for it to be attached.

   Depending on how much your baby's esophagus needs to grow, this may take between two and five weeks. During this time, your baby is on respiratory and nutritional supportive devices and closely monitored by her health care team.
3. Then, during a second operation, the sutures are removed, and the ends of the esophagus are sewn together.

Dr. Mooney, who works with Dr. Jennings, and performs surgery for long-gap esophageal atresia at Boston Children's Hospital, explained the downsides of the Foker process. The process requires multiple instances of surgery and continuous anesthesia during the course of surgery, which takes 2-5 weeks depending on the gap size. Also, the suture is frequently torn off, presumably due to the stress concentration on the tissue. In this case, another suture can be placed near the previous site, but the number of re-suturing is limited by the area of the esophageal end. These downsides and Dr. Mooney's suggestions motivated us to explore in-lumen bougienage method, which can in principle lead to non-invasive correction and can avoid the failure mode caused by the stress concentration.

Dr. Mooney provided chances to meet other surgical doctors, so that we could better understand the related issues. In the first meeting, we met Dr. John Foker, who

has developed the current standard method, and Dr. Russell Jennings, who is leading the Esophageal Atresia Treatment Program at Boston Children's Hospital. Dr. Foker expressed his concern with our in-lumen method by explaining his rule of thumb: making sutures on the outer surface of the esophageal pouch without penetrating the lumen. He also gave an example of esophageal atresia with an extremely long-gap, in which the stomach does not have an esophageal pouch at all. He related that the nominal tension he applies for the operation is about 20-250 grams force. He also introduced a research paper that describes how the tissue grows under a mechanical force [13]. Dr. Jennings mentioned that the tension during the Foker process decreases like a response of first order system. He also introduced his hypothesis on cell growing: cells grow well when excited at their natural frequency.

The second meeting was held at Boston Children's Hospital, where Prof. Trumper and I had a chance to meet more medical doctors in the Esophageal Atresia Team at Boston Children's Hospital. They have been exploring surgical solutions for esophageal atresia in various ways. For example, Dr. Pierre Dupont has been exploring other approaches, which have not been published yet. Dr. Mooney has been focusing on in-lumen methods using permanent magnets, which is the main strategy of our approach. Dr. Jennings is more interested in the general issue of tissue growing. At the meeting, Dr. Heung Bae Kim gave an idea of placing large permanent magnet outside of the body and inserting a permanent magnetic bougie in the proximal esophageal pouch in order to increase the magnetic force. Suggestions for future research are discussed in Chapter 7 in more detail.

2.2 Design Requirements

The goal of this project is to develop a least invasive method to correct long-gap esophageal atresia, thereby helping the babies with such a disorder to achieve normal digestion. The process can be divided into two steps: bougienage and anastomosis. In the bougienage step, we apply a mechanical stimulus, typically a tension, to the esophageal pouches so that the tissue grows into a desired shape. Once the esophageal

pouches grow by a sufficient length, the anastomosis can be performed either surgically or via magnetic compression anastomosis [32].

Below is the list of the design requirements, which are made based on meetings, personal conversations, and e-mail correspondence with surgeons at Boston Children's Hospital, especially with Dr. Mooney.

In lumen method

Esophageal stretching force should be applied by inserting a bougie in the lumen of the esophageal pouch.

Size of the bougie

The inner diameter of the proximal pouch is about 8-12 mm, and the inner diameter of the distal pouch is about 4-8 mm. The bougie diameter should be similar or smaller than the inner diameter of the pouches.

Bougienage force control

The bougie should apply the bougienage force in a controllable manner. The recommended bougienage force about 250 grams maximum force.

Directional bougienage

The bougienage force should be applied in the axial direction to stimulate the esophageal tissue lengthwise.

Esophageal gap size

The longest gap is 6 cm on a newborn baby and 10 cm on an older child.

Bougienage duration

The device should be designed to be able to be inside of a baby for 14 days. The device is expected to work all day, stretching the esophagus then relaxing, for example every 5 minutes.

Catheter type

For the compatibility, it is better to develop the device using the catheter currently being used at Boston Children's Hospital.

Catheter length

In a baby the distance from their lip to the end of the upper esophageal pouch is about 3 inches.

Catheter buckling

The catheter should not push against the inner wall of the esophagus, which can happen due to buckling. This might, with repeated applications of force, make a hole in the wall. To reduce the possibility of buckling, the catheter can be reinforced by inserting a steel wire. It is also recommended to use a mouthpiece with a firm curving sleeve to support the catheter in the lateral direction at the back of the mouth.

Gap measurement

The gap between the two esophageal pouches is currently measured by taking X-ray images. It would be helpful to have a real-time instrumentation system to measure the gap size, and to localize the position of the bougies as well.

Simple operation for physicians

The device should be simple to operate for surgeons and nurses.

Temperature

Temperature should be regulated at approximately the body temperature.

To satisfy the above requirements, we decided to use permanent magnets for a bougie design. Two permanent magnets attract to each other in alignment, which is advantageous to apply the bougienage force in the axial direction. We can easily satisfy the temperature requirement with permanent magnets, whereas electromagnets dissipate heat due to the current flow, and are much weaker than permanent magnnets at this size scale. Rare earth magnets can generate relatively large force with a small volume, which is advantageous to satisfy the size requirement. Permanent magnets can stay inside the body for a long time if properly protected to resist corrosion. The only concern with the permanent magnets is applying the bougienage

force in a controllable manner. To satisfy this requirement, we design a hydraulic piston mechanism on the magnet, which is discussed in detail in the next section.

2.3 Summary

In this chapter, we covered some background information on esophageal atresia. We also clarified the goal of the research, and listed the design requirements for the device to achieve the goal. In the next chapter, we develop a strategy and design concepts to satisfy the design requirements using permanent magnets and a hydraulic piston mechanism.

Chapter 3

Hydraulically Controlled Magnetic Bougienage

This chapter develops concepts for esophageal bougienage using permanent magnets and a hydraulic piston mechanism. The basic idea is to use an attractive force between two permanent magnets to stretch the esophageal pouches. In addition to the magnetic bougienage, a pushing mechanism and a hydraulic piston mechanism are designed so that the bougie can apply a complementary stretching force in a controllable manner. The chapter is closed by proposing several design concepts to realize the strategy along with listing pros and cons of each concept.

As a reminder, bougie is a cylindrical instrument inserted into a tubular organ for a medical treatment, and bougienage is the procedure of stretching or dilating tubal organs, e.g. the esophagus, with a bougie or bougies.

3.1 Strategy

The main strategy for esophageal bougienage is to use a force between two permanent magnets. Two permanent magnets generate a force attracting each other in an axial direction, which can be used to stretch the esophageal pouches. The magnets also generate a lateral stabilizing force so that the two magnets orient themselves in the lateral and rotational degrees of freedom. This property can guide the two magnetic

bougie to meet at one point ultimately, joining the two esophagus pouches together. Rare earth magnets with high remanence flux density, such as NdFeB magnets, are available at a reasonably low cost, and they can generate a relatively large force without power input. Also, the magnetic force can be exerted on a bougie without physical contact, so that the bougienage can be done in a least-invasive manner. A downside of using permanent magnets is that the magnetic force can be only controlled by changing the distance between the two magnets. That is, the force is only a function of the distance, given that geometry of the magnet and the remanence flux density are fixed. Also, the magnets cannot generate a sufficiently large force when the distance between them is more than about 2-3 cm. To complement such downsides of magnetic bougienage, a pushing mechanism and a hydraulic tip modulation mechanism are proposed in this section.

Instead of using permanent magnets, electromagnets are also possible to generate magnetic force. For example, Hendren and Hale have shown that bougienage can be done by inserting ferromagnetic steel bougies into the esophageal pouches as shown in Figure 3-1 and applying strong magnetic field with an external coil [6, 8].

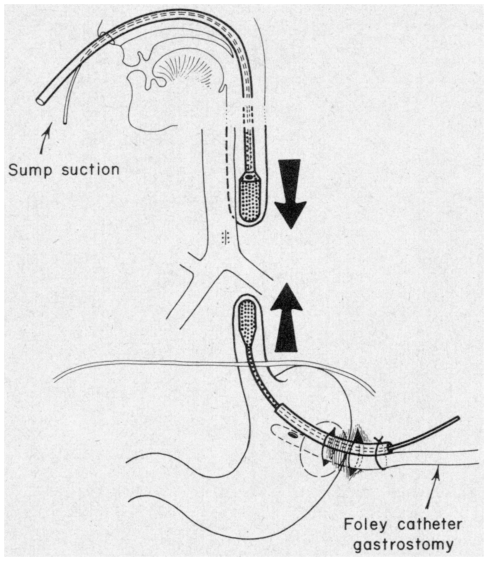

Figure 3-1: Bougienage with ferromagnetic steel bougies taken from [8]. An external coil generating magnetic field is not shown in the figure.

An advantage of using an electromagnet is that the force can be readily controlled

by modulating current through the external coil, which varies the intensity of the ambient magnetic field in which the ferromagnetic bougie is immersed. Under linear assumption, the resulting force is proportional to the product of average field intensity with the field gradient at the bougie. To generate sufficiently large force, however, the number of coil windings and the amount of the current through the coil should be made as large as possible. If a NdFeB magnet with remanence flux density of 1.3T was replaced with an electromagnet, the equivalent surface current density is calculated to be about 10 kilo amps per centimeter, which requires an active water cooling system to dump out the large amount of heat generated by the current. Also, the size of the coil should be large to have a sufficient air path to accommodate a baby's chest. For example, Takayasu et al. at MIT Plasma Science and Fusion Center [24] used an electromagnet with a bore of major diameter 330.6 mm and a minor diameter of 238.6 mm, with a height of 114.8 mm as shown in Figure 3-2. The electromagnet draws a maximum current of 800 A with water cooling (11 L/min), generating maximum magnetic field of 2719 Oe at the center of the magnet.

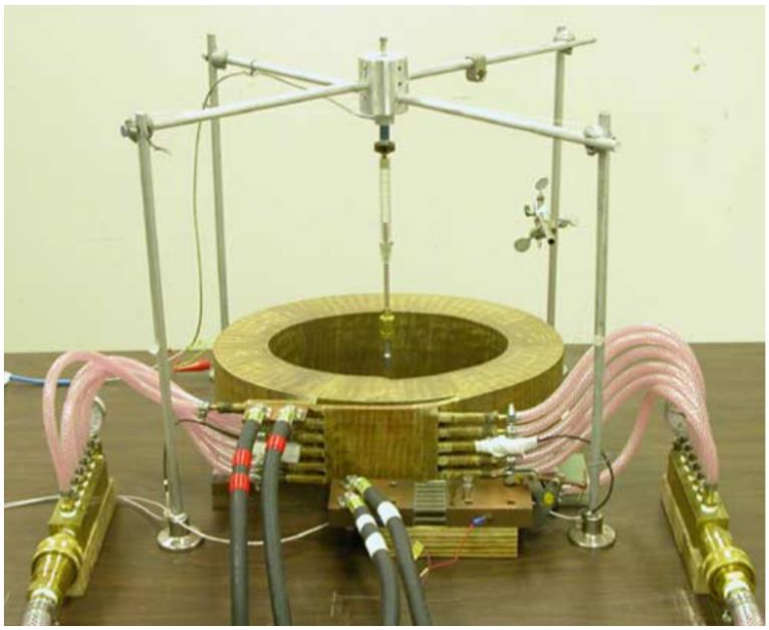

Figure 3-2: An electromagnet used by Takayasu et al. at MIT Plasma Science and Fusion Center [24]. Used to characterize the magnetic force for esophageal bougienage. Two ferromagnetic steel bougies are placed in the middle of the air path. Active water cooling (11 L/min) is required when the coil draws a maximum current of 800 A.

3.1.1 Bougienage with Permanent Magnets

The magnetic force between two cylindrical permanent magnets can be derived by modeling the north pole as a positive magnetic point charge q_m, and the south pole as a negative magnetic point charge $-q_m$, assuming that the magnets are uniformly magnetized, and that the axial distance between the two magnets is several times larger than the magnet radius. The magnetic charge of the north pole can be represented as

$$q_m = \mu_0 M \pi R^2 = B_r \pi R^2, \tag{3.1}$$

where μ_0 is permeability of free space, M is magnetization density of the permanent magnet, B_r is the permanent magnet remanence flux density, and R is radius of the magnet [7, p. 327].

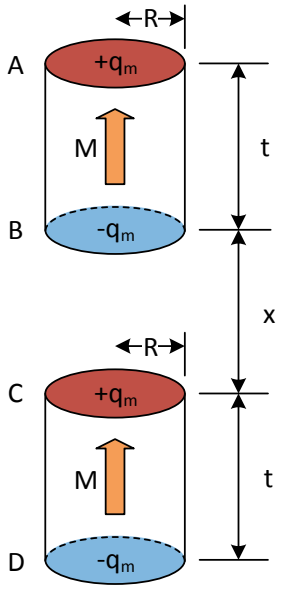

Figure 3-3: Magnetic force between two permanent cylindrical magnets.

Let us consider a case where two identical magnets with the same height, t, are separated by x in the same axis as shown in Figure 3-3. Here, A is the north pole of the top magnet, B is the south pole of the top magnet, C is the north pole of the bottom magnet, and D is the south pole of the bottom magnet. Each combination of two poles generate either a pushing force or a pulling force depending on their

polarities, and the magnitude of the force is a function of the distance between the two magnetic charges. For example, the force applied to B from C can be expressed as

$$F_{BC} = -\frac{q_m^2}{4\pi\mu_0}\frac{1}{x^2}. \tag{3.2}$$

In a similar way, we can evaluate the other forces applied to A and B as

$$F_{BD} = \frac{q_m^2}{4\pi\mu_0}\frac{1}{(x+t)^2}, \tag{3.3}$$

$$F_{AC} = \frac{q_m^2}{4\pi\mu_0}\frac{1}{(x+t)^2}, \tag{3.4}$$

$$F_{AD} = -\frac{q_m^2}{4\pi\mu_0}\frac{1}{(x+2t)^2}. \tag{3.5}$$

Finally, by adding the four forces F_{BC}, F_{BD}, F_{AC}, and F_{AD}, and substituting q_m with $B_r\pi R^2$ from (3.1), we can derive the magnetic force applied to the top magnet, F_m, as follows.

$$F_m = -\frac{\pi B_r^2 R^4}{4\mu_0}\left(\frac{1}{x^2} + \frac{1}{(x+2t)^2} - \frac{2}{(x+t)^2}\right), \tag{3.6}$$

where the negative sign denotes that the force is downward. (3.6) agrees with the work of Vokoun et al. [29], in which they derived an integral equation for the magnetic force between two cylindrical permanent magnets based on the total magnetostatic interaction energy of the system. They showed that the equation approximates to (3.6) when the axial distance between magnets is several times larger than the magnet radius. This approximate magnetic force (3.6) is considered to be sufficiently correct to develop a strategy for esophageal bougienage. For the detailed module design, FEA analysis is performed to calculate the accurate magnetic force, as described in Chapter 4.

We can conceptualize the bougienage method by inserting two permanent magnets into the esophageal pouches to stretch them as shown in Figure 3-4. In this case, the

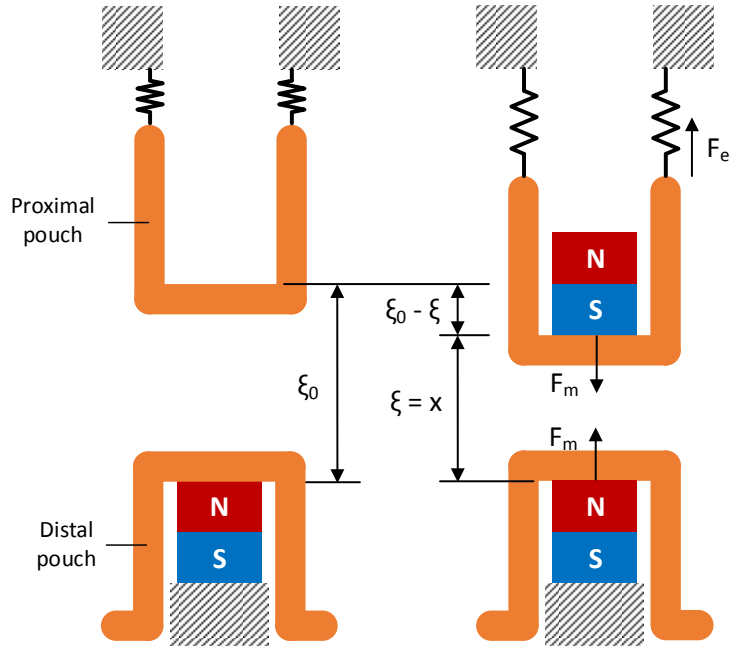

Figure 3-4: Esophageal bougienage with permanent magnets. The two esophageal pouches have a neutral gap of ξ_0 without a magnet in the proximal pouch (left). With a magnet in the proximal pouch, the gap size reduces from ξ_0 to ξ due to the magnetic force F_m stretching the proximal esophageal pouch (right). Static equilibrium is assumed in this figure.

gap between two esophageal pouches is equal to the distance between two magnets, or

$$x = \xi. \tag{3.7}$$

The magnet for the proximal pouch is inserted via the mouth, and the magnet for the distal pouch is inserted into the stomach via a gastrostomy, an artificial hole on the stomach for feeding, as shown in Figure 1-1. We assume that the magnet in the distal pouch is fixed. In many cases of long-gap esophageal atresia, the proximal pouch is longer and more spacious than the distal pouch, and therefore the bougienage is more often performed for the proximal pouch. We model the esophageal pouches as a linear spring, whose constitutive law can be represented as

$$F_e = K_e(\xi_0 - \xi), \tag{3.8}$$

where F_e is the esophageal stretching force, ξ is the gap size between two esophageal

pouches, ξ_0 is the neutral gap size with the esophageal pouches unstretched, and K_e is the stiffness of esophageal pouch. Although the actual biomechanics of esophageal tissue is viscoelastic and nonlinear rather than pure elastic [5], it is modeled here as a simple linear spring with a constant spring constant for simplicity during the strategy development stage.

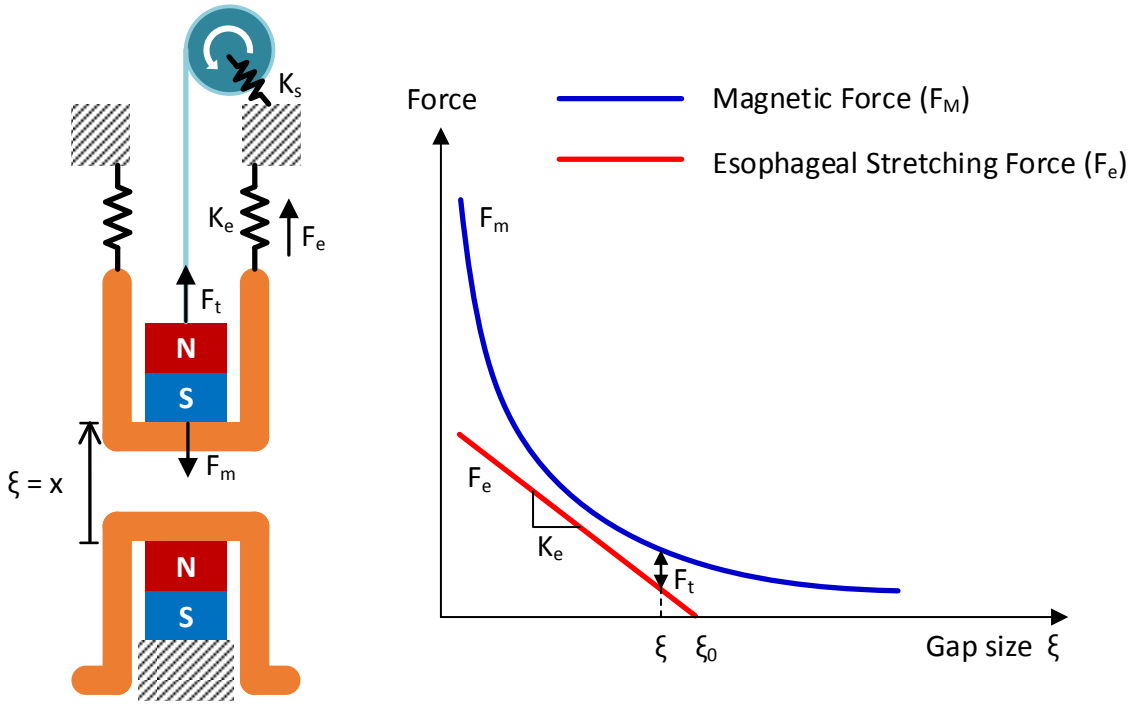

Figure 3-5: Magnetic bougienage with a pulling cable. Here, K_e is the stiffness of the esophageal pouch and K_s is the stiffness of the supporting structure. Magnetic force F_m is always larger than esophageal stretching force F_e. The bougienage can be accomplished by gradually releasing the magnet with a cable. Cable tension F_t is the distance between the two curves at a given gap size ξ.

Esophageal atresia with a relatively short gap, e.g. 2-3 cm, can be corrected by putting the permanent magnet into the esophageal pouch and gradually releasing it with the cable as shown in Figure 3-5 (left). For example, Zaritzky et al. used permanent magnets to perform bougienage for short-gap esophageal atresia in which the gap sizes were smaller than 3 cm [32]. This type of bougienage can be accomplished when the neutral gap between the two esophageal pouches ξ_0 is small. In this case the magnetic force is always larger than the required esophageal stretching force as shown in Figure 3-5 (right). In this case, the magnitude of the esophageal stretching

force F_e is determined by the difference between the magnitude of the magnetic force F_m and the tension of the cable F_t, or

$$F_e = F_m - F_t. \tag{3.9}$$

By modulating the cable length, thereby changing the gap size between the two esophageal pouches ξ, we can control the esophageal stretching force with an assumption that the cable does not elongate under the tension F_t. The stretching force F_e stimulates the esophageal tissue to grow, thereby decreasing the neutral gap size ξ_0. After the bougienage is done, releasing cable tension can lead to anastomosis. With the tension F_t is released, the two magnets squeeze the esophageal tissue between them with a large force F_m, so that the sandwiched tissue dies out (necrosis) and the wall tissue grows up naturally to connect the two esophageal pouches together. Zaritzky et al. performed magnetic compression anastomosis on esophageal atresia [32], and Jamshidi et al. showed magnetic compression anastomosis on the small intestine of a pig [10].

Ideally, the bougienage should be controlled to gradually lengthen the esophageal pouch to make the neutral gap size ξ_0 decrease down to zero. However, due to the finite stiffness of the cable and the compliance of the supporting structure k_s in Figure 3-5, the magnet could stick to the other magnet before achieving a sufficient amount of esophageal growth. Therefore, this type of bougienage concept can lead to a premature anastomosis.

3.1.2 Bougienage with Pushing Mechanism

The bougienage strategy suggested in the previous section will fail when the gap between two pouches is relatively large, e.g. 6-10 cm, because the magnets will not generate sufficiently large force to override the esophageal stretching force in such a large distance. In this case, we can implement a pushing mechanism to apply a complementary force to the magnetic force as shown in Figure 3-6 (left). The pushing mechanism is necessary when the neutral gap between the two esophageal pouches ξ_0

is large such that the magnitude of the magnetic force is not always larger than the magnitude of the esophageal stretching force as shown in Figure 3-6 (right).

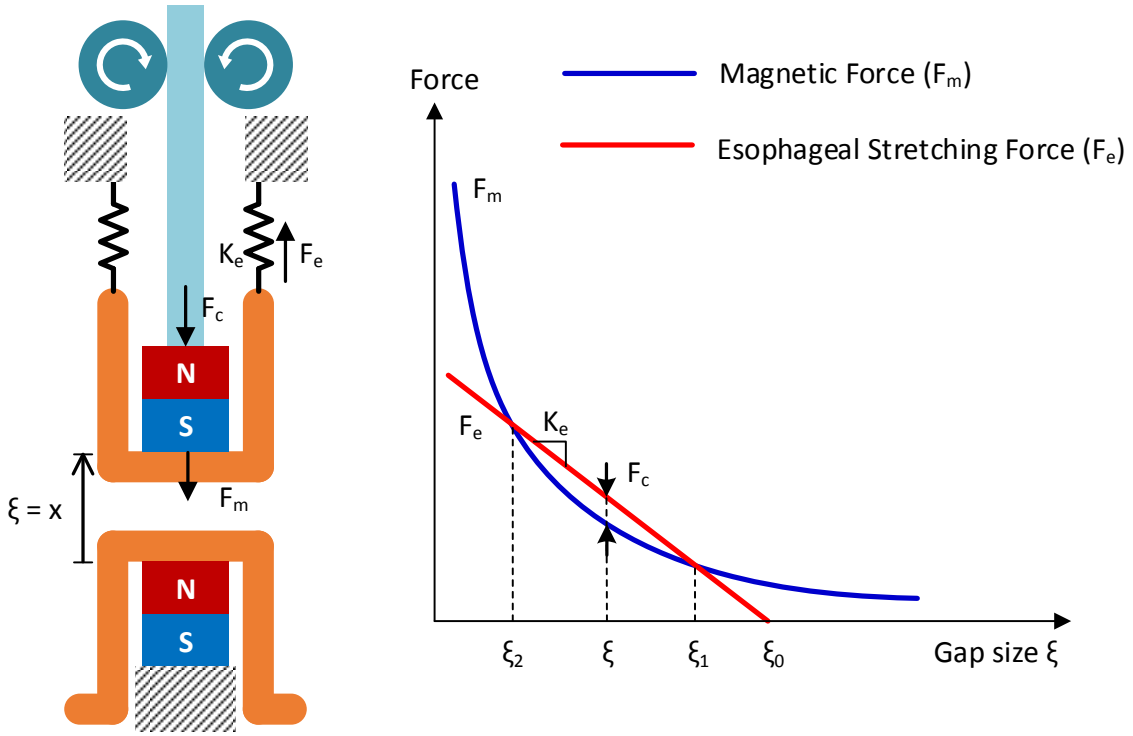

Figure 3-6: Magnetic bougienage with a pushing rod. The magnetic force F_m) intersects the esophageal stretching force F_e twice at ξ_1 and ξ_2. Here ξ_1 is a stable equilibrium point and ξ_2 is an unstable equilibrium point. To push the magnet further from ξ_1 to ξ, a pushing mechanism is required to apply a compressive force F_c.

Notice that the esophageal stretching force curve intersects the magnetic force curve twice at ξ_1 and ξ_2. Here, ξ_1 is a stable equilibrium point, where the magnetic force F_m and the esophageal stretching force F_e satisfy the following conditions.

$$(F_e - F_m)|_{\xi=\xi_1} = 0, \tag{3.10}$$

$$\frac{\partial}{\partial \xi}(F_e - F_m)\,|_{\xi=\xi_1} < 0. \tag{3.11}$$

In this case, just inserting a magnet and pulling it back and forth with a cable cannot control the bougienage force because the cable cannot drive the magnet beyond the stable equilibrium point ξ_1 due to the cable. To reduce the gap size smaller than ξ_1, we need a stiff rod that can apply a pushing force to the magnet without buckling as

shown in Figure 3-6. By feeding the rod back and forth, we can modulate the gap size ξ even smaller than the stable equilibrium point ξ_1. Here, the esophageal stretching force F_e is determined by the sum of magnetic force F_m and the compression force of the rod F_c, or

$$F_e = F_m + F_c. \tag{3.12}$$

By pushing the rod, thereby changing the gap size between the two esophageal pouches ξ, we can control the esophageal stretching force F_e. If the compressive force is released, the magnet is pulled back from ξ to ξ_1 due to the restoring force of the esophagus. In other words, a compressive force F_c is required in addition to the magnetic force F_m to stretch the proximal esophageal pouch to ξ.

Magnets might seem to be redundant for the bougienage if there is a pushing mechanism available. However, if the bougienage was implemented with a pushing mechanism only without the magnets, a thin rod could easily buckle because the net compression force on the rod would increase by the amount of the magnetic force. Also, pure pushing cannot guide the direction of stretching force, while magnetic bougienage can apply a stretching force guided by the magnets such that the esophageal pouches are stretched toward each other in alignment.

If we keep pushing the magnet further, we meet another equilibrium point ξ_2 in Figure 3-6. Here, ξ_2 is an unstable equilibrium point, where the magnetic force and the esophageal stretching force satisfy the following conditions.

$$(F_e - F_m)|_{\xi=\xi_2} = 0, \tag{3.13}$$

$$\frac{\partial}{\partial \xi}\left(F_e - F_m\right)|_{\xi=\xi_2} > 0. \tag{3.14}$$

In this case, positive displacement makes the bougie experience positive net force and negative displacement makes the bougie experience negative net force. Therefore, a small perturbation $\delta\xi$ around ξ_2 makes the bougie move in either the positive or the negative direction, and the bougie cannot come back to the neutral position ξ_2 by itself. In other words, the bougie experiences negative stiffness, which is caused by the magnetic force F_m. When the magnet is pushed beyond the unstable equilibrium

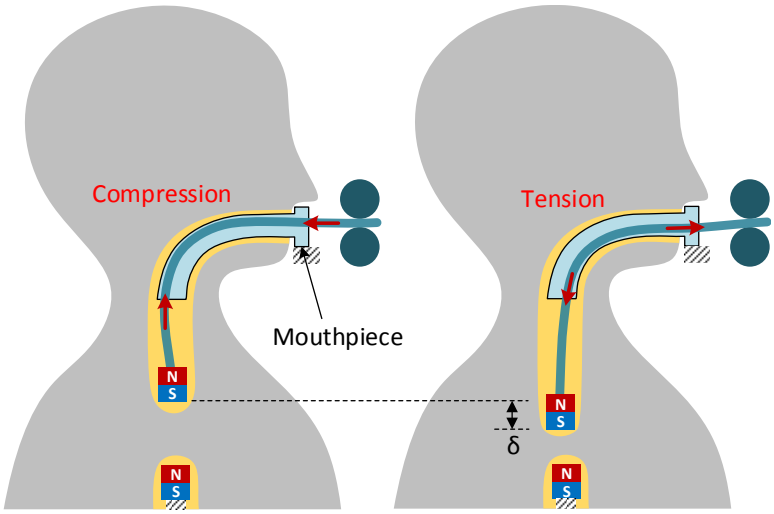

Figure 3-7: Force transition from the compression (left) to the tension (right) around the unstable equilibrium point ξ_2. The magnet could take a step change in position δ due to the clearance between the rod and the mouthpiece. The mouthpiece is required to carry the reaction force from the catheter and to provide a lateral guiding force to prevent the catheter from buckling.

point ξ_2, the compressive force of the pushing rod changes to a tensile force. The force transition around this point could make the magnet take a step change in position δ due to the clearance between the rod and the guiding mouthpiece as shown in Figure 3-7. This could make it difficult to control the position of the magnet around the unstable equilibrium ξ_2. A better fix would be mechanically modify the system such that the bougienage is not performed around the unstable equilibrium point, as described below.

3.1.3 Bougienage with Tip Extension Modulation

We can address the concern with controlling the magnet position around the unstable equilibrium by implementing an additional degree of freedom using a hydraulic piston mechanism as shown in Figure 3-8 (left). By injecting water into the barrel, we can modulate the tip extension of the bougie d, thereby controlling the esophageal gap size ξ without changing the distance between the magnets x. Here, the distance between the two magnets x is

$$x = \xi + d, \tag{3.15}$$

where ξ is the gap between two esophageal pouches and d is the tip extension.

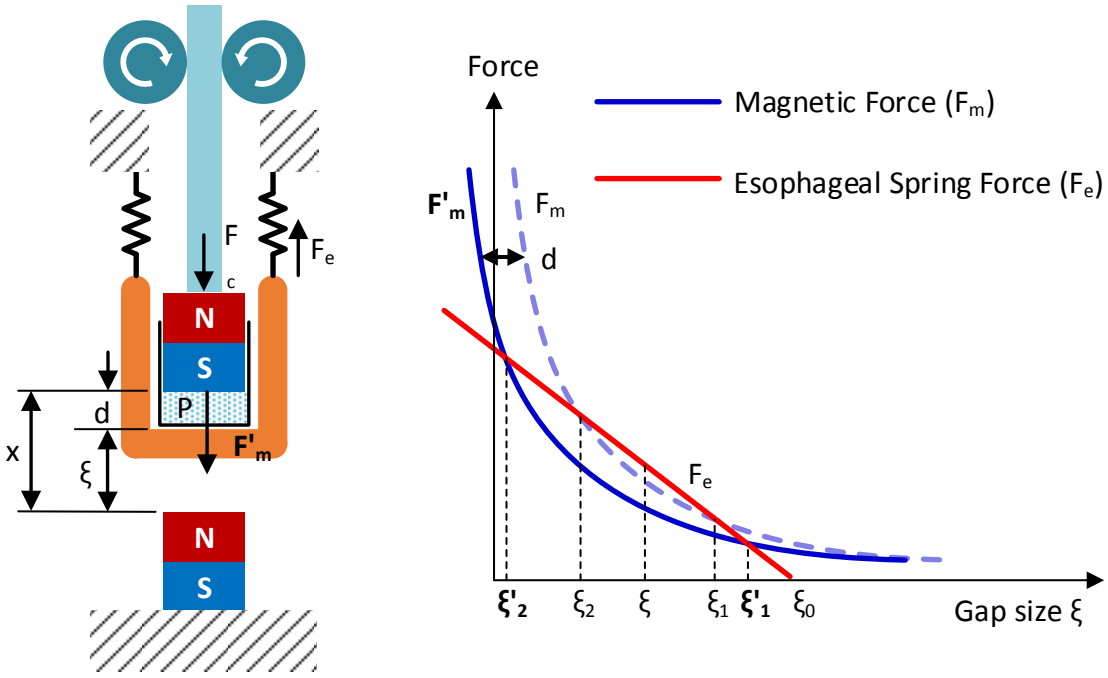

Figure 3-8: Magnetic bougienage with a piston mechanism. Modulating the tip extension d shifts the magnetic force curve in the ξ coordinate. The blue dashed line is the original magnetic force F_m, and the blue solid line is the shifted magnetic force F'_m.

Notice that (3.15) shifts the magnetic force curve expressed in (3.6) to the left by d in the ξ coordinate as shown in Figure 3-8 (right). The blue dashed line is the original magnetic force curve, and the blue solid line is the shifted magnetic force curve due to the tip displacement d. The new magnetic force curve intersects the esophageal stretching force curve twice at ξ'_1 and ξ'_2.

We can see in Figure 3-8 (right) that the original unstable equilibrium point ξ_2 is pushed to the left to ξ'_2. Therefore, the magnetic bougie can have more margin to avoid the unstable point with the tip displacement modulation. As the tip extension is increased, the unstable equilibrium point can be pushed further to the left such that ξ'_2 becomes negative, which means we can completely prevent the unstable equilibrium. However, having such a large tip extension sacrifices some of the benefits of magnetic bougienage, since the magnetic force is reduced.

The hydraulic piston mechanism also enable us to measure the esophageal stretch-

ing force. By measuring the pressure inside the barrel with an external pressure sensor, we can estimate the esophageal stretching force via

$$F_e = PA, \tag{3.16}$$

where F_e is the esophageal stretching force, P is the hydrostatic pressure inside the barrel, and A is the cross sectional area of the barrel. Since water is an essentially incompressible fluid, in principle the tip extension d does not change as the pressure varies. However, tubing flexibility does allow the tip extension to vary as a function of pressure. We have experimentally observed this effect, which is discussed in Chapter 6.

Bougienage Example

We can start the bougienage with inserting the magnetic bougie with the minimum volume of water in the barrel necessary to measure the pressure for the tip force estimation. Then, we feed the catheter to advance the magnetic bougie until the tip force reaches the nominal bougienage force, for example 3-4 N as shown in Figure 3-9. Dr. John Foker said the tension he applies to the esophageal pouch for bougienage is about 20-250 grams force, as related in a personal conversation. This force value has also been confirmed by Dr. David Mooney at Boston Children's Hospital. Here, we calculated the magnetic force curve using the finite element analysis software FEMM [14] with the actual device specifications, which is explained in more detail in Section 4.1.3. The esophageal pouch is assumed to have a stiffness of 0.3 N/mm and an initial gap of 20 mm. As shown in Figure 3-9, when the esophageal pouch is stretched by 10 mm to apply the bougienage force of 3 N, 1.3 N (43 %) comes from the magnetic force F_m and 1.7 N (57 %) comes from the compressive force of the catheter F_c.

We can increase the esophageal stretching force further up to 4 N. The first possible operating mode is to push the bougie directly by feeding the catheter without modulating the tip extension d. For example, as shown in Figure 3-9, we can increase the stretching force by 1 N by advancing the bougie by 3.3 mm. In this case, the total esophageal stretching force becomes 4 N, in which 2.7 N (68 %) comes from the

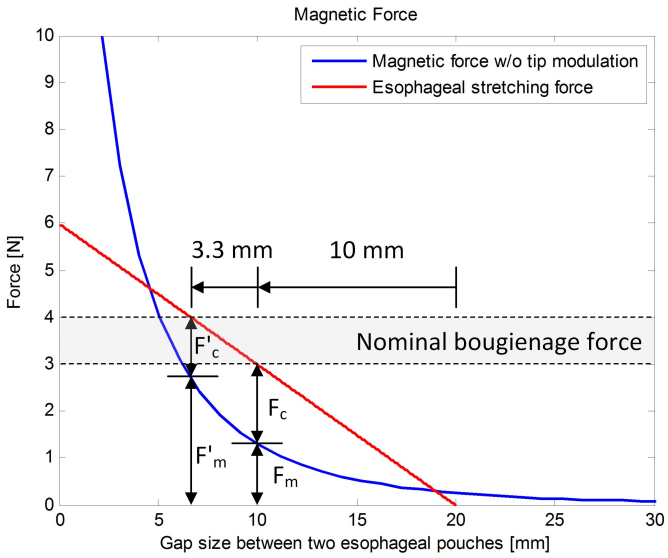

Figure 3-9: Force curve of bougienage with the tip extension $d = 0$.

magnetic force F_m and 1.3 N (32 %) comes from the compressive force of the catheter F_c. Notice that the magnetic force helps the catheter to prevent itself from buckling; although we push the magnetic bougie further, the amount of compressive force actually decreases, thereby reducing the possibility of buckling. Therefore, pushing the magnetic bougie without additional tip extension is advisable for long-gap esophageal atresia to utilize the magnetic force effectively.

The second possible operating mode is to fix the catheter feeding distance and to modulate the tip extension of the bougie only. For example, as shown in Figure 3-10, we can increase the stretching force by 1 N by increasing the tip extension by 3.3 mm. Notice that in this case the magnetic force curve is shifted to the left by 3.3 mm as explained in Section 3.1.3. The total esophageal stretching force becomes 4 N, in which 1.3 N (33 %) comes from the magnetic force and 2.7 N (67 %) comes from the compressive force of the catheter. Notice that the amount of magnetic force remains the same as before the stretch ($F_m = F'_m$) because the distance between two magnets does not change. That is, in this mode the stretch is caused by tip extension. Therefore, this operating mode requires the catheter to withstand more compressive force, which increases the possibility of buckling.

Suppose the esophageal pouch neutral position extends due to the bougienage

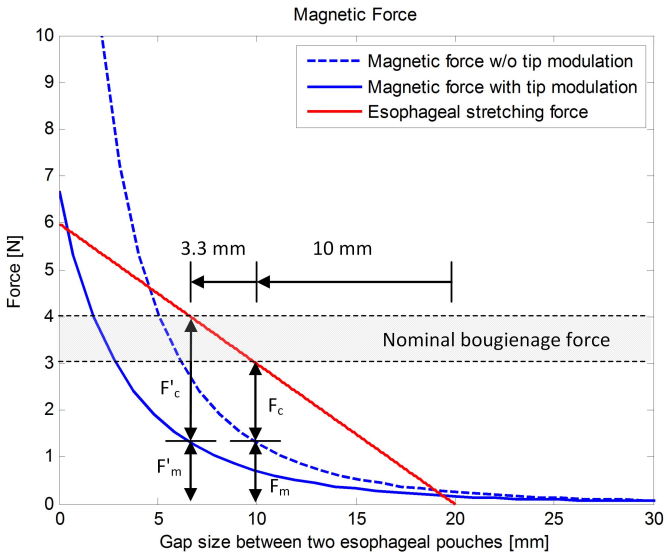

Figure 3-10: Force curve of bougienage in a mode with the stretch induced by the piston.

such that the initial gap size decreases from 20 mm to 17 mm as shown in Figure 3-11. We can keep performing bougienage by pushing the magnetic bougie until the tip force reaches 3 N. The gap size between the two esophageal pouches thus decreases from 17 mm to 7 mm and the esophageal pouch experiences a tensile force of 3 N,

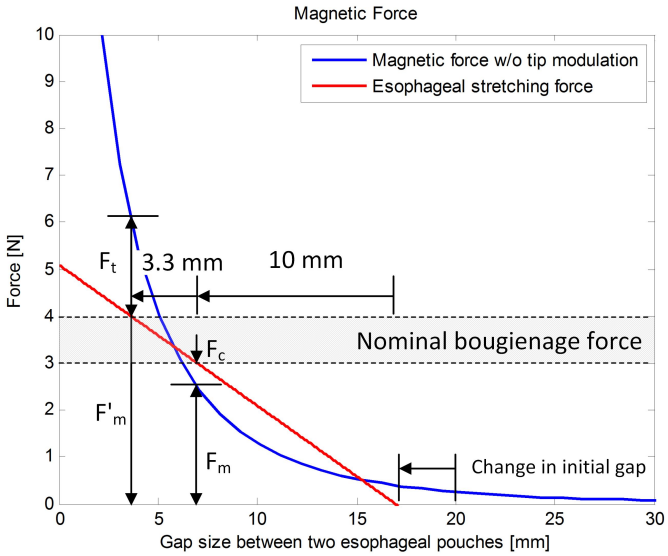

Figure 3-11: Force curve of bougienage with decreased initial gap of 17 mm, versus original 20 mm.

in which 2.5 N (83 %) comes from the magnetic force and 0.5 N (17 %) comes from the compressive force of the catheter. In this case, if we take the first operating mode, feeding the catheter without modulating the tip extension to increase the stretching force up to 4 N, the magnetic bougie passes an *unstable* equilibrium point and therefore the compressive force of the catheter changes to a tensile force. Notice that the intersection between the magnetic force curve and the esophageal stretching force is in the range of the nominal bougienage force shown as a shaded box in Figure 3-11. As discussed earlier in Section 3.1.2, such a force transition around the unstable equilibrium point makes it difficult to control the bougienage force.

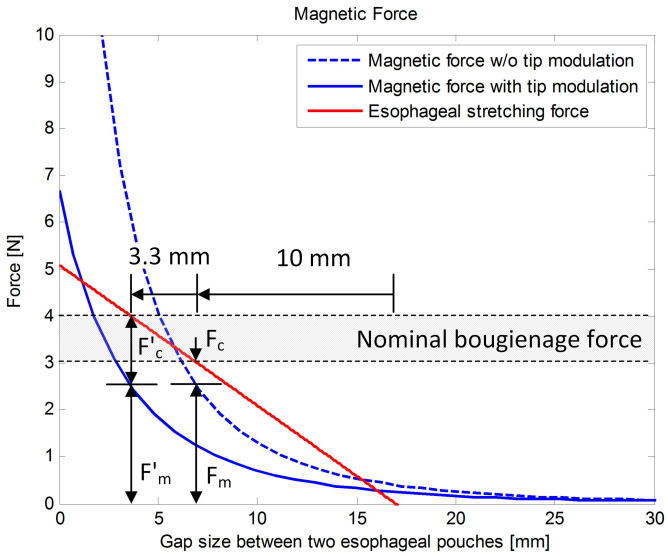

Figure 3-12: Force curve of bougienage with tip displacement = 3.3 mm.

Alternatively, we can take the second operating mode, modulating the tip extension with the catheter fixed, to avoid the unstable equilibrium point. For example, we can modulate the tip extension by 3.3 mm to increase the stretching force up to 4 N, in which 2.5 N (63 %) comes from the magnetic force F_m and 1.5 N (37 %) comes from the compressive force of the catheter as shown in Figure 3-12. Notice that the catheter experiences a compressive force continuously. Since the tip extension shifts the magnetic force curve as well, the magnetic bougie does not approach the unstable equilibium point and the catheter remains in compression during the bougienage. Therfore the second operating mode is recommended for esophageal atresia with a

relatively short gap so as to avoid instability.

3.2 Design Concepts

This section proposes several design concepts to realize the strategy developed in the previous section, especially focusing on the hydraulic mechanism for tip displacement modulation. The goal is to generate as many concepts as possible, and to analyze the pros and cons of each concept. We then select the most feasible one to carry forward into the detailed design of modules and components for prototyping.

Hydraulic bougie mechanisms enable us to keep the all electronics for actuation and measurement outside of the body. By pressurizing water from an external syringe pump, we can generate tip displacement inside the esophageal pouch. Also, the esophageal stretching force can be estimated by measuring the pressure change of the hydraulic bougie using an external pressure sensor. Three types of hydraulic bougie concepts were considered: a piston, a bellows, and a balloon type.

3.2.1 Piston

A piston mechanism is a standard way to transfer force and motion using a fluid medium. For the hydraulic bougie, we designed a piston mechanism in which a plunger consisting of permanent magnets is inserted into a barrel whose bottom is closed. The barrel can move back and forth with respect to the magnetic plunger as driven by pushing water through a catheter tube. There is a plunger seal to prevent leakage between the barrel and the plunger. We considered several designs for seals which can withstand high enough sealing pressure while minimally impeding the relative motion between the barrel and the plunger, as discussed below.

Tight Clearance Seal

Some glass syringes do not have a seal explicitly. Rather they have a tight clearance, e.g. 6-10 µm, between the barrel and the plunger.[1] Since a typical glass surface is

[1] http://wheaton.com/socorex/all-glass-syringes.html

hydrophilic, and the gap size is small, capillary effect makes the water evenly spread in the gap as shown in Figure 3-13. The thin fluid layer trapped in the small gap functions as a piston seal, whose static impedance for piston motion is almost zero. If the barrel moves with respect to the plunger at high speed, a viscous drag force is generated to impede the motion. However, the bougienage process for esophageal atresia is very slow so that any such drag effect can be ignored.

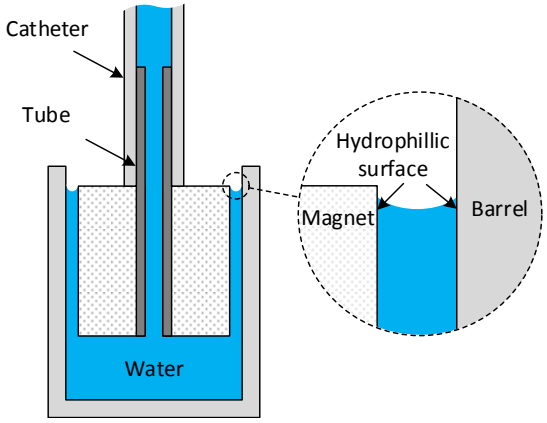

Figure 3-13: Piston seal with a gap of tight clearance.

One critical downside for this type of piston seal is the accumulated leakage, which makes it difficult to control the tip extension. The tip extension is controlled by an external syringe pump pushing water into the barrel. Without leakage, or with the conservation of the volume inside the barrel and the catheter guaranteed, we can control the tip extension by modulating the amount of water that the syringe pump pushes. However, in a tight clearance seal the pressurized fluid in the barrel can be gradually squeezed out through the gap. The leakage can be modeled as a flow between two parallel plates as shown in Figure 3-14, assuming that the radius of the plunger is much larger than the gap thickness ($R \gg 2h$). If the flow is slow such that it forms a laminar flow and the region of interest is far from the entrance, the velocity profile in the gap is represented as follows [31, p.272].

$$u = -\frac{dp}{dy}\frac{h^2}{2\mu}\left(1 - \frac{x^2}{h^2}\right), \tag{3.17}$$

where dp/dy is the pressure gradient in the y direction, h is a half of the gap thickness,

μ is the viscosity of the fluid. The parabolic velocity profile is called a *Poiseuille* parabola.

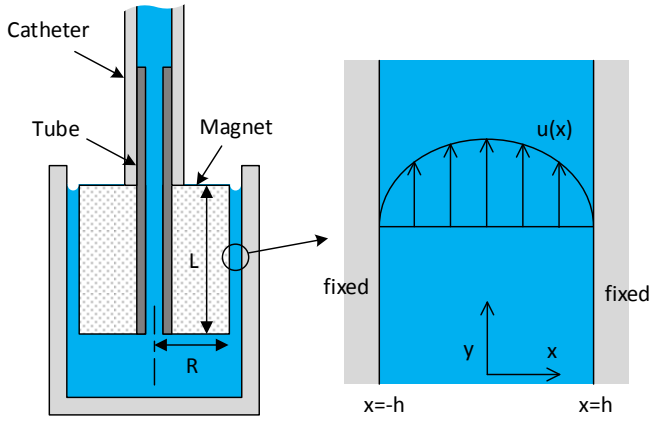

Figure 3-14: Flow between parallel plates: Poiseuille flow.

We can evaluate the net flow rate through the gap by integrating the velocity profile with respect to the cross sectional area of the gap.

$$Q = \int_A u \, da, \tag{3.18}$$

where Q is the net flow, A is the net cross sectional area of the gap, and da is the infinitesimal cross sectional area. Since the gap thickness is much smaller than the radius of the plunger, we can approximate the infinitesimal area da as.

$$da \approx 2\pi R \, dx. \tag{3.19}$$

Also, if we further assume that the entrance length is much shorter than the total length of the gap L, we can approximate the pressure gradient as a constant

$$\frac{dp}{dy} \approx \frac{\Delta p}{L}. \tag{3.20}$$

Finally, we can substitute (3.20) and (3.17) into (3.18) to get an approximate flow rate through the gap as

$$Q \approx \frac{2h^3}{3\mu} \frac{\Delta p}{L} 2\pi R. \tag{3.21}$$

If a piston with 1 cm diameter and 6 µm gap is loaded with a 1 N force continuously, the approximate amount of a leakage given by (3.21) is 2.6 mL per an hour. Such a small leakage can be neglected in some applications happening in a short time scale, but the accumulated amount of leakage is hard to neglect in this case, considering several weeks of bougienage process for esophageal atresia, and since any leakage has to be aspirated from the patient's esophageal pouch via suction. Thus, for the present purposes we discard this option.

Surface Tension Seal

Surface tension of a fluid can in principle seal the piston gap as shown in Figure 3-15. If we engineer the surfaces of the magnet and the barrel to be hydrophobic so that the water forms a convex meniscus, the surface tension can seal the water by withstanding the pressure up to certain level. The seal pressure is determined by the curvature of the meniscus.

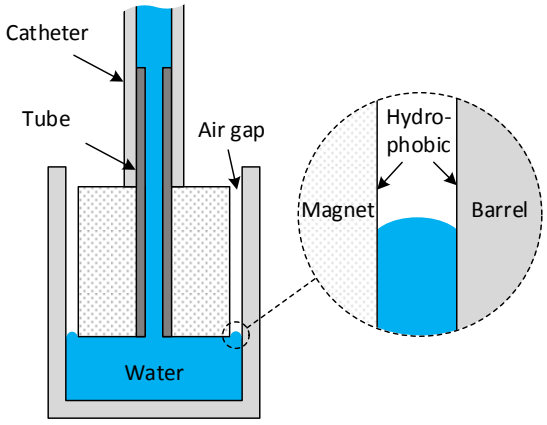

Figure 3-15: Piston seal with surface tension of water.

Fluids with strong cohesive forces between molecules are preferred for this purpose, because they generates stronger surface tension [19, p.132]. Therefore, we can think of using water because it has a strong intermolecular attraction due to the hydrogen bond.

A concern with this concept is that it does not have a strong mechanism to provide positive stiffness between the magnet and the barrel such that the magnet is

self-centered in the barrel in the radial direction and the rotational direction. The surface tension gives a positive stiffness at the bottom of the plunger, but the top of the plunger does not have such a mechanism. Therefore, the magnet pushed by the catheter can be tilted and even stuck in the barrel, which can introduce friction between two rigid surfaces.

O-ring Seal

O-rings can seal the gap between the magnetic plunger and the barrel as shown in Figure 3-16. Three ring type magnets and two spacers are inserted in a tube in turn to make a gland for each of the o-rings. The amount of the preload is determined by the diameter of the spacers. Notice that two O-rings provide positive stiffness, in the lateral and rotational directions, so that the plunger is centered with the barrel without the plunger touching any part of the barrel surface.

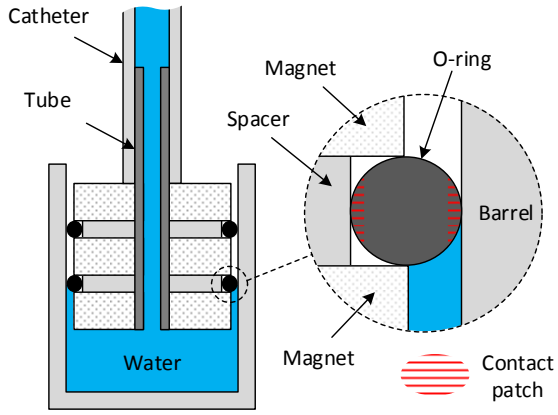

Figure 3-16: Piston seal with O-rings.

An O-ring is a standard solution to seal hydraulic systems. For a static seal, where there is no relative motion between two parts to be sealed, O-rings can create a high-quality seal in terms of robustness and reliability. However, for a dynamic seal, where there is a sliding motion between the two surfaces, O-rings are more problematic due to the friction. Although some companies provide a guideline for dynamic seal design and make some variations on the cross sectional shapes to reduce the friction[2],

[2]http://www.applerubber.com/seal-design-guide/introduction/

there is a fundamental trade-off between seal pressure and friction. An o-ring should be installed with a large preload to increase the seal pressure, where as the preload should be small to reduce the friction. The friction can be mitigated by applying a lubricant, which gives a thin fluid film between the O-ring and the rigid surface.

Mercury Seal

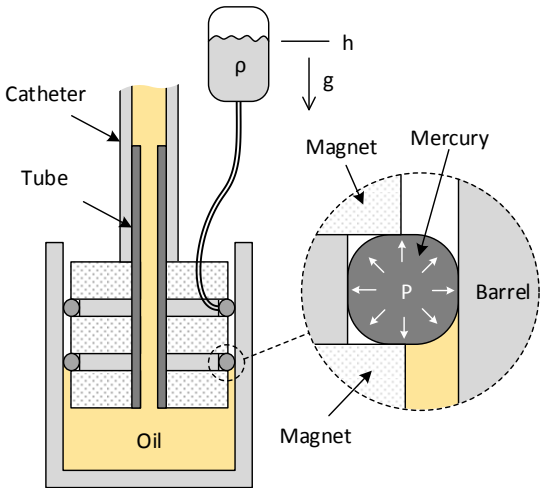

Figure 3-17: Piston seal with mercury concept, inspired by [30].

A fluid can seal the gap of a piston mechanism if it has sufficient surface tension. For example, the piston of a diffraction grating ruling engine was sealed with mercury [30]. The ruling engine requires extreme precision to engrave thousands of parallel grooves in 1 mm to fabricate a diffraction grating, and the mercury seal is one of the elements enabling such precision. A brief history of the ruling engine is described in a paper written by Loewen and Wiley [12], and more details are described in *Diffraction Grating Handbook* [20] available online. We can in principle use the same mechanism to seal the magnetic plunger as shown in Figure 3-17. The seal could be pressurized via a reservoir of mercury to pressure $P = \rho g h$, where ρ is the density of mercury, g is the gravitational acceleration, and h is the height of the mercury reservoir. The hydrostatic pressure as well as the surface tension of the mercury prevents the oil from leaking out through the gap. Although this mechanism enables us to get a high performance seal with essentially zero static friction and a self-centering characteristic,

it is not advisable to use mercury for such medical application, given the hazardous material.

Ferrofluid Seal

Ferrofluids are colloidal liquids made of nanoscale ferromagnetic particles. Due to the high magnetic permeability, they can be strongly magnetized and attracted by a magnetic field. The volumetric force density that a ferromagnetic material experiences under an ambient magnetic field is given by [7, p.517],

$$F_{KH} = J \times B - \frac{1}{2} H \cdot H \nabla \mu. \tag{3.22}$$

Here, J is current density, B is magnetic flux density, H is magnetic field intensity, and μ is the magnetic permeability. This equation, called the Korteweg-Helmholtz force density, explains how magnetic stress is imposed in the volume of a ferrofluid. In a material with magnetic permeability which is uniform as μ_1, the gradient operator gives a spatial impulse force density on the surface of a ferrofluid where the magnetic permeability takes a step from μ_0 to μ_1.

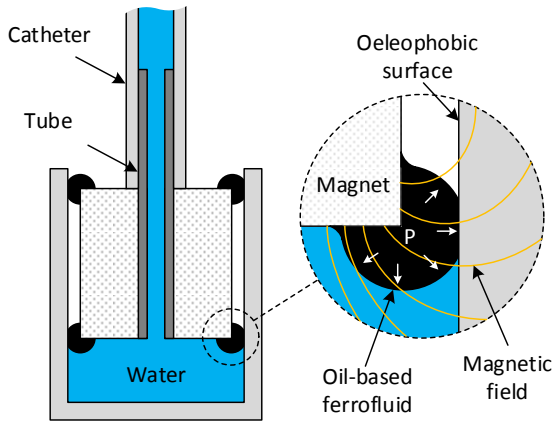

Figure 3-18: Piston seal with a ferrofluid.

The magnetic stress on the surface increases the pressure of the ferrofluid, thereby sealing the gap of the piston by withstanding the water pressure up to certain level as shown in Figure 3-18. Due to the relatively dense magnetic field at the edge of

the magnet, ferrofluid gathers around the circumference of the plunger to be in static equilibrium. In this case, the ferrofluid functions similar to an O-ring seal but can eliminate the friction issue. Also, the ferrofluid rings provide positive stiffness such that the magnetic plunger centers itself in the barrel.

There are two types of ferrofluids: water-based and oil-based. The water-based have more potential in terms of sealing capability due to the inherent large intermolecular attraction of water. For a long-lasting piston seal, however, oil-based ferrofluids are preferred to the water-based because water evaporates into the air with time. When using oil-based ferrofluids, the barrel surface needs to be oeleophobic so as to increase the surface tension. This also prevents the barrel being contaminated by wetting.

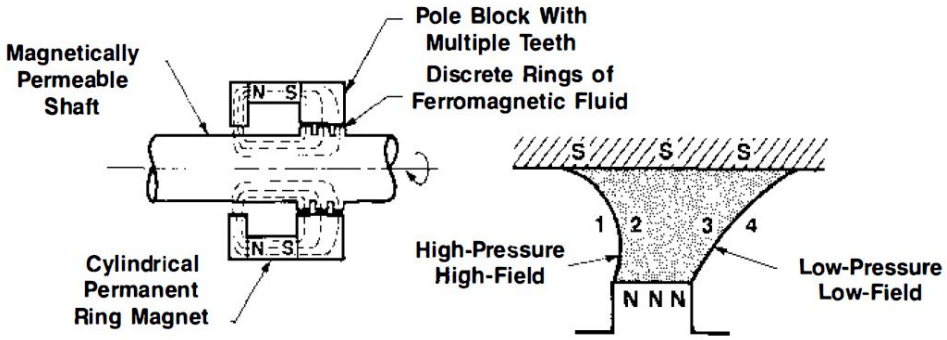

Figure 3-19: Ferrofluid seal for a rotary shaft taken from [23].

Sealing is a major application area for ferrofluids. For example, a ferrofluid can be used to seal the gap of a rotary shaft; a ferromagnetic rotary shaft and a ferromagnetic housing make up a magnetic circuit with an external permanent magnet as shown in Figure 3-19. The magnetic flux around the circuit concentrates at the narrow pole face of the tooth, which traps the ferrofluid in the gap between the shaft and the housing. The magnetic force due to the magnetic flux enables the ferrofluid to withstand the pressure difference [23].

Rolling Diaphragm Seal

A rolling diaphragm can be used to seal a linear hydraulic actuator that requires low friction loss. Dr. Piet Van Rens at Settels van Amelsvoort introduced me to this idea during a lab tour. For the hydraullic bougie seal design, a cylindrical thin rubber tube can be inserted between the barrel and the plunger, one end being turned inside out as shown in Figure 3-20. The ends of the rubber tube are glued on the barrel and the magnet respectively, while the tube is free to roll on the surface. The seal is robust because the water is directly sealed by the rubber diaphragm. As the barrel moves with respect to the magnet, the curved sleeve of the rubber tube rolls between the surfaces without slip. Since there is no slip between the tube and the surfaces, this type of seal can reduce the friction significantly. Also, positive stiffness of the curved rubber sleeve makes the plunger self-centered.

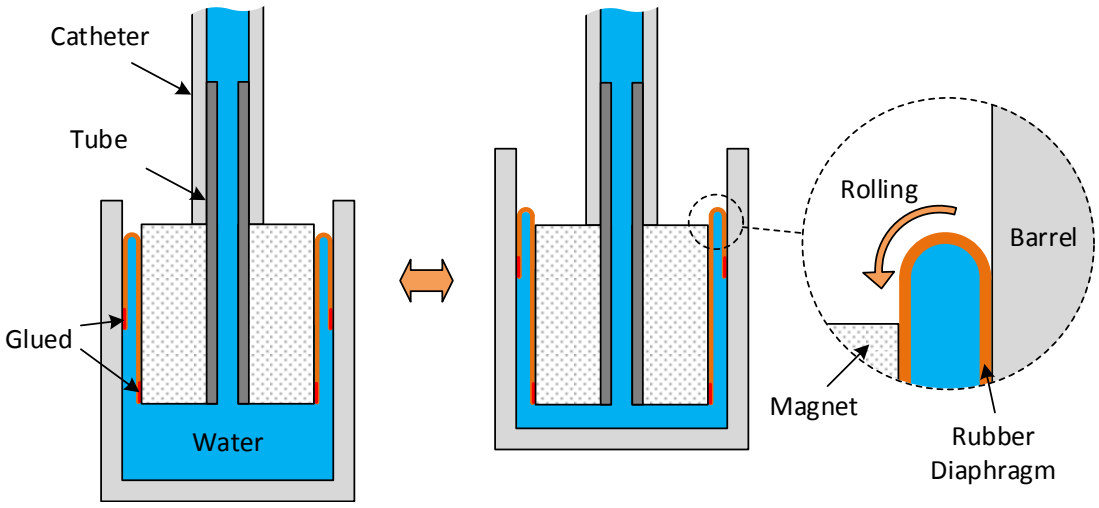

Figure 3-20: Piston seal with a rolling rubber diaphragm.

A downside of this mechanism is that it requires complicated structures in a small volume as well as glued joints on the seal interface. Also, there are fabrication issues to implement this mechanism because no standard parts are available, as apposed to O-rings. Nevertheless, the rolling diaphragm mechanism is a good candidate for the piston seal design, which gives a robust seal with potentially less friction.

3.2.2 Bellows

A bellows mechanism can be used to transfer a motion where a hermetic seal is required. In particular, metal bellows are commonly used to build a precision machine; although they have some stiffness to impede the motion, the stiffness is linear and repeatable, which enables us to design a machine which is easy to control. There are two main types of metal bellows based on how they are fabricated: edge-welded and electroformed.

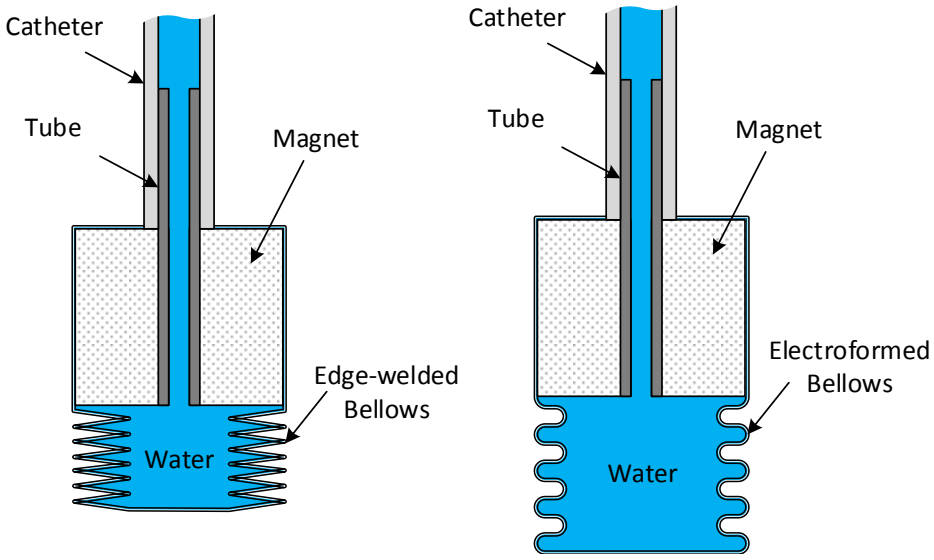

Figure 3-21: Edge-wedged Bellows (left) and electroformed bellows (right).

Electroformed bellows are fabricated by electroplating a thin metal layer, i.e. Ni alloy, on an aluminum mandrel machined in a bellows shape, and then dissolving out the mandrel electrochemically. The thickness of the each structure can be easily controlled, and it can be made with isotropic mechanical properties without any residual stresses. Multi-layered structures, such as copper, gold, and platinum, can be fabricated as well. A downside is that such a belllows has a relatively large solid height and a relatively small elongation range. Thus, this type of bellows is often used for a shaft coupling where the angular deflection is more dominant that the axial deflection. Electroforming is a general fabrication technique not just for bellows, suitable for fabricating a variety of thin-walled miniature parts.

Alternately, edge-welded bellows are fabricated by stacking layers of annular metal diaphragms and welding their edges. The thin metal layers have a relatively low bending stiffness, so that the overall structure can have a low spring coefficient. Therefore, this type of bellows are more suitable for generating long stroke than electroformed bollows. One concern with the edge-welded bellows is that the sharp welded-edge could damage the soft esophageal tissue. Also, although it is more compliant than the electroformed bellows in general, it requires a larger number of metal diaphragm folds to reduce the compliance, which increase the solid height of the bellows. Large solid height increases the default distance between the two magnets so that the maximum magnetic magnetic force the device can generate decreases.

3.2.3 Balloon

We can also potentially use a balloon for bougienage. For example, Vogel et at. employed a balloon catheter to stretch the distal esophageal pouch [28]. However, a typical rubber balloon expands isotropically, and therefore it generates unnecessary radial motion. If we can engineer a composite balloon with an anisotropic modulus such that it expands in the axial direction more than the lateral direction, we can make a soft hydraulic mechanism for esophageal bougienage.

The previous MIT student team developed a hydraulically controlled magnetic bougie with a rubber balloon [18] as shown in Figure 3-22. They designed a rigid outer casing around the balloon, such that the balloon expands in the axial direction only. However, the static friction between the balloon and the outer casing made the balloon experience stress concentration, so that the balloon was torn frequently. Nevertheless, the idea of combining a permanent magnet and a hydraulic mechanism to develop a new type of bougie showed promise, and inspired me to explore further on this topic.

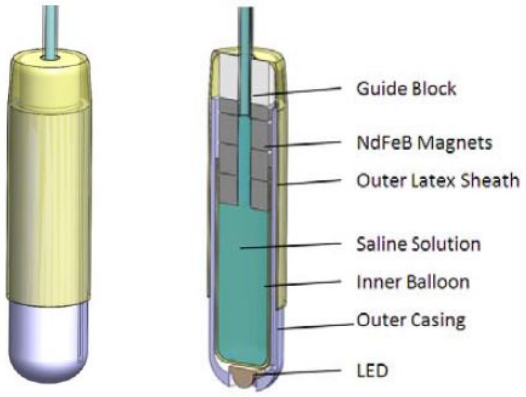

Figure 3-22: A magnetic bougie with a hydraulically controlled balloon developed by the previous MIT student team [18].

3.3 Concept Decision

The problem of the hydraulic bougie developed by the previous MIT student team was that the balloon was ripped too often. Also, they said it was hard to obtain a reliable tip force measurement using their bougie. Therefore, we decided to discard the balloon concept and focused on a bellows mechanism and a piston mechanism. First, we were fascinated by glass syringes with a tight clearance seal due to their extremely low friction. However, we found that there is a finite leakage through the gap, and calculated the amount of leakage to convince ourselves that the accumulated amount of such a leakage is not negligible as discussed in Section 3.2.1. Then, we moved our focus to metal bellows because of their high-quality seal and linear stiffness. I receive a sample of an edge-welded bellows from Senior Aerospace[3] to check the feasibility, and realized that the stiffness was larger than we expected although I ordered the least stiff bellows available. Their donation of the sample is appreciated though. Also, the welded edge of the bellows was too sharp, which made us concerned with hurting the soft esophageal tissue of babies. Finally, we decided to choose a piston mechanism with an O-ring seal. A piston mechanism with an O-ring seal is relatively easy to realize, and its sealing performance is quite reliable. The inherent friction issue of O-ring seals made us concerned but we thought that the friction can be mitigated by applying a lubricant and designing the gland appropriately.

[3]http://www.metalbellows.com/

3.4 Summary

In this chapter, we developed concepts for a magnetic bougienage with hydraulic tip modulation. We also discussed several design concepts for the hydraulic bougie, such as a piston, a bellows, and a balloon mechanism. The piston concept was discussed in more detail, focusing on variety of piston seal designs, such as tight clearance seal, surface tension seal, O-ring seal, mercury seal, ferrofluid seal, and rolling diaphragm seal. Among the concepts, we chose a piston mechanism and O-ring seal to carry forward into the detailed design for the prototype, which is covered in the next chapter.

Chapter 4

Modules and Components Design

This chapter introduces the detailed designs of the modules and the components for the hydraulically controlled magnetic bougienage. We especially focus on the design of two modules, a magnetic bougie and a friction drive, which are shown in Figure 4-1.

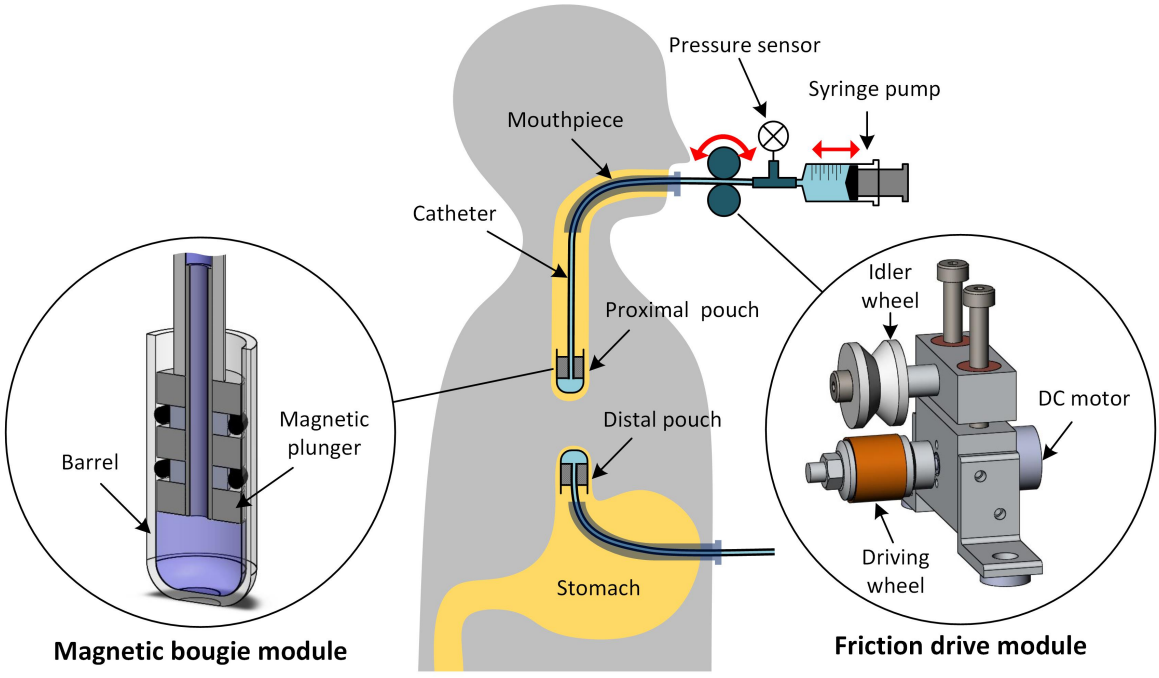

Figure 4-1: A schematic of the hydraulically controlled magnetic bougienage and two key modules: magnetic bougie and friction drive.

A magnetic bougie is an end-effector that applies a stretching force to the proximal

esophageal pouch. We designed the bougie based on a piston mechanism, where a plunger consisting of permanent magnets is inserted into a barrel. The magnet in the bougie generates a force by interacting with another magnet in the distal esophageal pouch to stretch the esophageal pouches. We can put either the same bougie in the distal pouch or different one without a hydraulic piston mechanism. The displacement of the barrel with respect to the plunger can be modulated by pushing water into the barrel through a catheter using an external syringe pump. A Tee connector is placed at the outlet of the external syringe pump to connect the pump to a pressure sensor as well as the catheter. The pressure sensor measures the water pressure in the catheter lumen, which approximates to the water pressure in the barrel of the bougie when the water flow rate is slow enough. From the measured pressure we can estimate the force at the tip of the bougie, which tells the esophageal stretching force.

A friction drive is designed to feed the catheter back and forth, thereby pushing the magnetic bougie into the esophageal pouch. A position-controlled servo motor rotates a driving wheel, which feeds the catheter. The hydraulic piston mechanism generates additional displacement at the tip of the magnetic bougie. In other words, the friction drive generates the long-stroke motion of the bougie, while the syringe pump generates short stroke at the tip of the bougie. The additional tip displacement enables the device to modulate the gap size between the esophageal pouches and the distance between the magnets independently as discussed in Section 3.1.3.

4.1 Magnetic Bougie

A magnetic bougie consists of a barrel and a magnetic plunger as shown in Figure 4-2. The barrel is a rigid thin-walled cylindrical structure with a closed end. The magnetic plunger is made with three ring-type NdFeB magnets and O-rings to seal the gap between the plunger and the barrel. The bougie is connected to an external syringe pump through a catheter as shown in Figure 4-1. The catheter is reinforced by inserting a thin stainless steel tubing inside to increase the structural rigidity, thereby reducing the possibility of buckling. The external syringe pump can modulate the tip

displacement of the bougie by pushing water into the barrel through the central hole of the magnetic plunger.

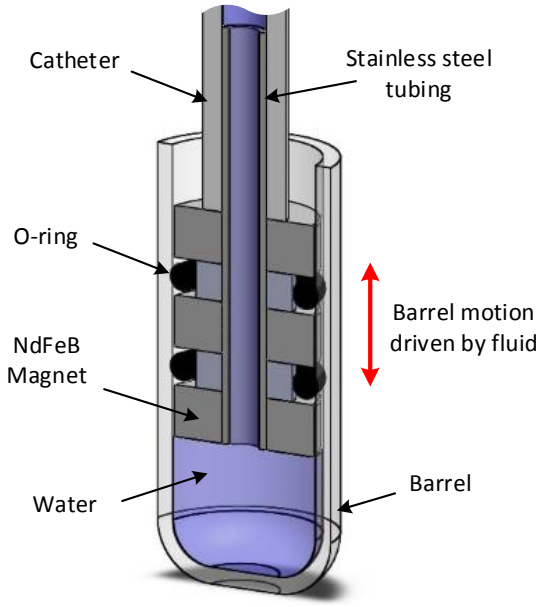

Figure 4-2: A cross-sectional view of the hydraulically controlled magnetic bougie.

O-rings are chosen for a seal mechanism due to their reliable sealing performance as discussed in Section 3.2.1. However, the O-rings in the magnetic bougie lead to a friction problem because there is relative motion between the barrel and the plunger. The friction makes it difficult to estimate the bougie tip force from the measured water pressure because some of the tip force is carried by the friction and only the rest of the tip force press the water in the bougie. There is a nice online seal design guide by Apple Rubber Products Inc.[1] which explains how to design O-ring seal in detail. In particular, the design guide lists various factors to be considered to reduce friction of O-ring seal: preloading, durometer, cross section, lubrication, compound additives, surface, gland machining, groove width, and material. In this section, however, we only focused on the gland design, material selection, and lubrication to reduce the friction.

[1] http://www.applerubber.com/seal-design-guide/

4.1.1 Barrel

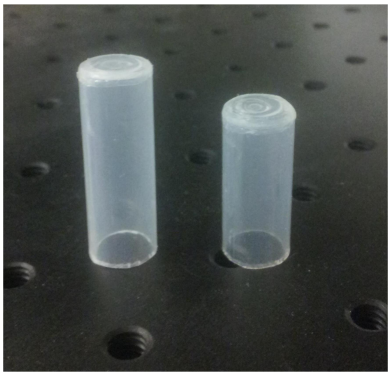

Figure 4-3: Barrels fabricated from polypropylene syringes.

A barrel is fabricated from an off-the-shelf syringe as shown in Figure 4-3. We purchased a polypropylene syringe of 3 cc volumetric capacity, whose inner diameter was 9.78 mm (0.385 inch) and the outer diameter was 11.56 mm (0.455 inch). Two methods have been tried to modify the syringe to make the barrel. We first tried to block the needle end side of the syringe with other materials, such as glue and epoxy, and cut the syringe as shown in Figure 4-4 (a). The barrel fabricated in this way worked well for a while, but after a course of bougienage tests, the clogging material was taken apart from the barrel. It turned out that both of the materials do not adhere well on the surface of the polypropylene barrel. Moreover, the fabricated barrel had a redundant overhead thickness, annotated as D in Figure 4-4 (a), which reduces the maximum magnetic force that the bougie can generate.

The second fabrication method that we came up with was to close the needle side by thermoforming as shown in Figure 4-4. In this way, we were able to make the unnecessary overhead thickness as small as possible, while achieving robustness of the closing. A cylindrical aluminum mold is machined for the thermoforming as shown in Figure 4-5, so that the barrel can maintain its cylindrical shape while the needle side is being deformed. This simple method enabled us to fabricate robust barrels with a minimal overhead thickness, whose quality was considered to be enough for the proof of concept.

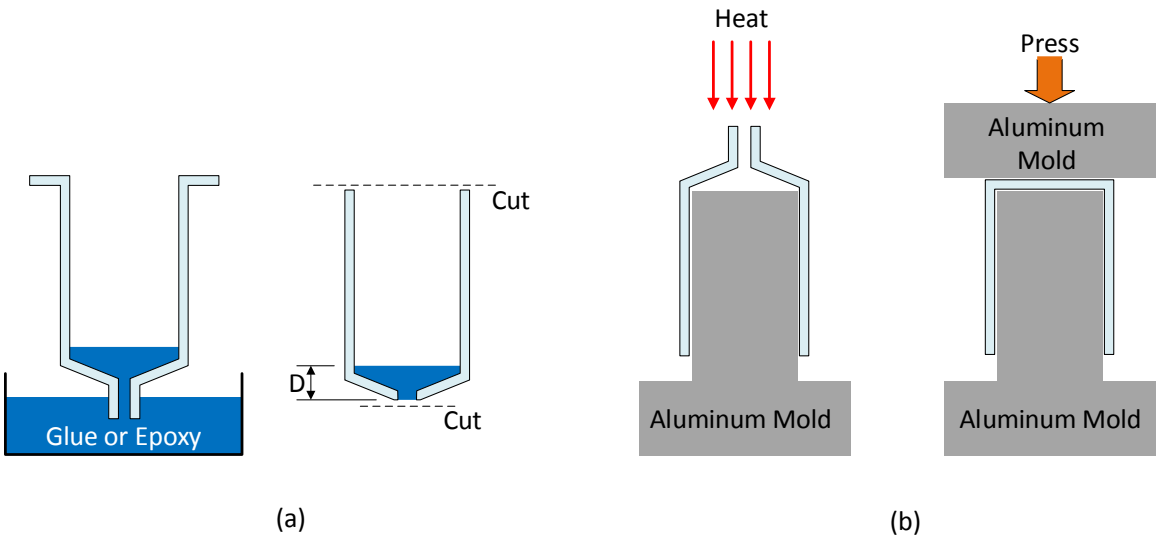

Figure 4-4: Two ways to fabricate the barrels.

4.1.2 Magnetic Plunger

A magnetic plunger is the central component of the magnetic bougie, which generates a magnetic force for the bougienage. It is made with three ring type NdFeB magnets, a core tubing, two spacers made of Delrin®, and two O-rings as shown in Figure 4-6. As shown in Figure 4-2, three ring type magnets and two spacers are placed on the core tubing by turns, and each spacer and the adjacent two magnets make a groove, or a gland, for an O-ring to be placed. The end of the core tubing is connected to the catheter via an interference fit into a lumen of the catheter.

Magnet Selection

We purchased ring type NdFeB magnets with the outer diamter of 9.53 mm (0.375 inch) so that it fits into the barrel with as small clearance as possible. The resulting diametrical clearance was 0.12 mm (0.005 inch), which was the minimum that we could achieve from the available magnet sizes. The magnet we finally selected had the inner diameter of 3.18 mm (0.125 inch), the thickness of 3.18 mm (0.125 inch), and the maximum remanence flux density of 1.32 T.

Figure 4-5: An aluminum mold to fabricate the barrel by thermoforming.

Table 4.1: Permanent Magnet Specification

Material	NdFeB
$B_{r,max}$	13,200 Gauss
Outer Diameter	9.53 mm (0.375 inch)
Inner Diameter	3.18 mm (0.125 inch)
Thickness	3.18 mm (0.125 inch)

Core Tube Fabrication

We tried two materials to fabricate the core tube within the plunger. At first, we used a PEEK plastic tubing with the outer diameter of 3.18 mm (0.125 inch). A PEEK plastic is known to be a good substitute for a stainless steel tubing because of its relatively high mechanical strength (90-100 MPa) and inertness to most chemicals. We assembled the PEEK tubing and the magnets via interference fit. However, the cross sectional shape of the tubing was somewhat oval, and therefore water leaked through the gap gradually.

Next, we used a stainless steel tubing to fabricate the core. One end of the stainless steel tubing was turned in a tight tolerance for a slip fit. A liquid retainer is applied between the machined surface of the stainless steel tubing and the magnets to retain the assembly. We employed Loctite® 7649 primer and Loctite® 609 retainer,

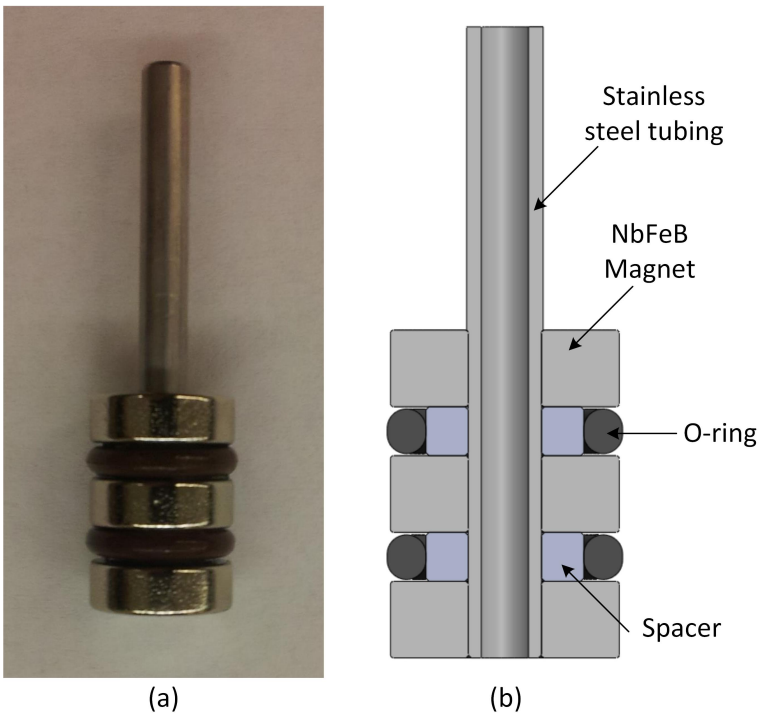

Figure 4-6: Magnetic Plunger: (a) the prototype and (b) 3D model.

which gives maximum shear strength of 16 MPa (2300 psi) and seals the diametrical clearance up to 0.13 mm (0.005 inch). The maximum force that the liquid retainer can withstand is about 1506 N, which is calculated by multiplying the maximum shear strength, 16 MPa, by the contact surface area between the core tubing and the magnets, 95 mm^2. The maximum force is about 50 times larger than the maximum magnetic force and therefore the liquid retainer is considered to be safe for the assembly.

O-ring Selection and Gland Design

We selected the O-ring size such that its outer diameter is slightly smaller than the inner diameter of the barrel. From the standard AS568 O-ring sizing chart, we chose AS568-010 whose inner diameter is 6.07 mm (0.239 inch), the outer diameter is 9.63 mm (0.379 inch), and the cross section is 1.78 mm (0.07 inch).

Compression of the O-ring, which is set by the size of the gland, is an important factor that determines the sealing performance [21, p.7]. In our bougie design shown

Figure 4-7: Stainless steel tubing. The right end is turned with a lathe to fit the ring type magnets inner diameter. Tube provides structural support as well as a fluid connection from the plunger to the catheter.

in Figure 4-8, the O-ring compression can be tuned by varying the size of the spacer. As we increases the spacer's outer diameter OD_s, the gland depth A and the groove depth D decrease, and therefore the O-ring experiences more compression. More compression enhances the sealing performance, but it also increases the friction between the O-ring and the barrel. In other words, there is a fundamental trade-off between the sealing performance and the friction. By trial and error, the outer diameter of the spacer is designed to be 6.60 mm (0.26 inch) for a satisfactory trade-off between the seal and the friction. The thickness of the spacer is designed to be 2.3 mm (0.09 inch) such that the O-ring does not experience compression in the axial direction, following the seal design guide [21, p.17].

To find a material that gives less friction, we tried four different materials of O-rings: Buna-N, Silicone, Viton® Fluoroelastomer, and PTFE (Polytetrafluoroethylene). We expected PTFE to give the best lubricity among them, but the one we purchased from McMASTER-CARR[2] was too rigid (durometer hardness D55) to set the appropriate preloading for the seal. The other three materials gave similar performance in terms of friction especially when they were lubricated with a silicone grease. Viton® Fluoroelastomer O-ring a silicone O-ring lubricant manufactured by PolySi Technologies (PST-841) were selected to use for the seal. We have also studied using a controlled dither signal to reduce the effect of friction, as explained in Section 6.1

[2]http://www.mcmaster.com/

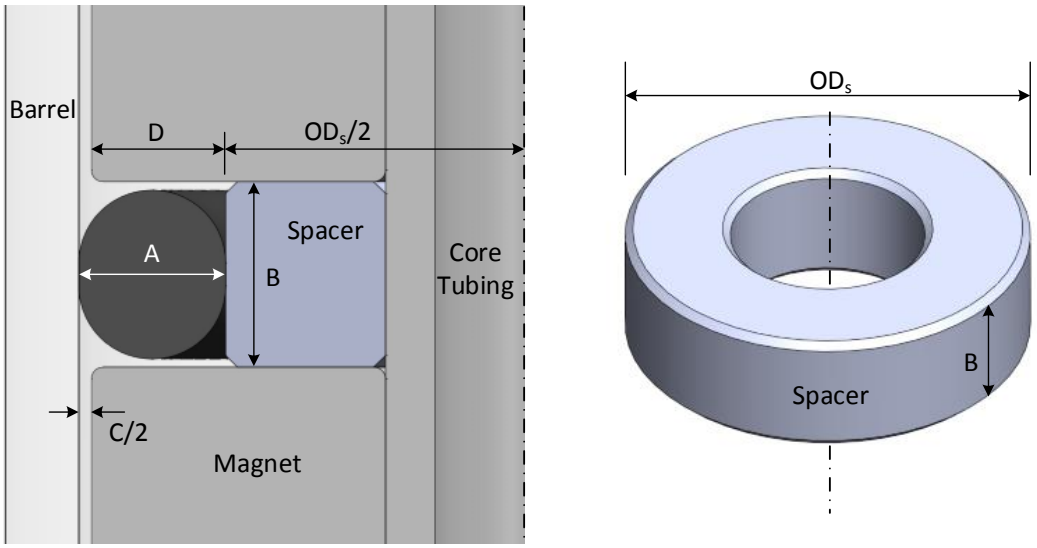

Figure 4-8: O-ring gland design. A is the gland depth, B is the groove width, C is the diametrical clearance, and D is the groove depth. The outer diameter of the spacer OD_s determines A and D.

For future research, we recommend to try different types of seals, such as the ferrofluid seal discussed in Section 3.2.1 and rolling diaphragm seal discussed in Section 3.2.1 to resolve the friction problem.

4.1.3 Magnetic Force Analysis

Calculating the magnetic force that the magnetic bougie can generate is important to design other modules quantitatively. However, the magnetic force is not simply governed by (3.6) especially when the gap between the two magnets is small. For more accurate calculation, a finite element analysis is performed with FEMM software [14]. The result is compared with the experimentally measured magnetic force as well as the simple model result from (3.6) as shown in Figure 4-9.

In Figure 4-9, the green curve is the magnetic force calculated from the simple model (3.6), the blue curve is calculated from the finite element analysis performed in FEMM software, and the red circles are the experimentally measured magnetic force with a load cell. The experimental result matches with the FEA result well, whereas the simple model shows a discrepancy from the measured date as the gap size decreases. This is because the simple model (3.6) considers each pole face of

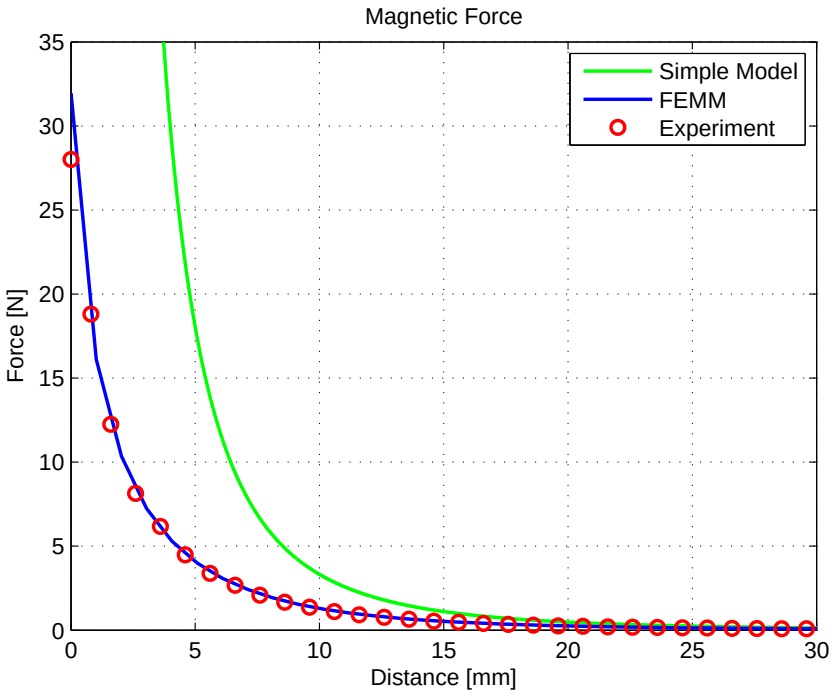

Figure 4-9: Attractive force between two permanent magnets. The green curve is the result of the simple model (3.6), the blue curve is the FEA result with FEMM software, and the red circles are measured data.

the magnet as a magnetic point charge, which give infinite attraction when the gap size approaches to zero. However, the real magnetic force between two permanent magnet cannot be infinitely large. The maximum magnetic force that our bougie can generate is about 30 N as shown in Figure 4-9.

4.2 Friction Drive

A friction drive, or a traction drive, is a type of transmission mechanism that transfers mechanical power by means of friction. It can be used in a transmission system where placing gears and screws is difficult. In this research, a friction drive is designed to feed the catheter back and forth so that the position of the magnetic bougie at the tip of the catheter can be controlled. A brushless DC motor rotates a driving wheel, which applies a friction force to the catheter to move the bougie into the esophageal pouch by a commanded displacement. The friction drive is attached to a rigid reference

frame, which carries the reaction force from the catheter.

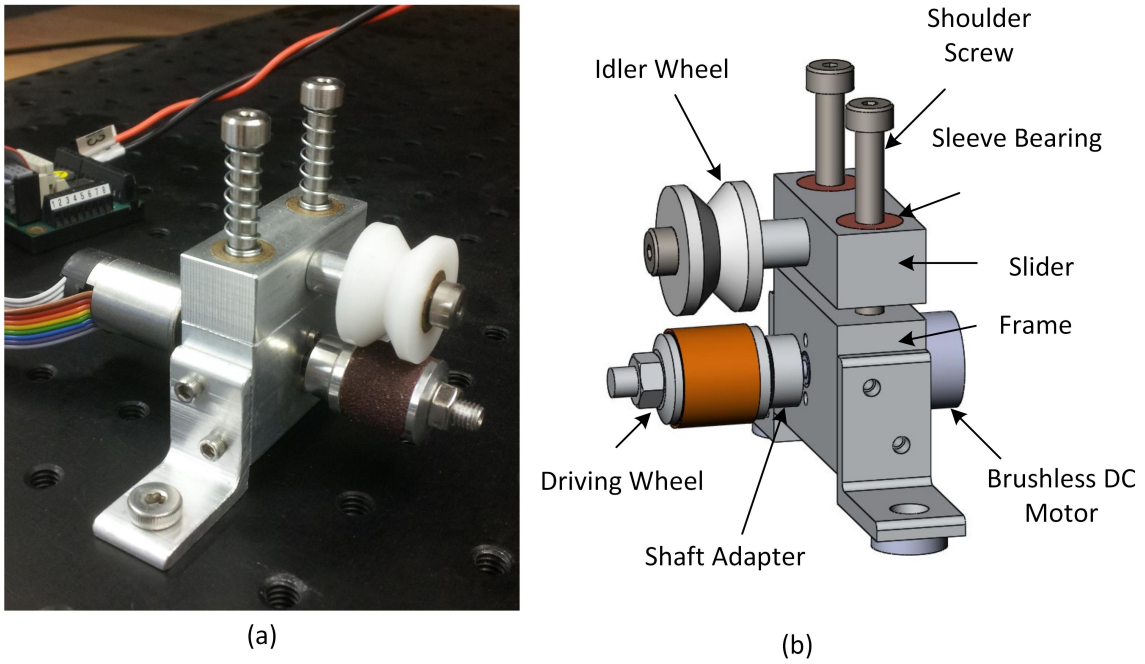

Figure 4-10: Friction Drive: (a) the prototype and (b) 3D model.

The friction drive consists of a driving wheel, an idler wheel, a main frame, and a slider frame as shown in Figure 4-10. The driving wheel and the V-grooved idler wheel make a triangular opening for a catheter to be placed. The size of the opening between the driving wheel and the idler wheel can be adjusted by moving the slider frame up and down. The slider frame runs on two parallel shoulder screws, which function as rails for the slider frame. These shoulder screws, fixed on the main frame, constrain the slider so that it can move only in the direction parallel with the screws. Two flanged-sleeve bearings are installed on each shoulder screw to reduce the friction, and two linear stainless steel springs are inserted on each shoulder screw to generate controllable normal force to compress the idler wheel against the catheter. This provides the preload for the friction drive to feed the catheter. The driving wheel is connected to a brushless DC motor via a collet-type shaft adapter, and the motor is mounted on the main frame. The friction drive module is fixed on an optical table in our experiment so that it can carry the reaction force from the driving wheel, and provides a position reference for the whole system.

Table 4.2: Brushless DC Motor Specifications.

Motor type	Brushless
Torque constant	7.8 mNm/A
Nominal torque	3.23 mNm
Stall torque	5.95 mNm

Table 4.3: Motor Gearhead Specifications.

Radial play, 6 mm from flange	max. 0.06 mm
Max. permissible axial load	8 N
Max. permissible force for press fits	100 N
Max. radial load, 6mm from flange	16 N
Max. continuous torque	0.20 Nm
Intermittently permissible torque at gear output	0.300 Nm
Reduction	84:1

4.2.1 Brushless DC Motor

A brushless DC motor is the central component of the friction drive module, which generates a torque required for controlling the position of the magnetic bougie. At the beginning of this project, I got a brushless DC motor and a driver board from Phillip Nadeau, who was a member of the previous MIT undergraduate team for esophageal atresia project. The motor is manufactured by Maxon Motor (EC-max 16 #283828), which has a gearhead (GP 16A #110323) and an encoder (MR #201940) integrated together. Some of the specifications are listed in Table 4.2 and Table 4.3. I checked whether the specifications of the motor and the geargead meet the design requirement for the friction drive. I especially focused on two specifications: the maximum torque load of the gearhead and the maximum torque load of the motor.

The force between two permanent magnets is calculated as a function of the gap size with FEMM software as shown in Figure 4-9. It turned out that the maximum force that motor gearhead must withstand is about 30N, which occurs when the two magnets are put together and the motor needs to pull them apart. For a given force load, the amount of the torqe load increases proportional to the radius of the driving

wheel ($\tau = F \times r$). The radius of the driving wheel is designed such that the maximum torqe load does not exceed the maximum torque that the gearhead can withstand, which is 300 mNm for an intermittent load. The actual driving wheel is designed to have 15mm diameter considering a safety margin, so that the maximum torque load becomes 225 mNm.

The gearhead has a reduction of 84:1, so that the maximum torque that motor should withstand is scaled down from 225 Nm to 2.68 mNm. According to the motor datasheet, the motor generates a nominal torque of 3.24 mNm and a stall torque of 5.95 mNm. Thus, it turned out that the motor and the gearhead that I got from the previous team satisfies the specifications if I design a driving wheel of 15 mm radius.

An off-the-shelf motor driver, Maxon EPOS2, is used to control the rotational position of the brushless DC motor. A PID control algorithm, whose gains are auto-tuned, is implemented on top of a current control loop. The board communicates with a host PC via an USB cable to get a position command.

4.2.2 Driving Wheel

The driving wheel converts a torque generated from the DC motor to a translational force to move the catheter. It consists of a sand paper sleeve, a rubber drum, and an aluminum shaft, whose one end has a three jaw collet for connection to the motor shaft, as shown in Figure 4-11. A sandpaper sleeve, which is originally manufactured to be used with Dremel Tool™, is put on the driving wheel to increase the friction coefficient. The random asperity pattern of the sand paper can also prevent the catheter from a drift; the transient pattern imprinted on the catheter by the sandpaper helps the catheter moves in such a way that the autocorrelation function between the two patterns is maximized. For the design procedure, the friction coefficient was assumed to be larger than 1 ($\mu \geq 1$). A rubber drum is used as a central component to assemble the driving wheel parts. As compressed in the axial direction, the rubber drum deforms and bulges out radially to apply a normal force on the inner wall of the sandpaper sleeve to fasten it (See Figure 4-11). The rubber drum also expands inward to grab the aluminum shaft. The compression force of the rubber drum is

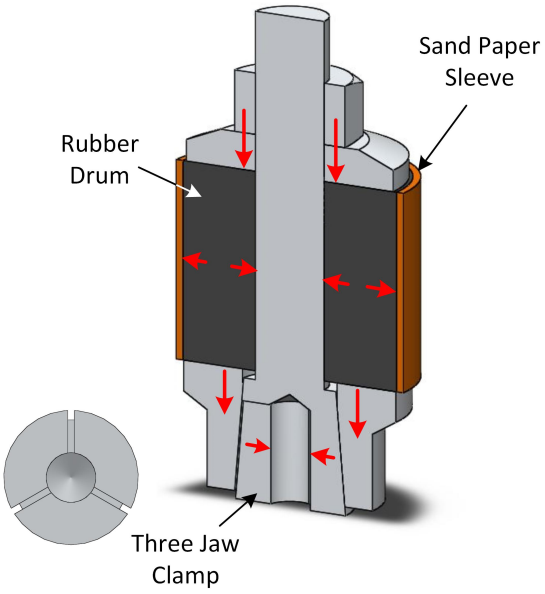

Figure 4-11: Cross sectional view of the driving wheel. The red arrows denote a compressive force flow through the rubber drum to the motor shaft.

also transfered to the wedge of the three jaw collet at the end of the shaft, thereby increasing the clamping force between the collet and the motor shaft. The aluminum shaft is originally manufactured for a propeller adapter in RC airplanes, which I purchased from Hyperion[3] (See Figure 4-12). The idea of using a rubber drum for the assembly is inspired from the mechanism of Dremel Tool™, and enabled to attach the friction sleeve to the motor shaft with a small number of parts.

Attaching a wheel to a DC motor sounds like a straightforward task, but one needs to think carefully if the connection requires precision and robustness. There are several typical ways for motor shaft coupling: set-screw, interference fit, and collet. Using a set-screw is handy, but in general it is a bad idea because the set-screw can concentrate stress at a small portion of the part. Interference fit is usually recommended for coupling, but it is not appropriate for prototyping where parts need to be taken apart several times. Using a collet is a good compromise between ease of disassemble and robustness, but it increases the length of moment arm, thereby increasing the radial load that the motor gearhead should withstand.

[3]http://www.hyperion-world.com/products/

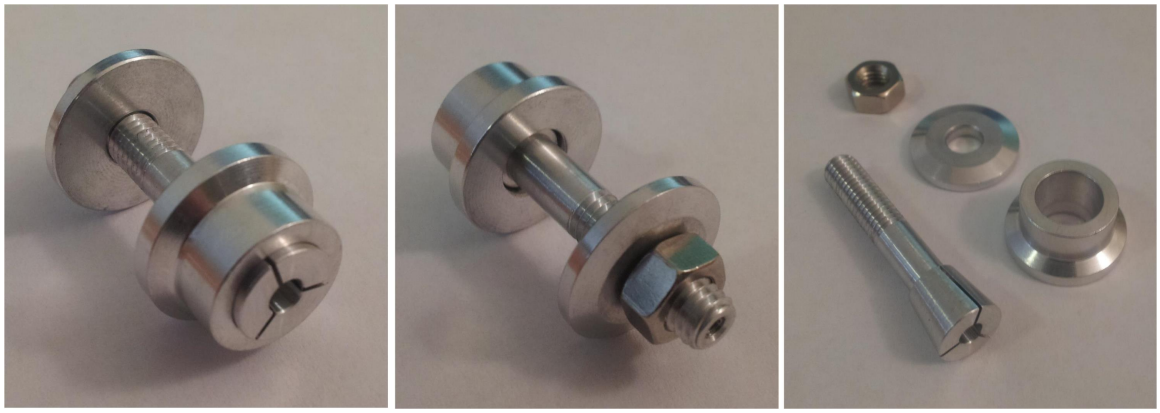

Figure 4-12: A propeller adapter manufactured by Hyperion, which is used as a shaft for the driving wheel.

4.2.3 Idler Wheel

The idler assembly consists of an idler wheel, a choulder screw, a flanged-sleeve bearing, and a spacer as shown in Figure 4-13. It sets the amount of normal force between the catheter and the driving wheel so that the driving wheel can generate sufficient friction force to move the catheter. Two preloaded compression springs push the slider frame down (See Figure 4-15) so that the idler wheel and the driving wheel squeeze the catheter. The idler wheel has a V-groove, which constrains the catheter tube in the lateral direction. A plane bearing is inserted on the axle for the idler wheel to reduce the sliding friction.

The concept of a contact patch was taken into account in designing the friction drive. Due to the finite stiffness, a material driven by a friction drive contacts with wheels on a finite area rather than at a point or on a line, which is called a contact patch. In our design of the friction drive, the catheter contacts with the driving wheel on one contact patch, and with the V-grooved idler on two contact patches as shown in Figure 4-14. If the material velocity on the contact patch is not uniform, it can generate differential velocity at the material contact patch, which twists the surface of the driven material on the contact patch. This local twist can rub the surface of the material to result in plastic deformation or damage. To avoid this phenomenon, the driving wheel is designed as a flat roller to generate relatively uniform material velocity on the contact patch. The idler wheel, however, is designed as a V-grooved

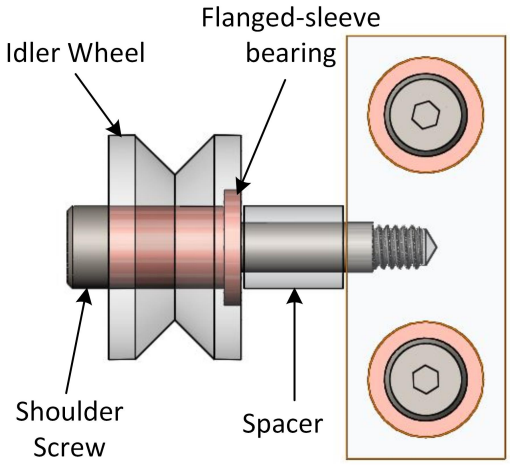

Figure 4-13: Top view of the idler wheel.

wheel so that the catheter can be constrained in the lateral direction. The V-grooved wheel generates non-uniform material velocity on the contact patch as shown in Figure 4-14. To avoid unnecessary surface rubbing, the idler wheel is made of Delrin®, which has a relatively low friction coefficient, so that the catheter can easily slip on the contact patch.

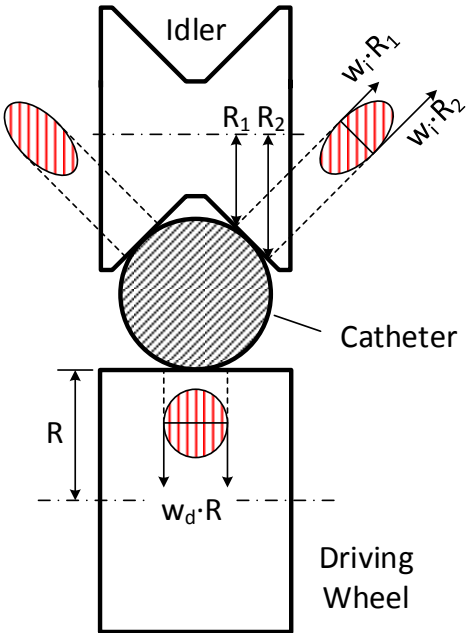

Figure 4-14: Contact patches on the catheter surface.

The compression springs are designed such that they provide sufficient normal force for the driving wheel, with the radial load to the motor gearhead not exceeding the maximum value that the motor gearhead can withstand continuously. According to the datasheet, the maximum admissible radial load for the gearhead is 16 N at 6 mm from the flange (36 mNm). Since the actual length of the moment arm is about 15 mm as shown in Figure 4-15, the load that the gearhead should withstand for a continuous operation is calculated to be 6.4 N. I inserted two compression springs whose spring constant was 0.54 N/m, which is relatively compliant so that the force variation due to the change of the catheter diameter would be as small as possible. The springs were compressed by about 5.5 mm to set the preload about 6 N.

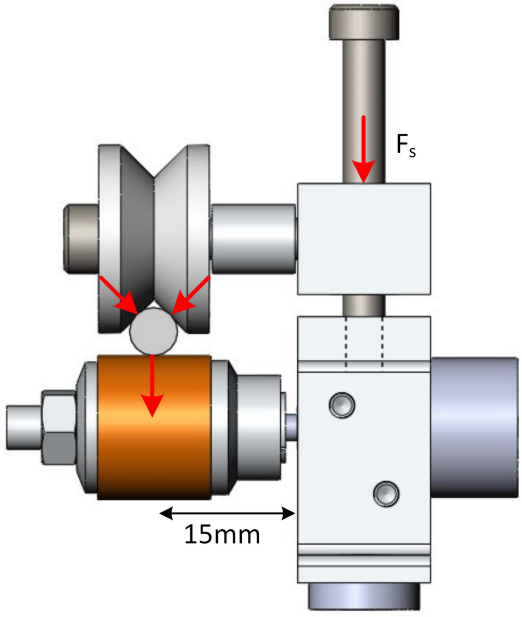

Figure 4-15: The force flow from the compression spring to the driving wheel.

During the bougienage test we found that the catheter gradually slips on the friction drive if more than about 3 N force is applied, which is not consistent with the design specification. This is because the surface of the catheter is rubbed off, or yields, due to the stress concentration on the contact patch. The experimental result is discussed in more detail in Section 6.2.1.

4.3 Summary

In this chapter, we discussed the design details of modules and components for the hydraulically controlled magnetic bougie. Specifically, we covered the design details of the magnetic bougie module and friction drive module, and also explained how they were fabricated for the prototype. In the next chapter, we integrate the modules on a test bench and design a control architecture for the test.

Chapter 5

System Integration and Control

This chapter describes how the modules and the components designed in the previous chapters are integrated to build a test bench as shown in Figure 5-1. This chapter also discusses how the control architecture is designed and implemented for the test bench to demonstrate the magnetic bougienage for esophageal atresia.

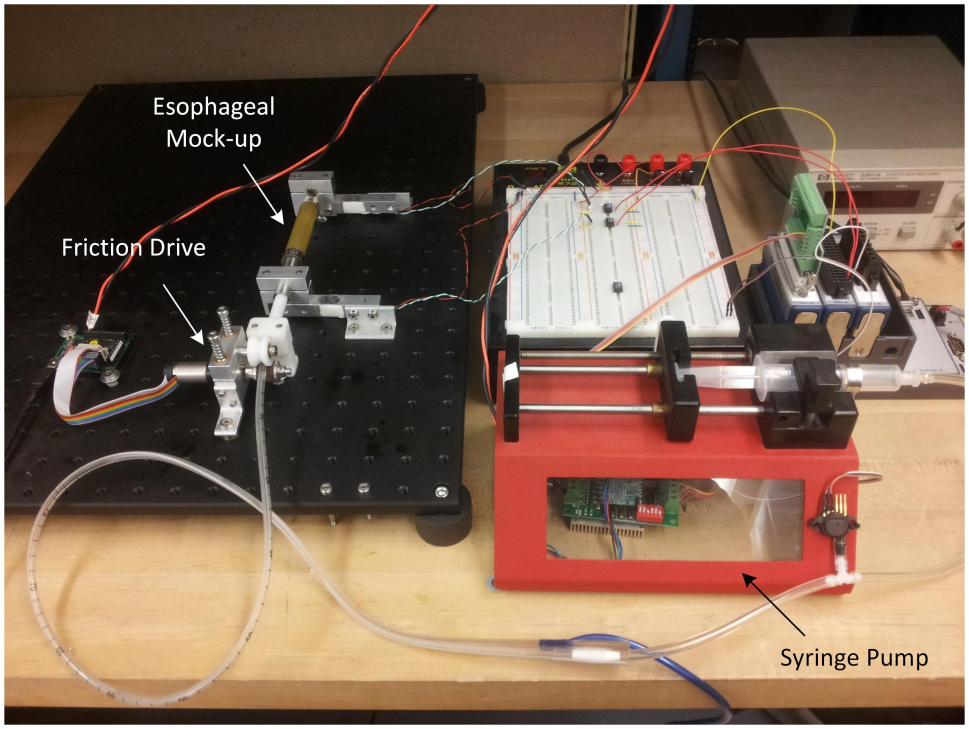

Figure 5-1: Overview of the bench setup.

5.1 Test Bench Setup

The test bench is built on an aluminum optical breadboard as shown in Figure 5-1. A mock-up of the proximal esophageal pouch is fabricated and mounted on the test bench, which is explained more in Section 5.1.1. The friction drive designed in Section 4.2 is built and placed on the test bench to feed the catheter, thereby advancing the magnetic bougie into the esophageal mock-up. Section 5.1.2 explains how the friction drive is integrated in the test bench in detail. A syringe pump is placed next to the optical breadboard and connected to the catheter to inject water into the magnetic bougie. The syringe pump integration is further discussed in Section 5.1.3.

5.1.1 Esophageal Mock-up

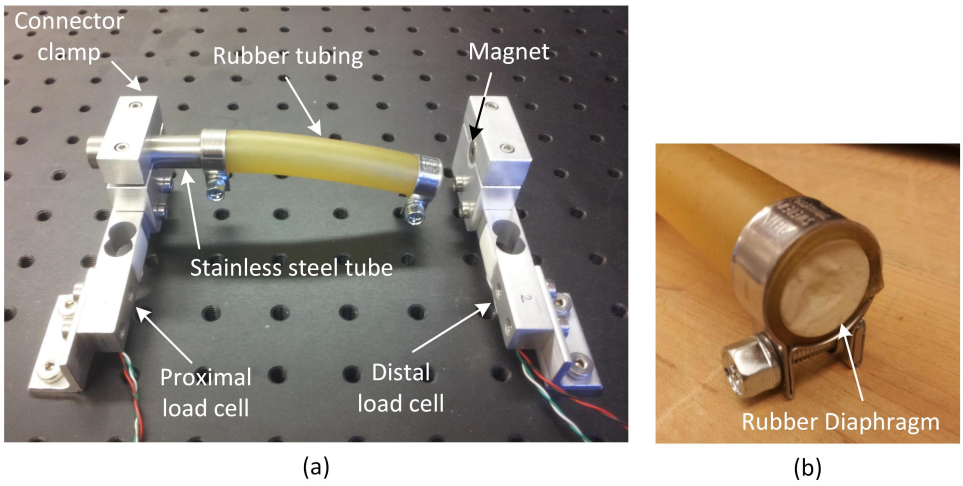

Figure 5-2: A mock-up of an esophageal pouch: (a) overview and (b) the end closing.

A mock-up of the esophageal pouch is made of a surgical rubber tubing whose inner diameter is 12.7 mm (0.5 inch), the outer diameter is 15.88 mm (0.625 inch), and the thickness is 1.59 mm (0.063 inch). The rubber tubing is cut at the length of about 90 mm. One end of the rubber tubing is closed with a rubber diaphragm as shown in Figure 5-2 (b) to emulate the proximal esophageal pouch. The rubber diaphragm is used to increase the overall compliance of the esophageal mock-up because the surgical rubber tubing is considered to be stiffer than the actual esophagus. The

other end of the surgical rubber tubing is connected to a stainless steel tube via a tube clamp, where the stainless steel tube has the outer diameter of 12.7 mm (0.5 inch) and the inner diameter of 11.68 mm (0.46 inch).

Two load cells are set up on the optical breadboard as shown in Figure 5-2 (a). The esophageal mock-up is mounted on the proximal load cell via a connector clamp machined out of aluminum. The connector clamp fastens the stainless steel tube of the mock-up such that the proximal load cell measures the tensile force of the esophageal mock-up. The distal load cell does not mount a mock-up of the distal esophageal pouch. We simply clamped a permanent magnet to the distal load cell such that the magnetic bougie in the surgical rubber tubing experiences a magnetic force.

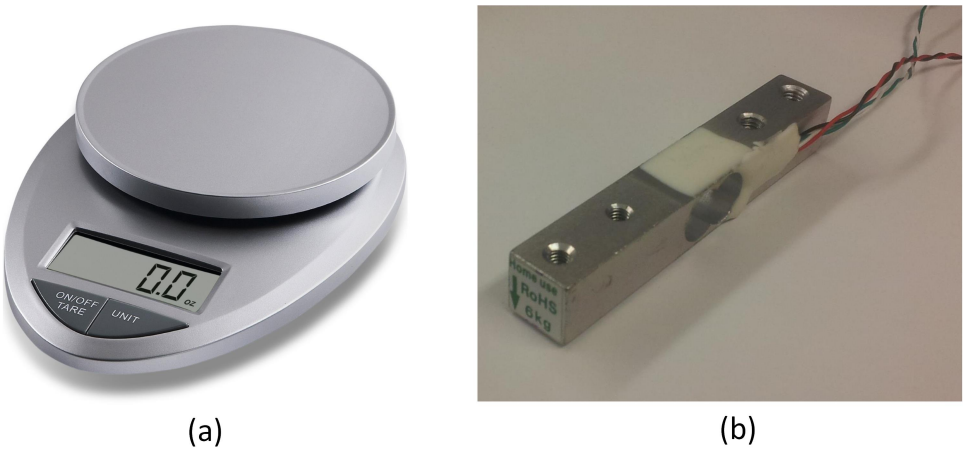

Figure 5-3: (a) A kitchen scale purchased from EatSmart and (b) a bending beam load cell taken from the kitchen scale.

We purchased kitchen scales manufactured from EatSmart[1] as shown in Figure 5-3 (a) and took the load cells from them (See Figure 5-3 (b)) because it was cheaper than purchasing load cells only. The load cells are bending beam and strain gauge type made of aluminum. The load cell has a through hole in the middle to have two thin walls around the hole. A full-bridge strain gauge based on Wheatstone bridge circuit is attached on the thin wall of the load cell under the protective white silicone rubber seen in the figure. We applied 5 V across the red and the black leads, and

[1]http://www.eatsmartproducts.com/

the voltage difference between the white and the green leads is amplified via an INA 128 instrumentation amplifier manufactured from Texas Instruments. The circuit schematic for the load cell and the amplifier is shown in Figure 5-4.

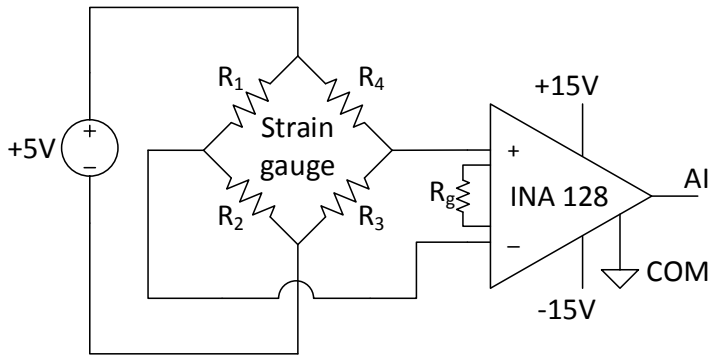

Figure 5-4: An instrumentation amplifier circuit for a load cell. The amplifier gain is set to 5000 with $R_g = 10\ \Omega$.

The outputs from the instrumentation amplifiers are transmitted to an NI 9205 analog input module manufactured by National Instrument to be processed by the CompactRIO 9076 real-time target manufactured by the same company. The control architecture is discussed in detail in Section 5.2. The load cell measures the tensile force of the esophageal mock-up.

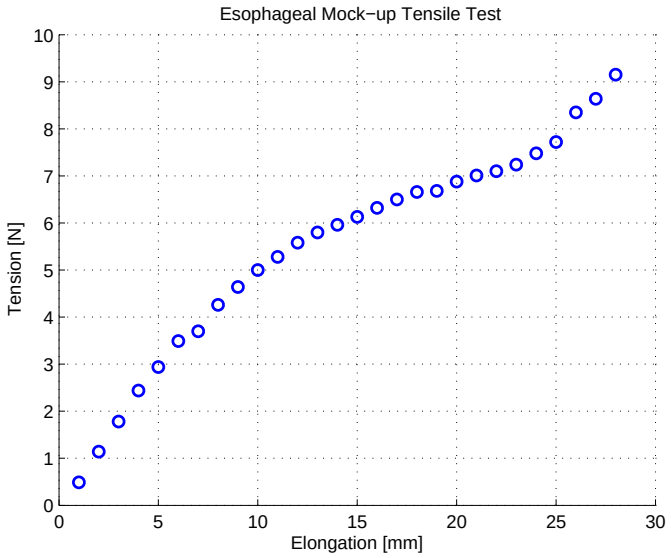

Figure 5-5: Measured esophageal mock-up tension-elongation curve.

As shown in Figure 5-5, the tensile force of the esophageal mock-up is measured

as a function of its elongation. The experimental result shows that the stiffness of the mock-up is not constant, rather the tension-elongation graph shows an S-shape curve. Although we have not proved any mechanical similarities between the real esophagus and the mock-up, we perform bougienage tests on this mock-up to demonstrate the performance of the bougie. The experimental result is discussed in Chapter 6.

5.1.2 Friction Drive

The friction drive designed in Section 4.2 is fabricated out of aluminum and mounted on the optical breadboard as shown in Figure 5-6 (a). Also, the magnetic bougie designed in Section 4.1 is integrated with the friction drive as the catheter engages the driving wheel of the friction drive. By controlling the position of the driving wheel, which is discussed in detail in Section 5.2.1, we can feed the catheter and thereby drive the magnetic bougie by commanded displacement.

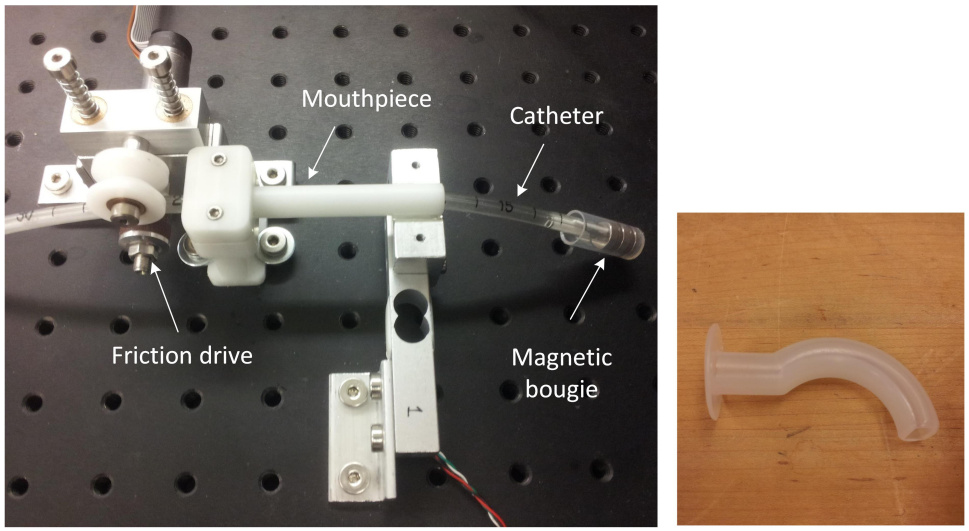

Figure 5-6: (a) An overview of the friction drive integration and (b) a sample mouthpiece.

A mouthpiece is placed near the friction drive to support the catheter in the lateral direction. Instead of using the real mouthpiece shown in Figure 5-6 (b)[2], we fabricated a straight mouthpiece simulation out of Delrin® tube for the test bench as

[2]Courtesy of Dr. David Mooney in Boston Children's Hospital

shown in Figure 5-6 (a) because the sample mouthpiece had a too-narrow channel and a sharp turn, which generated too much friction to move the catheter. This friction and geometry remains a significant issue to be resolved in future work. In Figure 5-6 (a), the esophageal mock-up is dismounted from the load cell to show how the mouthpiece supports the catheter. Note that the mouthpiece does not contact the stainless steel tube which supports the esophageal mock-up tubing (See Figure 5-7).

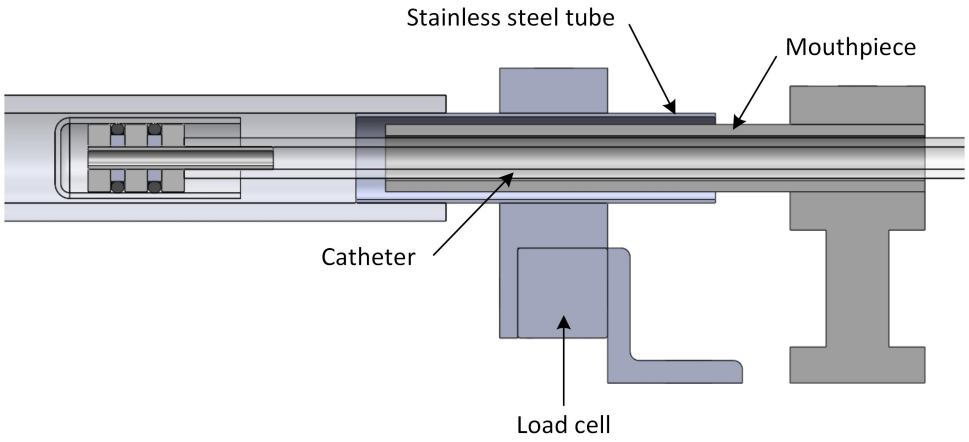

Figure 5-7: A cross-sectional view of the esophageal mock-up and mouthpiece. Note that the mouthpiece does not contact the stainless steel tube which supports the esophageal mock-up tubing.

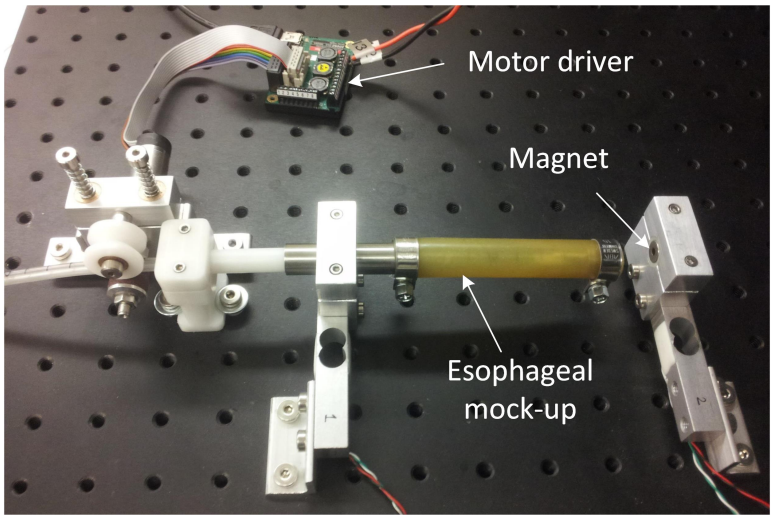

Figure 5-8: An overview of the test setup for the magnetic bougienage.

In Figure 5-8, the mock-up of the esophageal pouch is mounted on the load cell. Not visible in the figure is the magnetic bougie which is inserted into the esophageal mock-up to apply stretching force. This force includes both pushing and magnetic forces which are measured by the proximal load cell. The magnetic bougie interacts with the other magnet mounted on the distal load cell. Due to the magnetic force, the magnetic bougie in the esophageal mock-up is pulled to the right, and therefore the mock-up is straightened and lifted up compared to the one in Figure 5-2 (a) in which the rubber tubing is bent down due to the gravitational force.

5.1.3 Syringe Pump

A syringe pump is integrated in the test bench as shown in Figure 5-9 (a). The pump pushes water into the catheter to modulate the tip displacement of the magnetic bougie hydraulically. A syringe is mounted on the pump, whose barrel is fixed to the chassis and the plunger is driven by a lead screw. A stepper motor, mounted inside the chassis as shown in Figure 5-9 (b), engages a timing belt to transmit power to the lead screw. As the stepper motor rotates by a commanded profile, it drives the lead screw and pushes the plunger of the syringe to inject water.

The outlet of the syringe barrel is connected to a polyurethane tubing via a barbed Luer connector, and the polyurethane tubing is connected to the catheter via interference fitting, in which a PTFE (Polytetrafluoroethylene) thread seal tape is employed for sealing. This joint can be seen in the lower left of the photo. In the middle of the polyurethane tubing is placed a Tee connector to branch out the tubing to connect to a pressure sensor. We use a silicon piezoresistive pressure sensor (MPX2200AP) manufactured by Freescale Semiconductor. The pressure sensor measures hydrostatic pressure in the polyurethane tubing, which approaches the pressure inside the magnetic bougie when the flow rate in the lumen is low enough. The tip force of the magnetic bougie can be estimated from the pressure measurement, which is compared with the load cell measurement in Chapter 6. The voltage output from the pressure sensor is transmitted to the NI 9205 analog input module, manufactured by National Instruments, to be processed by the CompactRIO 9076 real-time target,

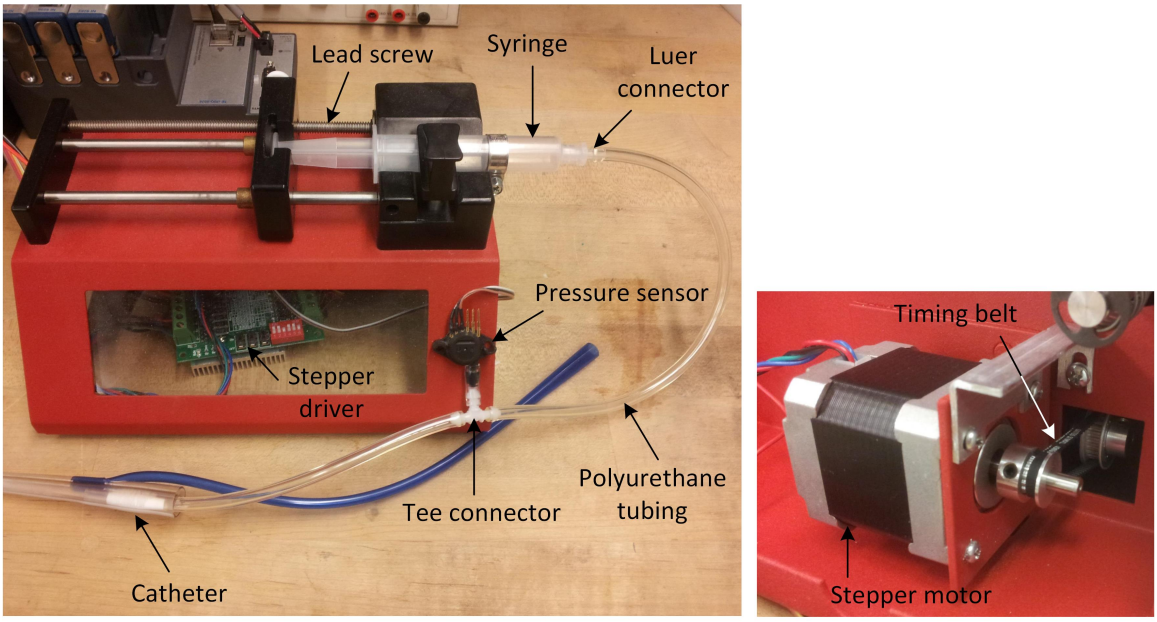

Figure 5-9: Syringe pump: (a) an overview and (b) stepper motor inside the chassis.

manufactured by the same company.

5.2 Control Design

The control architecture for the magnetic bougienage system is shown in Figure 5-10. Functional units are represented as white blocks, while physical modules, in which the functional units are integrated, are represented as blue rectangles. The yellow arrows represent information flows between the functional units.

A CompactRIO real-time target, manufactured by National Instruments, is employed as the hub of the control system, in which the LabVIEW graphical programming language is used to implement the control algorithm and the software user interface. The target has a 400 MHz industrial real-time processor and FPGA (Field Programmable Gate Array) embedded in the chassis. As shown in Figure 5-11, the target has four slots for different types of input and output modules to be inserted. We mounted one digital input/output module (NI 9403) and one analog input module (NI 9205). The analog input module is used to read analog signals from the pressure

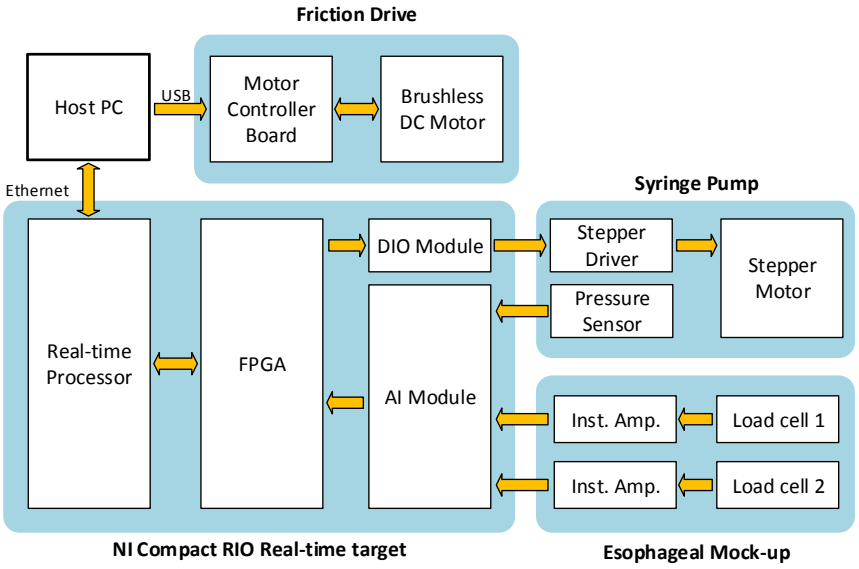

Figure 5-10: Control architecture for the magnetic bougienage system.

sensor and the two load cells. The digital input/output module is used to transmit the control signal to the stepper motor driver. The stepper motor control is discussed in Section 5.2.2 in detail.

Figure 5-11: CompactRIO real-time target manufactured by National Instuments.

The host PC communicates with the CompactRIO target via an Ethernet cable. The PC provides an interface for users to program the target. The host PC also communicates with the EPOS2 brushless DC motor controller board, manufactured by Maxon Motor, via a USB cable. The brushless DC motor control is discussed in Section 5.2.1 in detail.

5.2.1 Brushless DC Motor Control

The EPOS2 Positioning Controller shown in Figure 5-12 (b), a controller board manufactured by Maxon Motor[3], is employed to control the position of the brushless DC motor of the friction drive. The motor is mounted on the friction drive and connected to the controller board via two bus cables as shown in Figure 5-12. The gray bus cable transmits the encoder output to the controller board and the color cable transmits the motor coil currents from the board to the motor.

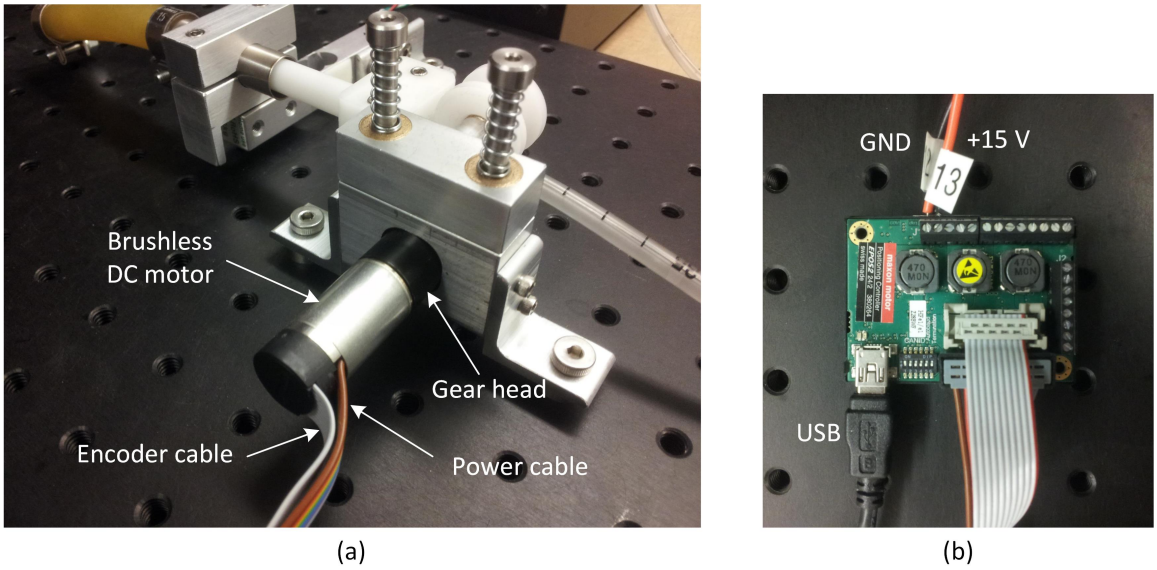

Figure 5-12: (a) A brushless DC motor mounted in the friction drive and (b) the EPOS2 controller board for the motor.

The controller board contains a switched-mode power supply, an electronic commutation circuit, and a microprocessor in which a feedback control algorithm is implemented. The parameters of the feedback controller can be tuned with EPOS Studio, an application software provided by the same company, either in a manual mode or in an auto-tuning mode. Instead of designing the feedback controller by myself, I used the auto-tuning function to set the parameters of the position controller.

Figure 5-13 is a block diagram for the position control of the brushless DC motor. The controller board has a feedback controller implemented, in which the current loop is closed with a PI controller and the position loop is closed with a PID controller and

[3]http://www.maxonmotorusa.com/maxon/view/content/products

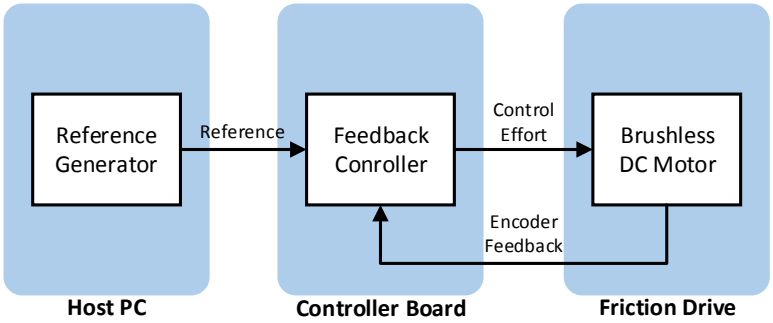

Figure 5-13: Brushless DC motor position control architecture.

the encoder feedback. The gain parameters of the feedback controller is auto-tuned with EPOS Studio software. The host PC generates a reference profile and transmits it to the controller board via a USB cable. The software interface is programmed in the host PC using LabVIEW.

5.2.2 Stepper Motor Control

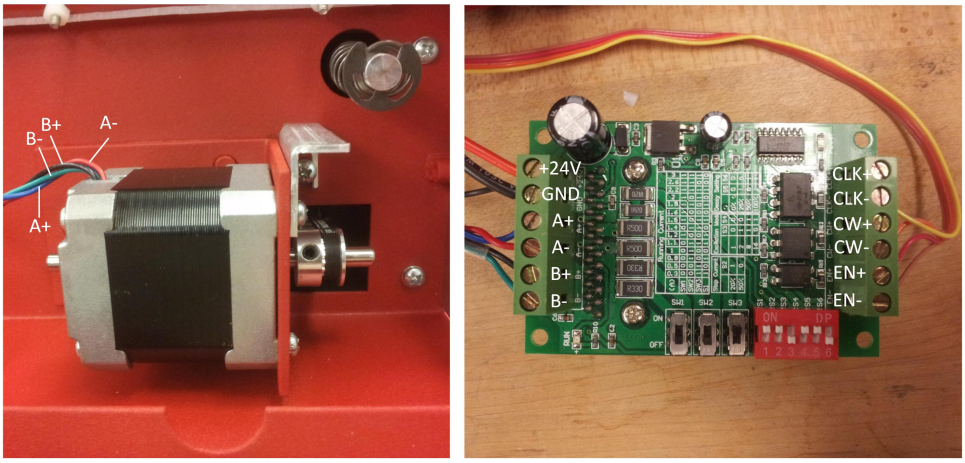

Figure 5-14: (a) Stepper motor in the syringe pump and (b) the driver board for the stepper motor.

The TB6560 Stepper Motor Driver shown in Figure 5-14 (b). It is manufactured by Toshiba, and is employed to drive the stepper motor of the syringe pump. The board has four output terminals, A+, A-, B+, and B-, which are connected to the stepper motor mounted on the chassis of the syringe pump as shown in Figure 5-14

(a). The driver board generates control effort and transmits it to the stepper motor through these output terminals. The board has six input terminals, CLK+, CLK-, CW+, CW-, EN+, and EN-, which are connected to the digital output module of the CompactRIO target. The EN+/EN- terminal pair enables and disables the board and the CW+/CW- terminal pair determines the rotational direction of the stepper motor. When the CLK+/CLK- pair receives a square pulse signal, the driver board generates a change of state in the coild drives such that the stepper motor rotates by one micro step.

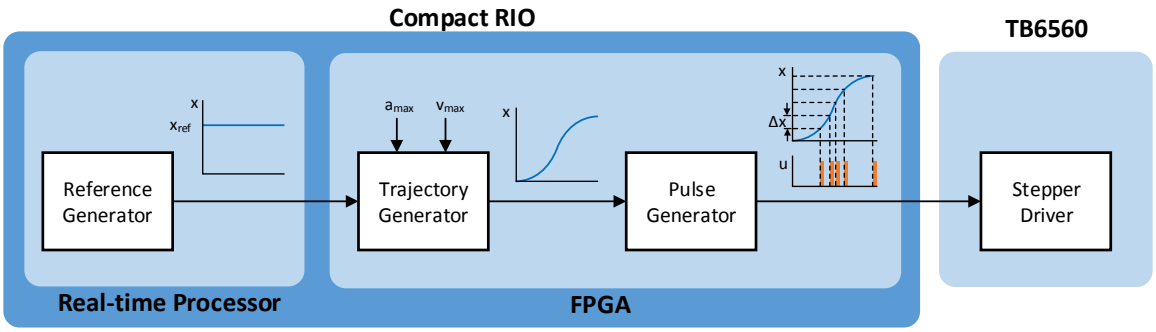

Figure 5-15: Stepper motor controller architecture.

The stepper driver board controls the stepper motor in open-loop. That is, we control the rotation of the stepper motor by transmitting a train of square pulses to the CLK+/CLK- terminal pairs of the stepper driver. The amount of the rotation, or the number of micro steps, of the stepper motor is determined by the number of square pulses transmitted to the stepper driver. Due to the limited torque, the stepper motor could slip some steps if the commanded trajectory requires too high velocity (pulse/sec) or acceleration (pulse/sec^2). To prevent the stepper motor from missing any steps, we implemented a trajectory generator and a pulse generator in FPGA as shown in Figure 5-15, which is discussed in detail in the rest of this section.

Trajectory Generator

The trajectory generator is designed to generate a trapezoidal velocity profile, in which the velocity and the acceleration are bounded. An example of such a trajectory is shown in Figure 5-16. To move toward the reference position, x_{ref}, the trajectory

first speeds up with the maximum acceleration, a_{max}, until it reaches the maximum velocity, v_{max}. Then, it keeps the velocity constant for a while and slows down with the maximum deceleration, $-a_{max}$, to reach the reference position with zero velocity.

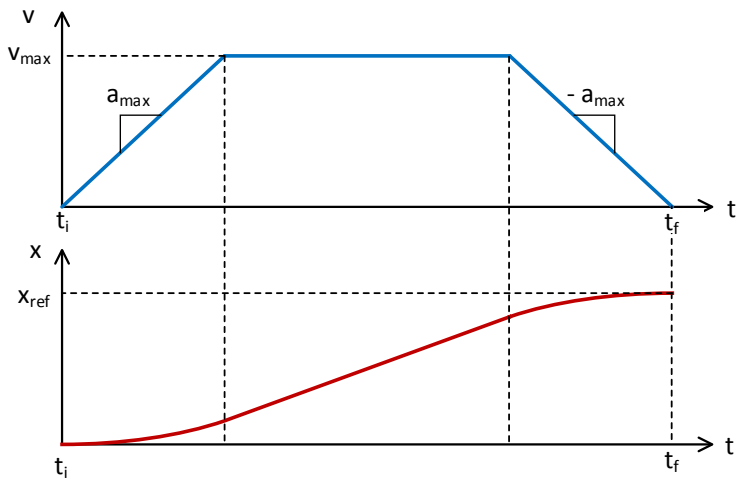

Figure 5-16: A trapezoidal velocity profile and the associate position profile.

The example trajectory in Figure 5-16 starts from zero initial velocity, $v(t_i) = 0$. However, in some cases, e.g. changing the reference position while the stepper motor is running, we need to generate a new trajectory from a non zero initial velocity. To facilitate designing such a trajectory generator, we perform a state space analysis as shown in Figure 5-17.

Let us define a state vector $\mathbf{x} = (x_1, x_2)$ such that

$$\begin{pmatrix} x_1 \\ x_2 \end{pmatrix} = \begin{pmatrix} x(t) - x_{ref} \\ v(t) \end{pmatrix},$$

where x_{ref} is the motor angular reference position, $x(t)$ is the motor angular position, and $v(t)$ is the motor angular velocity of the trajectory. The velocity limit of the trajectory bounds the state x_2 such that

$$-v_{max} \leq x_2 \leq v_{max}. \tag{5.1}$$

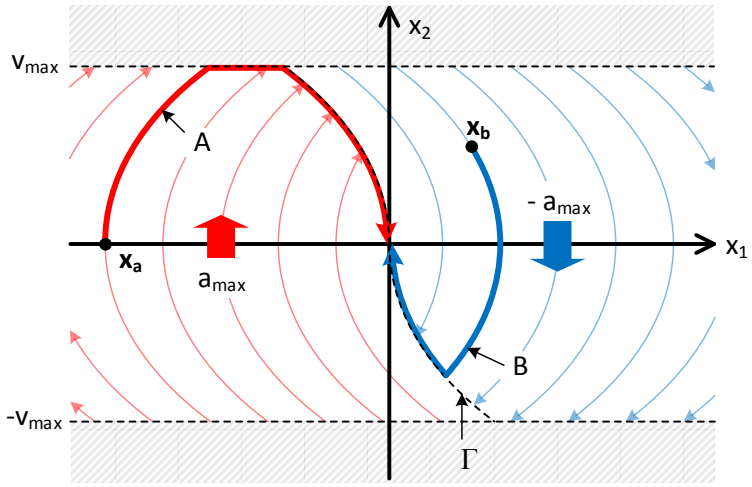

Figure 5-17: A phase plot for the design of a trapezoidal motor angular position trajectory generator. Variables x_1 and x_2 are position error and angular velocity, respectively. Red curve (A) shows a trajectory with initial position error x_a and initial velocity $x_2 = 0$. Blue curve (B) shows a more general initial condition.

The acceleration limit constrains the state $\mathbf{x} = (x_1, x_2)$ to transit along a parabola

$$x_1 = \frac{1}{2}\frac{x_2^2}{\pm a_{max}} + C_1, \tag{5.2}$$

where the sign of a_{max} depends on whether the trajectory accelerates or decelerates, and C_1 is determined such that the parabola passes through the current state.

Now, we design an algorithm to generate a trajectory such that the state $\mathbf{x} = (x_1, x_2)$ departs from any initial value and converges to the origin while satisfying (5.1) and (5.2). First, let us define a curve

$$\Gamma : x_1 + \frac{1}{2}\frac{x_2^2}{\text{sign}(x_2)\, a_{max}} = 0, \tag{5.3}$$

which passes through the origin and divides the domain into two areas as shown in Figure 5-17. Next, we assign positive acceleration to the state on the left of Γ, negative acceleration to the state on the right of Γ, and zero acceleration to the state on the velocity limits. In other words,

- If the current state is on the left of Γ, then we assign positive acceleration to

the trajectory, or $a = a_{max}$. If the current state is on the right of Γ, then we assign negative acceleration to the trajectory decelerates, or $a = -a_{max}$.

- If the current state is on the velocity limits, or $x_2 = \pm v_{max}$, then we assign zero acceleration to the trajectory, or $a = 0$

Here are two examples to show how the algorithm works.

Example 1

The phase plot A in Figure 5-17 departs from the initial state $\mathbf{x_a}$, which has zero initial velocity and is to the left of Γ. At the beginning, the state transits upward along the associated parabola due to the positive acceleration. After it reaches the upper velocity boundary $x_2 = v_{max}$, the state transits to the right horizontally due to the zero acceleration. As soon as it passes across the curve Γ, the state transits downward along the associated parabola due to the negative acceleration condition. Finally, it converges into the origin.

Example 2

The phase plot B in Figure 5-17 departs from the initial state $\mathbf{x_b}$, which has non-zero initial velocity. At the beginning, the state transits downward along the associated parabola due to the negative acceleration. As soon as it intersects the curve Γ, the state transits upward along the associated parabola due to the positive acceleration. Finally, it converges into the origin.

Algorithm 5.1 is programmed using MATLAB for a simulation ($dt = 0.001$ sec, a_{max}=100 pulse/sec^2, v_{max}=100 pulse/sec).

Algorithm 5.1 Trapezoidal trajectory generator

$$f(x_2) \equiv -\frac{1}{2}\frac{x_2^2}{\text{sign}(x_2)a_{max}}$$

loop
  if $x_1 < f(x_2)$ **then**
    if $x_2 < v_{max}$ **then**
      $a \leftarrow a_{max}$
    else
      $a \leftarrow 0$
    end if
  else
    if $x_2 > -v_{max}$ **then**
      $a \leftarrow -a_{max}$
    else
      $a \leftarrow 0$
    end if
  end if
  $x_2 \leftarrow x_2 + a\,dt$
  $x_1 \leftarrow x_1 + x_2\,dt$
  return $\{x_1, x_2\}$
end loop

The simulation result for Example 1 (Trajectory A) with the initial state $\mathbf{x_a} = (0, -200)$ is shown in Figure 5-18. In this simulation, velocity is in units of pulse/sec, and position is in units of pulse.

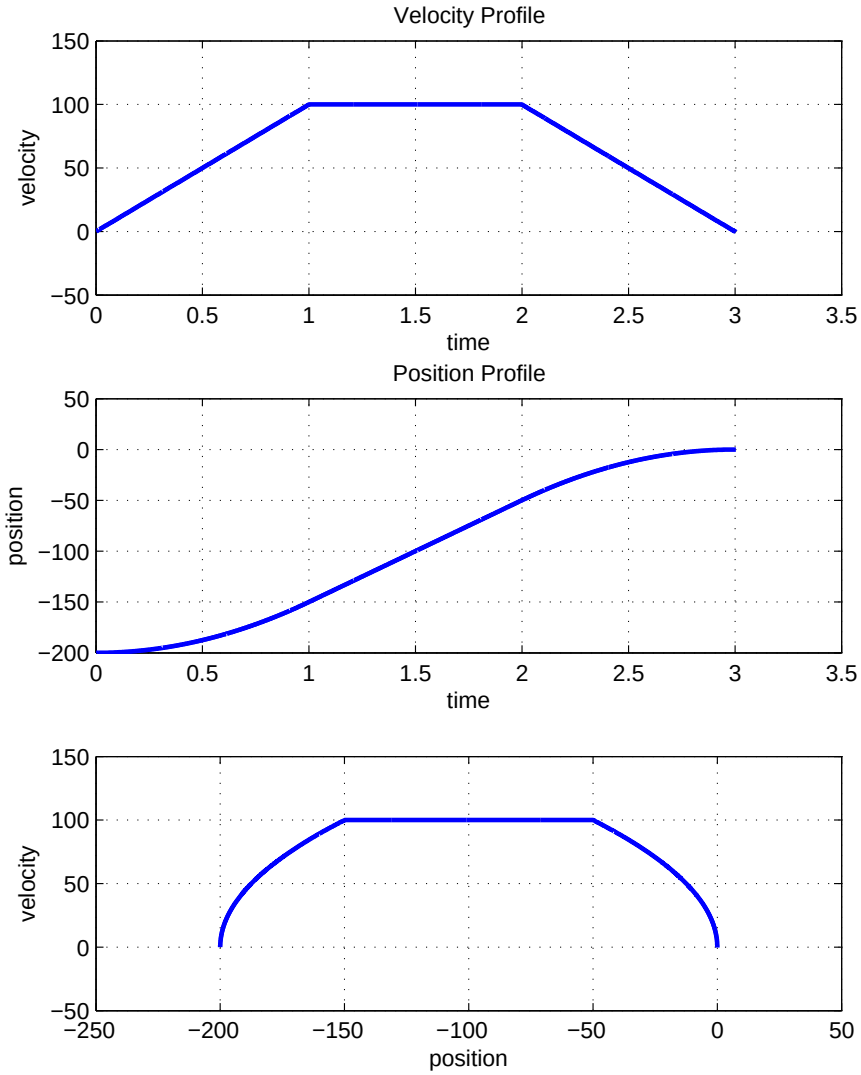

Figure 5-18: Example 1 with $\mathbf{x_a} = (0, -200)$. Velocity is in units of pulse/sec. Position is in units of pulse.

The simulation result for Example 2 (Trajectory B) with the initial state $\mathbf{x_b} = (50, 50)$ is shown in Figure 5-19.

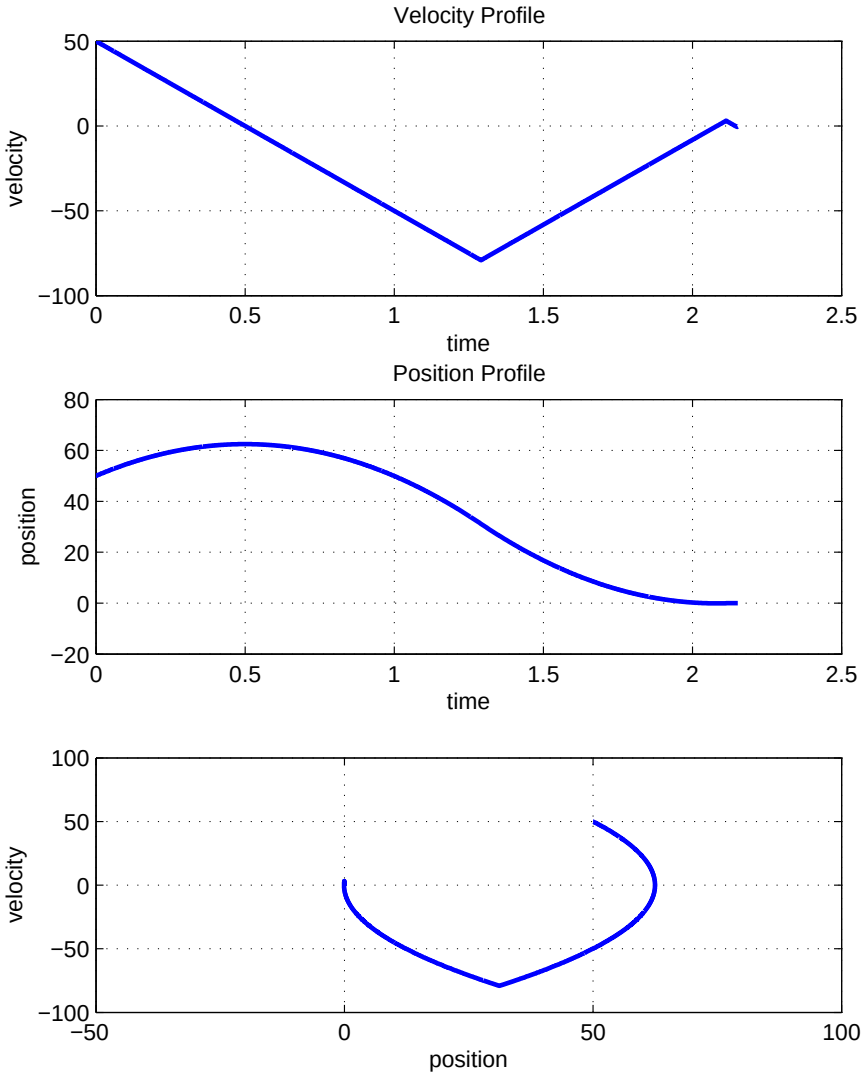

Figure 5-19: Example 2 with $\mathbf{x_b} = (50, 50)$. Velocity is in units of pulse/sec. Position is in units of pulse.

There is a small oscillation at the end of the trajectory due to numerical drift given the finite sampling time. The amount of the residual oscillation reduces as the loop time decreases. The same algorithm is implemented on FGPA using LabVIEW ($dt = 5$ µs, $a_{max} = 20000$ pulse/sec^2, $v_{max} = 37000$ pulse/sec). This smaller step size

effectively eliminates numeric drift.

Pulse Generator

A pulse generator quantizes the position profile generated from the trajectory generator and outputs a square pulse when it detects an incremental change in position. The pulse generator also outputs a *true* or *false* signal depending on whether the incremental change is positive or negative so that the stepper driver can determine the rotational direction. We implemented such a pulse generator on the FPGA using LabVIEW as shown in Figure 5-20.

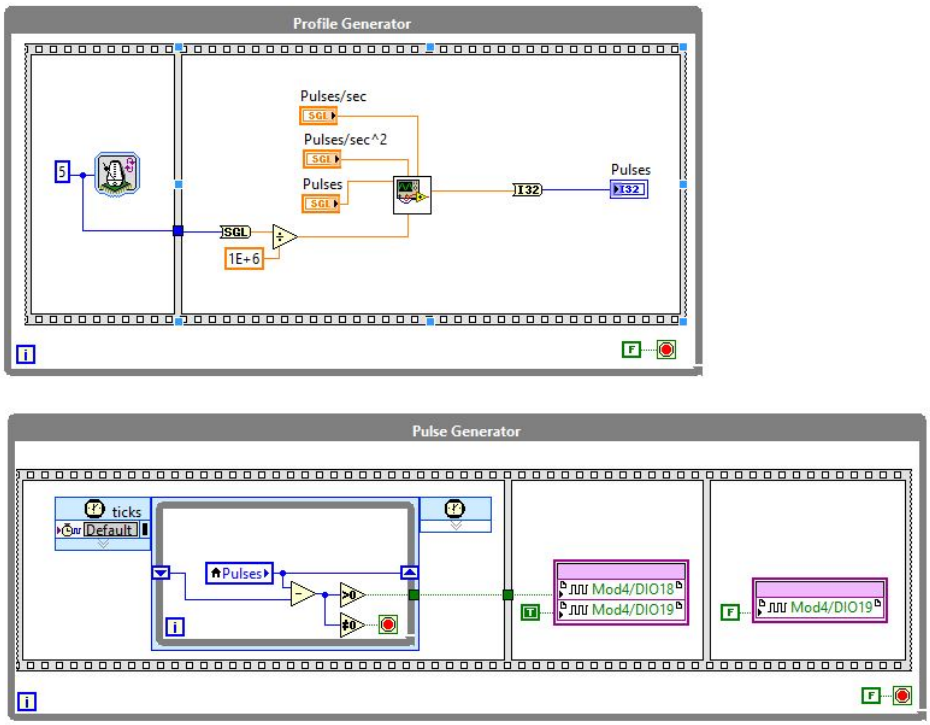

Figure 5-20: Pulse generator implementation using LabVIEW.

The pulse generator can output a square pulse every 27 µs as a maximum rate (37000 pulse/sec), which is determined by the speed of the digital output module (NI 9403). This corresponds to a motor rotation rate of 72.65 rad/s if the stepper driver is set to 1/16 micro-stepping mode, which is fast enough for our application.

5.3 Summary

In this chapter, we discussed how the test bench is built and the control architecture is designed and implemented for the hydraulically controlled magnetic bougie. An esophageal mock-up is fabricated, and the friction drive, magnetic bougie, and the syringe pump are integrated with the mock-up for the experimental bougienage test. In the next chapter, we perform experiments on the test bench to show how the bougie can apply a controllable stretching force to the esophageal mock-up, and how the bougie can measure the mock-up stretching force in a reliable manner.

Chapter 6

Experimental Results

This chapter shows experimental results to demonstrate the hydraulically controlled magnetic bougienage system designed and built in the previous chapters. Specifically, we demonstrate that the bougie can reliably measure the stretching force of the esophageal mock-up, and 2) the bougie can apply a stretching force to the esophageal mock-up by a desired amount.

Section 6.1 discusses the effect of O-ring friction, and introduces *dither* to compensate the friction. Section 6.2 shows the results of the bougienage test. Section 6.3 introduces an alternative bougie design using a ferrofluid seal, and shows some preliminary test results to show pros and cons of the ferrofluid seal.

6.1 O-ring Friction

The friction of the O-rings makes it difficult for the bougie to measure the bougienage force accurately. If the friction force is much smaller than the nominal bougienage force, which is about 3-4 N as discussed in Section 3.1.3, then we could neglect the friction. To measure the friction force between the O-rings and the syringe barrel, the test bench is configured as shown in Figure 6-1. A syringe barrel, whose end is open and filled with air, is mounted on a load cell, and the magnetic plunger is inserted into the barrel. Two O-rings of the magnetic plunger contact with the inner wall of the syringe barrel, thereby applying a friction force to the syringe barrel when there

is relative displacement. The O-ring and syringe barrel are lubricated with a silicone O-ring lubricant manufactured by PolySi Technologies (PST-841).

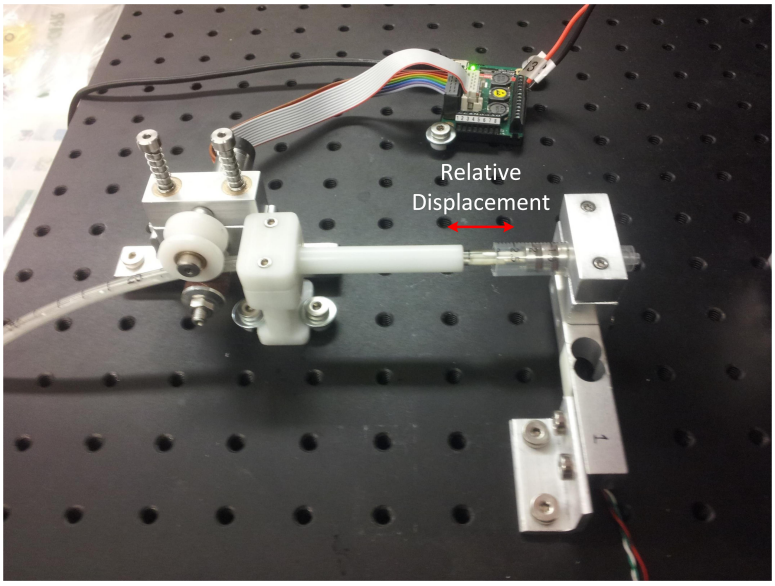

Figure 6-1: The test bench set up for O-ring friction measurement.

The friction drive modulates the displacement of the catheter sinusoidally to generate the relative displacement. Different amplitudes of sinusoidal displacement are applied: ±1 mm, ±2 mm, and ±5 mm, at 0.1 Hz. Notice that although we command the friction drive to feed the catheter by a certain amplitude back and forth, it does not necessarily mean that the plunger moves by the same amplitude because of the finite stiffness of the catheter. As shown in Figure 6-2, the friction force in the case of ±1 mm peak amplitude gives the highest maximum friction force among the three cases, which is about 2 N. This is presumably because the O-ring does not slip on the inner wall of the barrel with such a small displacement, and therefore all the friction force comes from static friction. Here, the maximum friction force of 2 N is the same order of magnitude as the nominal bougienage force, and thus not negligible.

As shown in Figure 6-2, the maximum friction force decreases as the amplitude of the sinusoidal displacement increases. This is presumably because the O-ring starts to slip as the amplitude of the relative displacement increases. In this case, most of the friction force comes from kinetic friction, which is usually smaller than the maximum static friction. In the case of ±5 mm amplitude shown in the bottom of

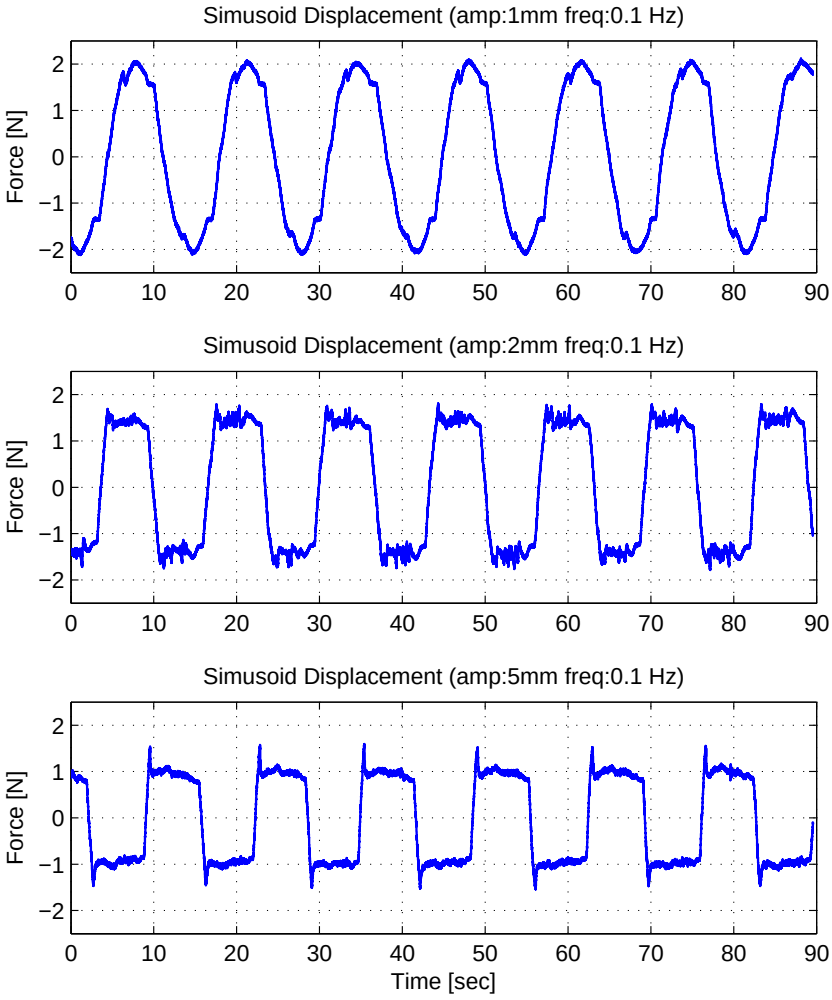

Figure 6-2: O-ring friction for different amplitudes of sinusoidal displacement.

Figure 6-2, the sharp peak at the beginning of each stair case is considered to be due to the transition from the static friction to the kinetic friction regime. Although the maximum friction force is decreased compared to the case of ± 1 mm amplitude, still the order of magnitude of the friction force is not negligible.

Another test was performed to show how the the O-ring friction prevents the bougie from measuring the tip force accurately. In this case, the bougie and the catheter are filled with water as shown in Figure 6-3, and we pushed and pulled the barrel of the bougie while measuring the water pressure inside the bougie with an external pressure sensor. From the water pressure, we can then estimate the bougie

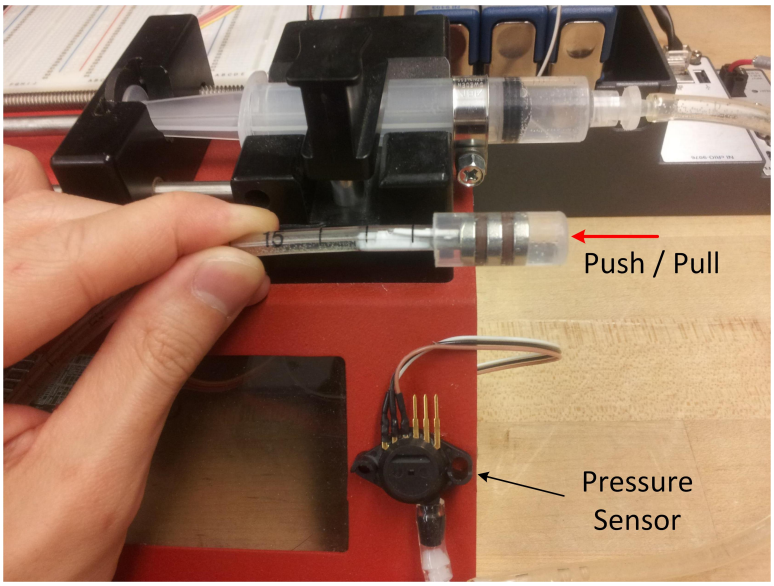

Figure 6-3: Dithering test for and to compensate the O-ring friction.

tip force by multiplying the pressure by the cross sectional area of the barrel.

A pushing force was applied to the barrel of the bougie and released rapidly. Relative motion between the plunger and barrel occurs due to the tubing compliance. Accordingly, as shown in Figure 6-4, the tip force measured with the bougie increased at around 8 seconds when the pushing force was applied and decreased after the pushing force was removed. However, the bougie measurement did not get back to zero completely, leaving a positive residual force of about 0.5 N. Next, a pulling force was applied to the barrel of the bougie at about 27 seconds and released rapidly. Accordingly, the tip force measured with the bougie decreased at around 27 second and increased after the pulling force was removed. However, the bougie measurement again did not approach to zero completely. In this case, the residual force is negative, whereas the residual force of the pushing force was positive. A positive push is also shown at about 45 seconds, with similar results. The hysteretic residual force of the bougie measurement comes from the O-ring friction.

To compensate the O-ring friction, thereby removing the residual force, we pushed water sinusoidally into the bougie using the syringe pump with a volumetric amplitude of about ± 100 mm^3 and a frequency of 0.4 Hz. Then, we took a one period moving average of the pressure by passing it through a moving average filter with an averaging

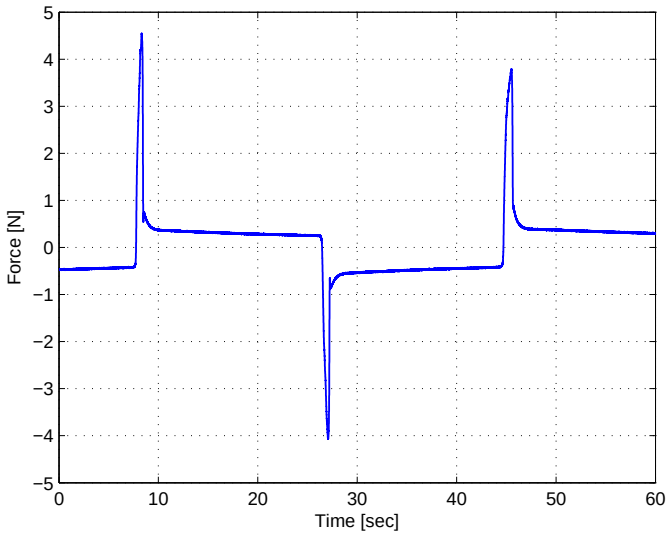

Figure 6-4: Residual force due to the O-ring friction after applying a bougie push.

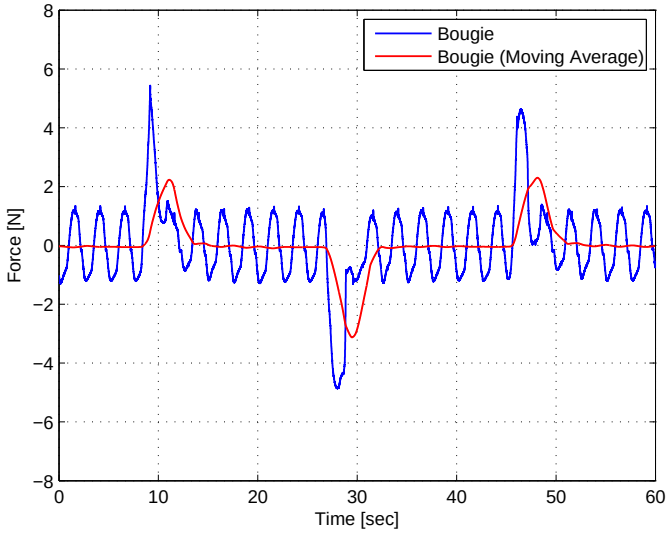

Figure 6-5: O-ring friction is compensated with dither.

interval of 1/0.4 Hz = 2.5 sec, and calculated the bougie tip force with (3.16). This averaging interval rejects the 0.4 Hz pressure signal. The resulting force data are shown in Figure 6-5. The blue curve is the force calculated directly from the pressure sensor measurement, and the red curve is the same force passed through the moving average filter. Notice that the red curve gets back to zero when the external force is removed. This technique to compensate the friction by generating sinusoidal motion

is called *dither*. This is a classical approach in the controls literature for reducing the effect of friction. If we can remove the friction by using different types of seals, such as a rolling diaphragm seal and a ferrofluid seal introduced in 3.2.1, we do not need to rely on dither, and could obtain more reliable sensing performance. However, the dither is sufficient to allow good results even in the presence of friction. Some preliminary experimental result on a ferrofluid seal is discussed in Section 6.3. The ferrofluid seal is essentially frictionless.

6.2 Bougienage Test

Bougienage, or stretching the esophageal mock-up with the bougie, is performed by modulating the displacement of the catheter. Figure 6-6 shows the setup for a bougienage test. We set the neutral gap size of the esophageal mock-up to two different values, $\xi_0 = 10$ mm and $\xi_0 = 5$ mm, to show that the bougienage can be performed for different gap sizes. Then, for each case, we set the tip extension of the bougie to two different values, $d_0 = 10$ mm and $d_0 = 5$ mm, to see how the additional tip extension helps the bougienage.

First, we insert the magnetic bougie into the esophageal mock-up and advance the catheter such that the bougie reaches the closed end of the mock-up. Then, we modulate the displacement of the catheter using the friction drive such that the mock-up experiences maximum tension of 3 N as measured by the load cell. The tip force of the bougie is estimated with the external pressure sensor. The tension of the esophageal mock-up is measured with the load cell, which is used as a reference to verify the bougie tip force estimate using the pressure sensor.

6.2.1 Bougienage Test Result ($\xi_0 = 10$ mm)

We first perform bougienage for the esophageal mock up with a neutral gap size of 10 mm ($\xi_0 = 10$ mm) along with $\xi_0 = 10$ mm. The displacement of the catheter is modulated in a sinusoidal or step profile with the peak amplitude of ± 2 mm and the frequency of 0.04 Hz. The length of the catheter average position is adjusted such

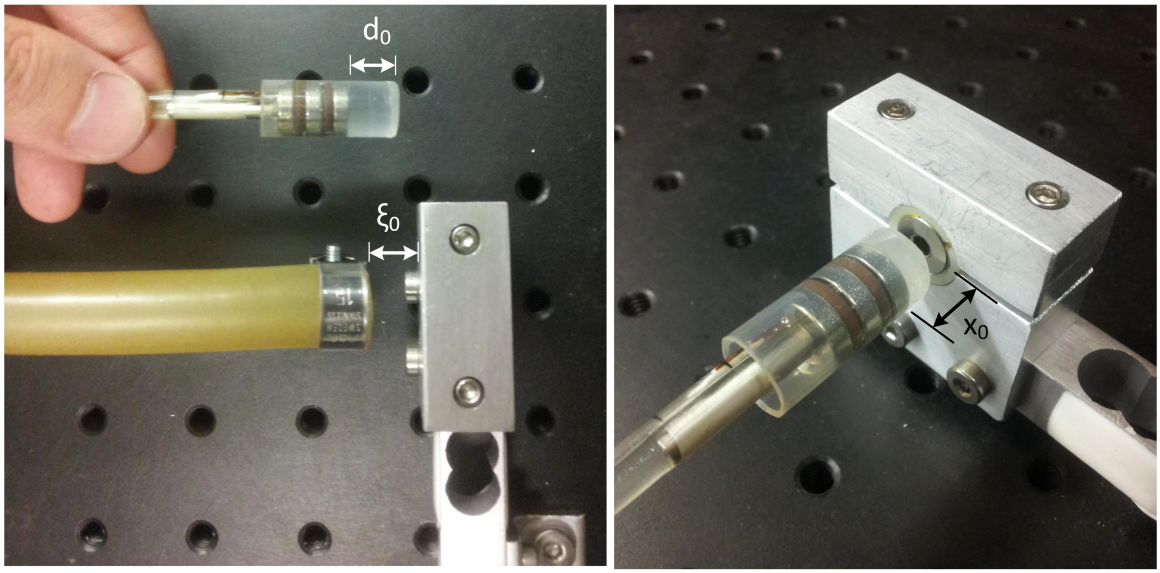

Figure 6-6: The setup for bougienage test. Distance ξ_0 is the neutral gap size of the esophageal mock-up, d_0 is the tip extension of the bougie, and x_0 is the distance between the magnetic plunger and the other magnet mounted on the load cell.

that the maximum stretching force approaches 3 N.

Bougienage Test Result ($\xi_0 = 10$ mm and $d_0 = 5$ mm)

We set the tip extension of the bougie to 5 mm ($d_0 = 5$ mm). This sets the initial distance between the two magnets to about 15 mm ($x_0 \approx 15$ mm).

The displacement of the catheter is modulated in a sinusoidal profile and experimental data are recorded as shown in Figure 6-7. In this figure, the upper plot is without dither and the lower plot is with dither. The red dashed line is the bougie tip force estimated with the pressure sensor after filtering through a moving average filter with a time window of 2.5 second. The blue solid line is the tension of the esophageal mock-up measured with the associated load cell. The green solid line is the distal magnetic force measured with its associated load cell (on the right in Figure 6-6).

The top figure of 6-7 shows the experimental results without dither. We can see that the esophageal mock-up experiences a sinusoidal tension with the maximum of 3 N. However, there is a large discrepancy between the bougie tip force estimated

with the pressure sensor and the tension measured with a load cell. It is thus difficult to estimate the mock-up tension from the bougie tip pressure-based force estimate. This discrepancy is due to the sliding O-ring friction between the plunger and barrel, which changes the push/pressure relationship.

The bottom of Figure 6-7 shows the experimental results with dither, where we have added a 0.4 Hz sine wave. We can see that the tension of the esophageal mock-up has small ripples with a frequency of 0.4 Hz caused by the dither. Now, since the dither averages out the friction, the bougie pressure-based tip force estimate matches well with the mock-up tension measurement. Therefore, we can reliably estimate the mock-up tension from the bougie measurement in this case.

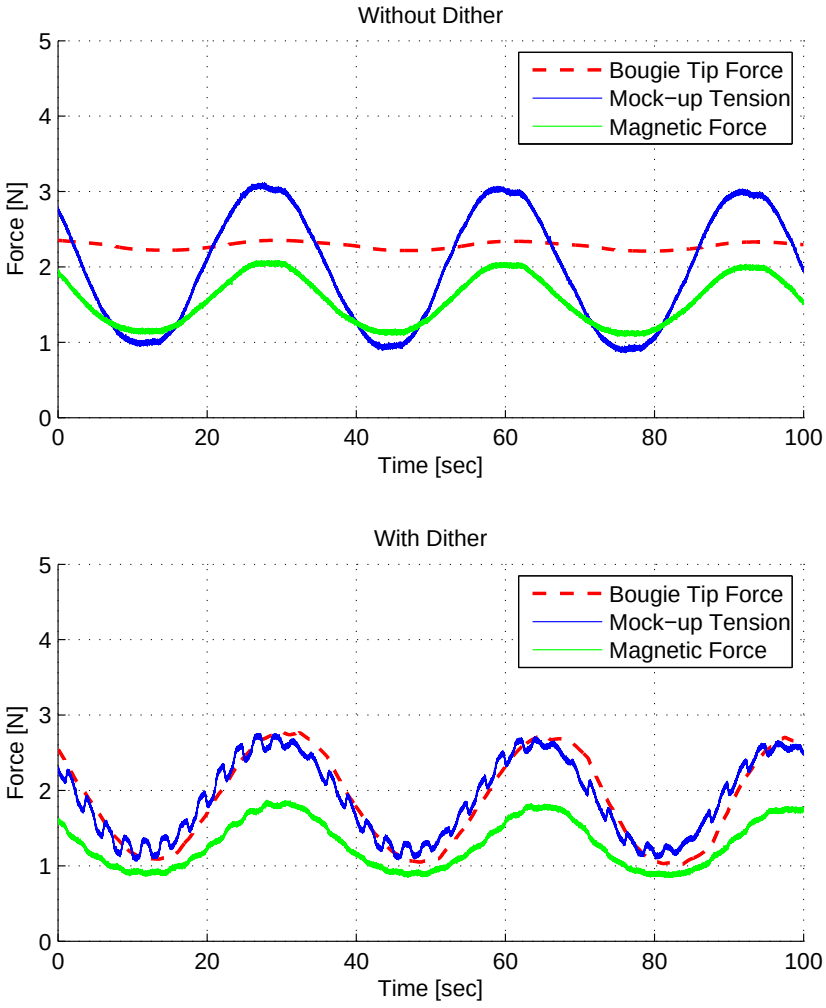

Figure 6-7: Sinusoidal bougienage ($\xi_0 = 10$ mm and $d_0 = 5$ mm). Top trace is without dither. Bottom trace is with dither.

Figure 6-8 shows the experimental result with the same experimental conditions, but we command a step displacement profile to the friction drive to modulate the catheter. Again, the pressure-based force estimate is inaccurate due to friction in the plunger/barrel. The addition of dither effectively averages the friction, increasing the estimate accuracy.

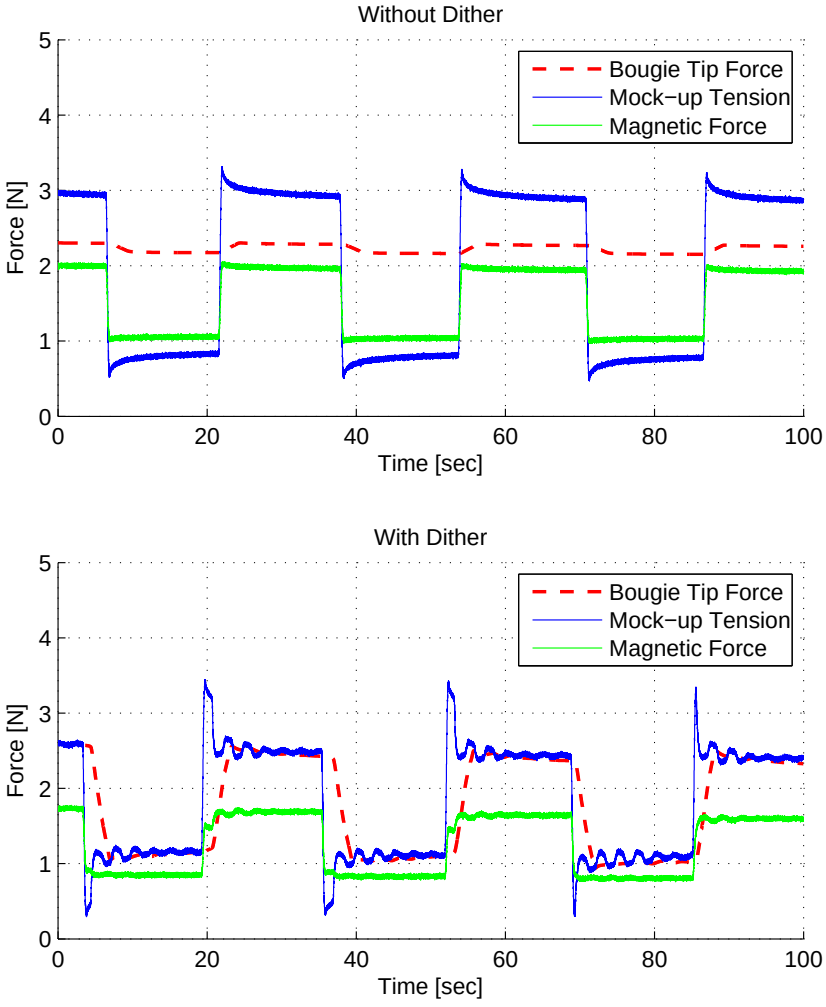

Figure 6-8: Step bougienage ($\xi_0 = 10$ mm and $d_0 = 5$ mm). Top trace is without dither. Bottom trace is with dither.

Bougienage Test Result ($\xi_0 = 10$ mm and $d_0 = 10$ mm)

We now adjust the tip extension of the bougie to 10 mm ($d_0 = 10$ mm) along with $\xi_0 = 10$ mm. This adjusts the initial distance between the two magnets to about 20 mm ($x_0 \approx 20$ mm).

The displacement of the catheter is modulated in a sinusoidal profile and experimental data are recorded as shown in Figure 6-9. In this figure, the upper plot is without dither and the lower plot is with dither. The red dashed line is the bougie tip force estimated with the pressure sensor after filtering through a moving average filter with a time window of 2.5 second. The blue solid line is the tension of the esophageal mock-up measured with the associated load cell. The green solid line is the distal magnetic force measured with its associated load cell (on the right in Figure 6-6).

Because the distance between the two permanent magnets has increased, the magnetic force in this case, the green curve in Figure 6-9, is smaller than the magnetic force in the previous case, the green curve in Figure 6-7. That means the bougie does not get sufficient assistance from the magnetic force to stretch the mock-up, and therefore the friction drive is burdened with applying more pushing force on the catheter.

The catheter is pushed with the friction drive such that the maximum mock-up tension approaches 3 N, but the tension gradually has decreased and settles to the maximum of 2 N as shown in the blue curves in Figure 6-9. We found that the catheter slipped on the friction drive and the surface of the catheter was rubbed off, which did not happen in the previous case, in which more magnetic force was contributing to the bougienage. During the design process, we had not considered this failure mode of catheter yielding and slipping. A better design to resolve this issue is suggested in Section 7.

The top of Figure 6-9 shows the experimental result without dither, whereas the bottom figure shows the result with dither. We can reliably estimate the mock-up tension from the bougie tip pressure measurement if the bougienage is performed with dither. One potential downside of dither is that it imposes unnecessary oscillatory

tension on the mock-up, and may lead to premature seal wear. Also, it is not clear whether such oscillatory motion would be tolerated by the patient. This might be a cause of irritation or tissue damage.

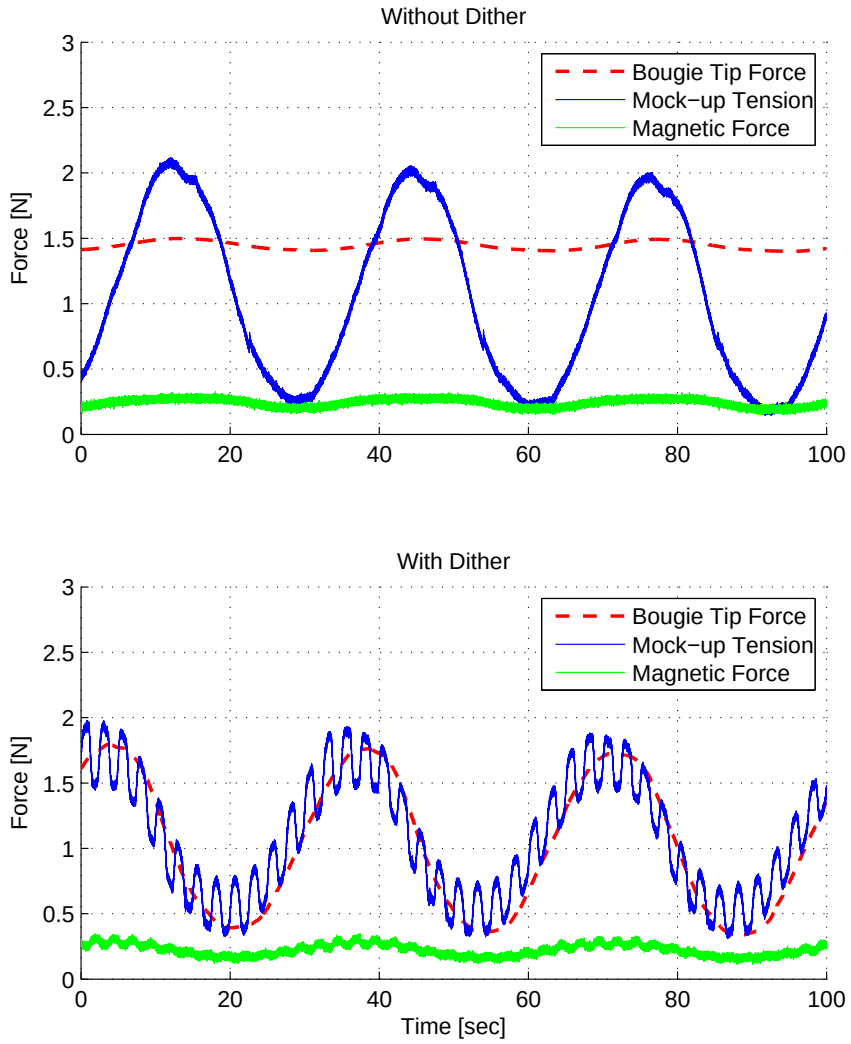

Figure 6-9: Sinusoidal bougienage ($\xi_0 = 10$ mm and $d_0 = 10$ mm). Top trace is without dither. Bottom trace is with dither.

Figure 6-10 shows the experimental result with the same test conditions, but we command a step displacement profile to the friction drive to modulate the catheter. Again, the pressure-based force estimate is inaccurate due to friction in the plunger/barrel. The addition of dither effectively averages the friction, increasing the estimate accuracy.

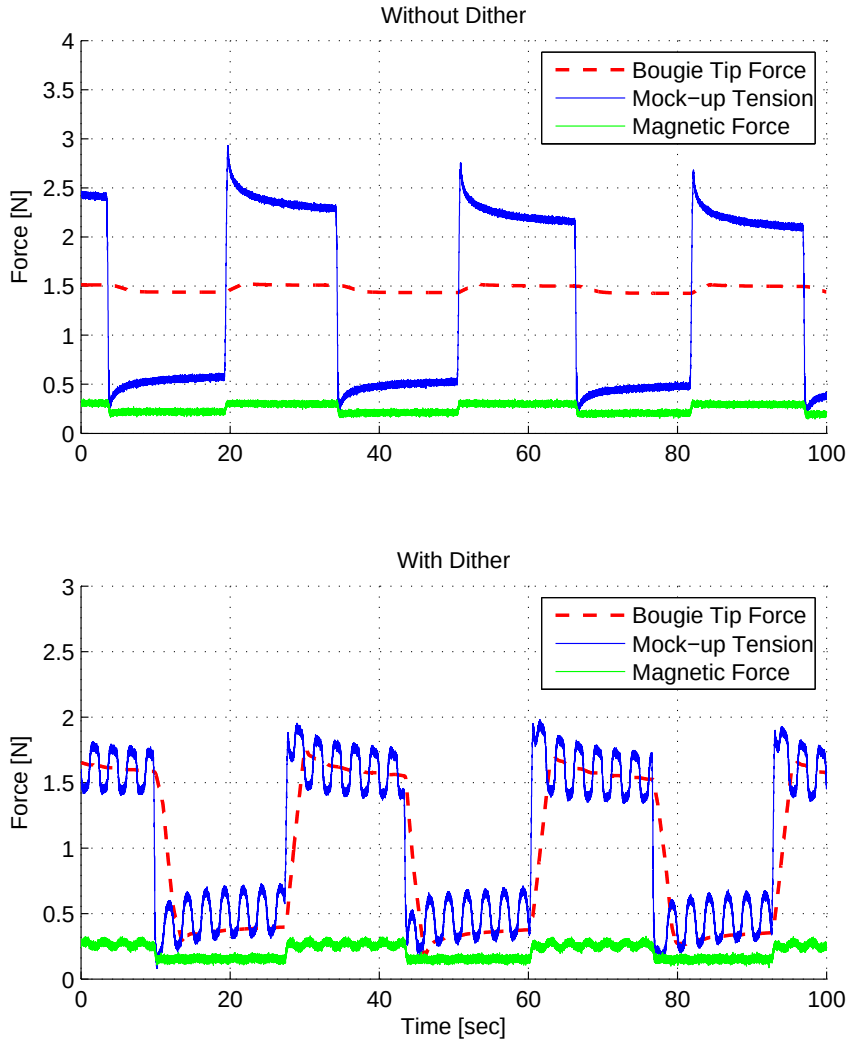

Figure 6-10: Step bougienage ($\xi_0 = 10$ mm and $d_0 = 10$ mm). Top trace is without dither. Bottom trace is with dither.

6.2.2 Bougienage Test Result ($\xi_0 = 5$ mm)

We next adjust the neutral gap size of the esophageal mock-up to 5 mm ($\xi_0 = 5$ mm) along with $\xi_0 = 5$ mm. Again, the displacement of the catheter is modulated in a sinusoidal or step profile with the peak amplitude of ± 2 mm and the frequency of 0.04 Hz. The length of the catheter average position is adjusted such that the maximum stretching force approaches 3 N.

Bougienage Test Result ($\xi_0 = 5$ mm, $d_0 = 5$ mm)

We set the tip extension of the bougie to 5 mm ($d_0 = 5$ mm) along with $\xi_0 = 5$ mm. This sets the initial distance between the two magnets to about 10 mm ($x_0 \approx 10$ mm). First, we tried to modulate the displacement of the catheter in a sinusoidal profile such that the maximum stretching force approaches 3 N. However, we were not able to continue the bougienage because the catheter slipped on the friction drive and the magnetic bougie stuck on the other magnet. An alternative bougienage test is performed to better understand this failure mode, as discussed below. We adjust

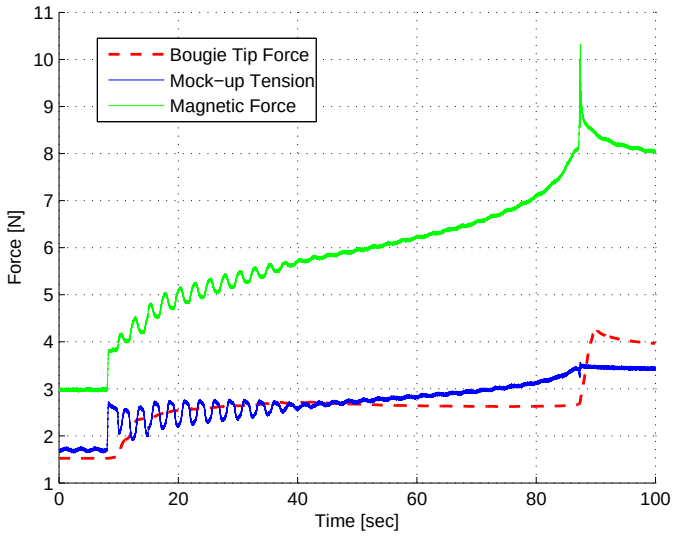

Figure 6-11: Step bougienage ($\xi_0 = 5$ mm and $d_0 = 5$ mm). Note runaway force and ultimate contact at about 87 seconds, due to slipping of the friction drive.

the catheter average position such that the maximum stretching force becomes 3 N, and make a step change by 1 mm. Dither is performed during the bougienage. As

the catheter displacement takes a step change, the magnetic force and the mock-up tension take step changes as well at about 8 second in Figure 6-11. Then, the catheter gradually slips on the friction drive and magnetic bougie drifts to the other magnet, and accordingly the magnetic force and the mock-up tension increase. Finally, the magnetic bougie sticks to the other magnet at around 87 second.

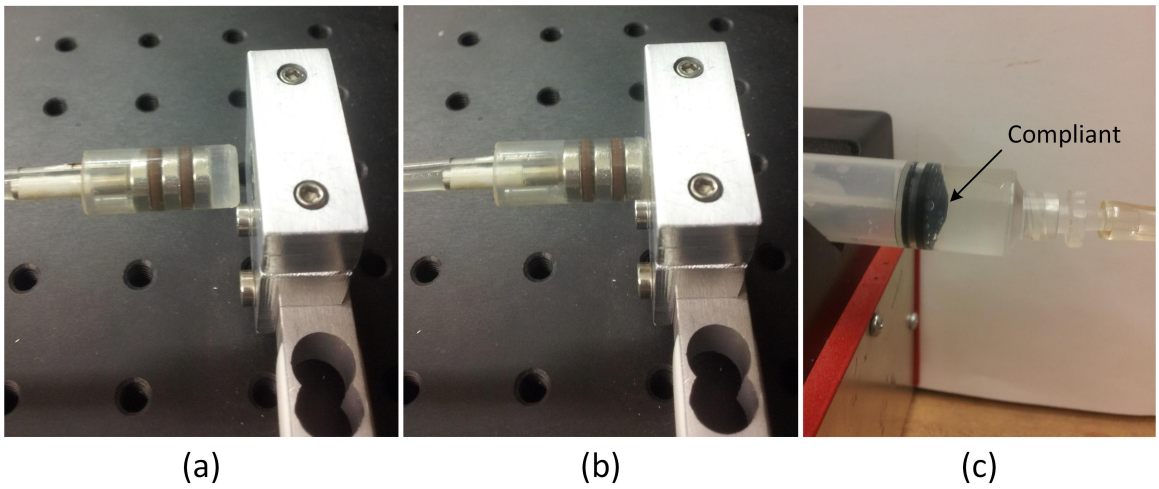

Figure 6-12: The magnetic bougie sticks to the other magnet: (a) before sticking and (b) after sticking. Compliance of the catheter tubing and syringe rubber plunger tip allows magnet motions which can runaway at small gaps.

Initially the bougie pressure-based tip force estimate follows the mock-up tension well, but as the tension increases the bougie tip force estimate does not follow the mock-up tension any more, especially from about 40 seconds in Figure 6-11. Also, the oscillatory behavior of the mock-up tension and the magnetic force gradually disappear from about 40 seconds. Based on these two observations, we can presume that dither can fail when too much compression is applied to the bougie. For a successful dither, we should generate oscillatory relative displacement between the barrel and the magnetic plunger of the bougie with a sufficient amplitude. The way we generate such a displacement is commanding a sinusoidal displacement to the syringe pump. However, due to the flexibility of the tubing and the compliance of the plunger of the syringe pump as shown in Figure 6-12 (c), the sinusoidal displacement of the syringe pump cannot guarantee the same amplitude of oscillation for the barrel of the bougie. Although the tip extension of the bougie is not explicitly shown in

Figure 6-11, we can infer from the mock-up tension curve that the amplitude of oscillation of the tip extension decreases as it experiences more compression. When the amplitude of the oscillation is not enough, dither cannot compensate the O-ring friction effectively.

Figure 6-12 shows the effect of the tubing flexibility on the tip extension of the bougie. In Figure 6-12 (a), the bougie is filled with water to have a tip extension of 5 mm. When the bougie approaches the other magnet, the magnetic plunger sticks to the other magnet and the water inside the bougie is squeezed out through the catheter (See Figure 6-12) (b). Although water itself is essentially incompressible, compliance of the catheter, polyurethane tubing, and the rubber plunger of the syringe pump can cause this phenomenon. Also, the transition from Figure 6-12 (a) to Figure 6-12 (b) explains why there was a step change in bougie pressure-based tip force estimate in Figure 6-11 at about 87 seconds. As the two magnets stick to each other, the water inside the bougie is pushed out, thereby increasing the pressure of the water in the channel.

Bougienage Test Result ($\xi_0 = 5$ mm and $d_0 = 10$ mm)

We now adjust the tip extension of the bougie to 10 mm ($d_0 = 10$ mm) along with $\xi_0 = 5$ mm. This adjusts the initial distance between the two magnets to about 15 mm ($x_0 \approx 15$ mm).

The displacement of the catheter is modulated in a sinusoidal profile and experimental data are recorded as shown in Figure 6-13. In this figure, the upper plot is without dither and the lower plot is with dither. The red dashed line is the bougie tip force estimated with the pressure sensor after filtering through a moving average filter with a time window of 2.5 second. The blue solid line is the tension of the esophageal mock-up measured with the associated load cell. The green solid line is the distal magnetic force measured with its associated load cell (on the right in Figure 6-6).

In this case, we were able to control the mock-up tension such that the maximum force approaches 3 N as shown in the top figure of Figure 6-13. The catheter did not slip on the friction drive. This is because some of the force that the friction

drive should apply to the catheter is compensated with the magnetic force. In other words, the bougie gets appropriate amount of assistance from the magnetic force for the bougienage. Notice that the average of the magnetic force looks similar to the average of the mock-up tension in Figure 6-13, where as the magnetic force was too small in Figure 6-9 and too large in Figure 6-11.

The bottom of Figure 6-13 shows the result with dither. We can reliably estimate the mock-up tension from the bougie pressure-based tip force estimate if the bougienage is performed with dither, although it introduces unnecessary oscillation in tension.

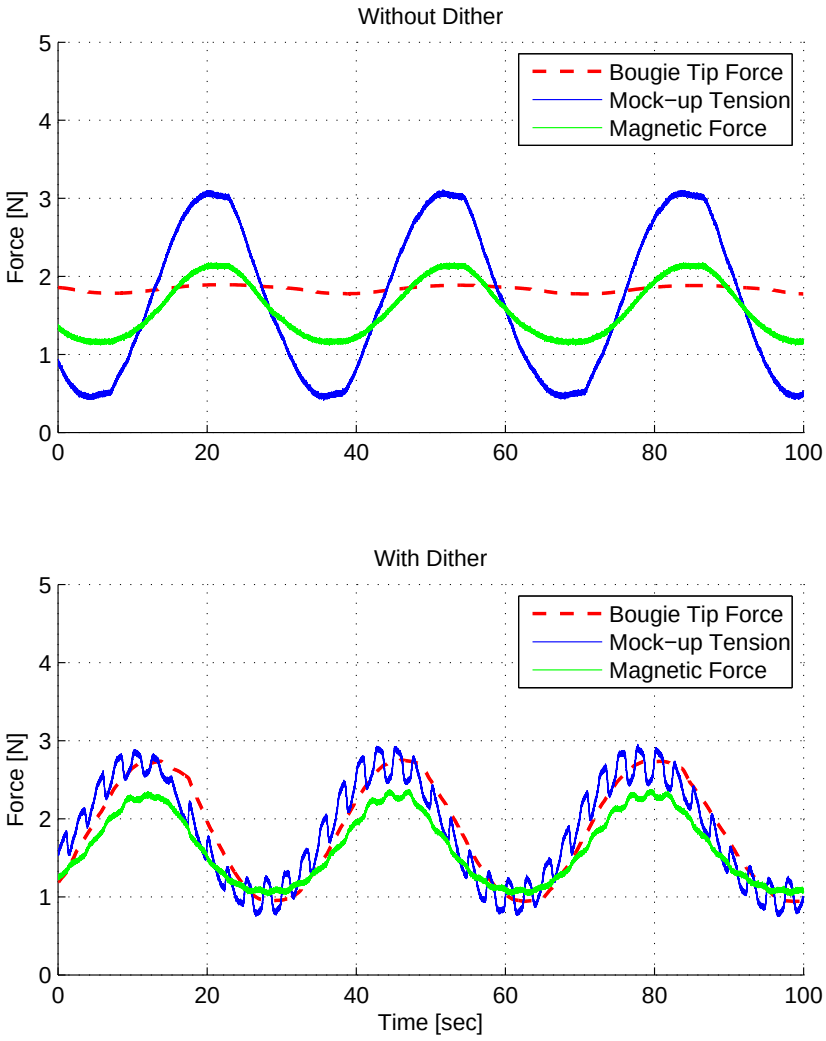

Figure 6-13: Sinusoidal bougienage ($\xi_0 = 5$ mm and $d_0 = 10$ mm). Top trace is without dither. Bottom trace is with dither.

Figure 6-14 shows the experimental result with the same condition as before, but we command a step displacement profile to the friction drive. Again, the pressure-based force estimate is inaccurate due to friction in the plunger/barrel. The addition of dither effectively averages the friction, increasing the estimate accuracy.

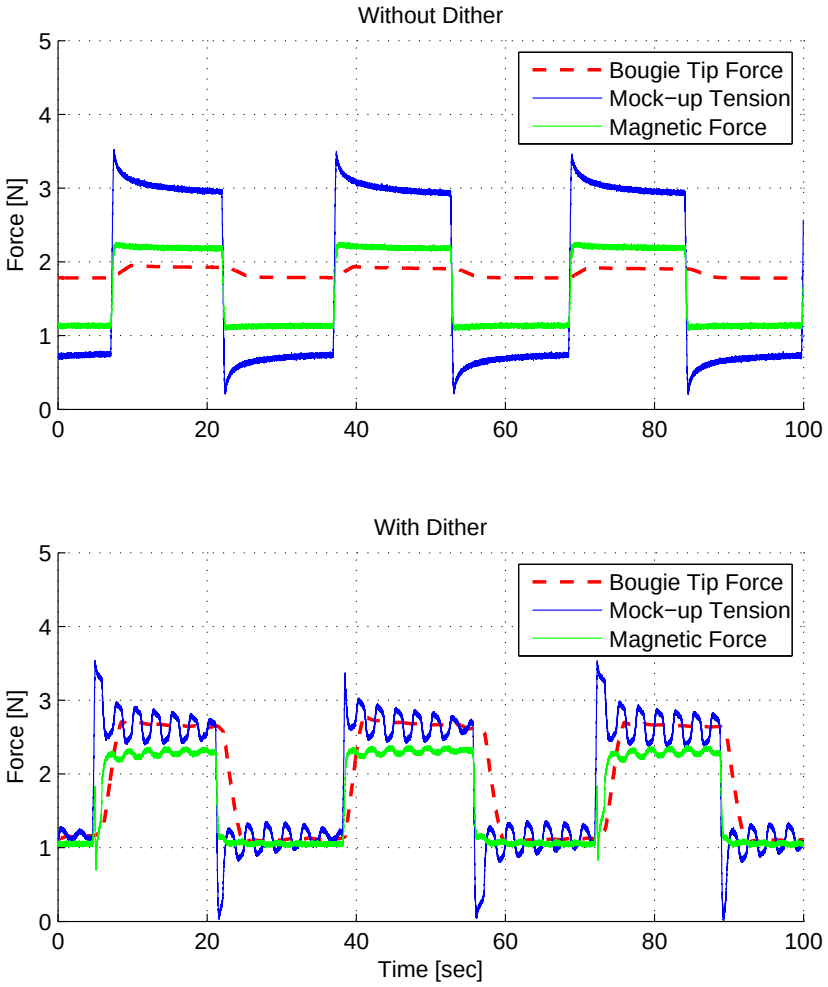

Figure 6-14: Step bougienage ($\xi_0 = 5$ mm and $d_0 = 10$ mm). Top trace is without dither. Bottom trace is with dither.

6.3 Ferrofluid Seal Test

The prototype bougie in previous sections employed O-rings for sealing. The O-ring gives a satisfactory sealing performance, but its inherent friction issue prevents the bougie from estimating the tip force accurately as discussed in Section 6.1. Although we perform dither to compensate the friction, such a technique could lead to another issue, for example wearing the syringe and the lubricant, as well as irritating the patient's esophagus.

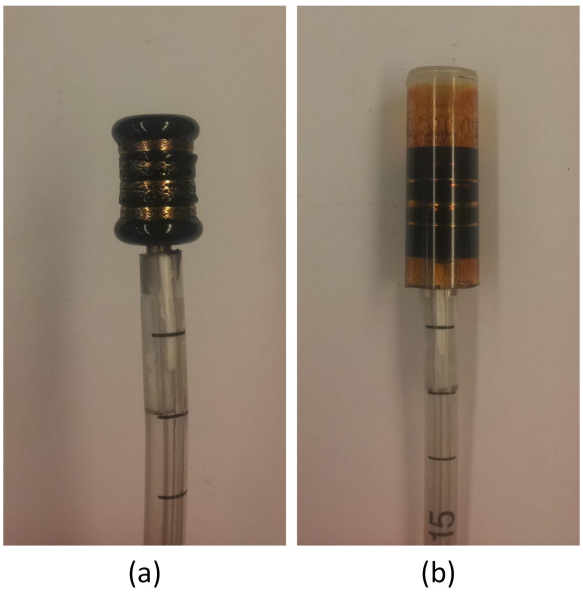

Figure 6-15: Ferrofluid seal: (a) a ferrofluid is applied on the magnetic plunger and (b) the plunger is inserted into the barrel. Note that the ferrofluid wets plunger barrel, as seen by brown film.

Among the alternative piston seal concepts discussed in 3.2.1, we performed some preliminary tests on ferrofluid seal. These results are discussed in the rest of this section. We recieved two bottles of ferrofluid samples from FerroTec[1]; their donation of these samples is appreciated. The specifications of the samples are listed in Table 6.1. For the test, an ester-based ferrofluid, APG S12N, is appplied on the magnetic plunger as shown in Figure 6-15 (a). Note the fluid concentration near the magnet corners, due to magnetic forces on the ferrofluid. The ferrofluid which seals the gap

[1]https://www.ferrotec.com/

between the plunger and the barrel as shown in Figure 6-15 (b). The inner wall of the barrel has a brown film because the ferrofluid wets the surface. Two types of experiments are performed to test the friction and the maximum sealing pressure of the ferrofluid seal, as discussed below.

Table 6.1: Specifications of ferrofluid samples from FerroTech.

	Base Material	Saturation Magnetization	Viscosity
APG E18	Hydrocarbon	125 Gauss	90 mPa s
APG S12N	Ester	375 Gauss	250 mPa s

6.3.1 Friction Test

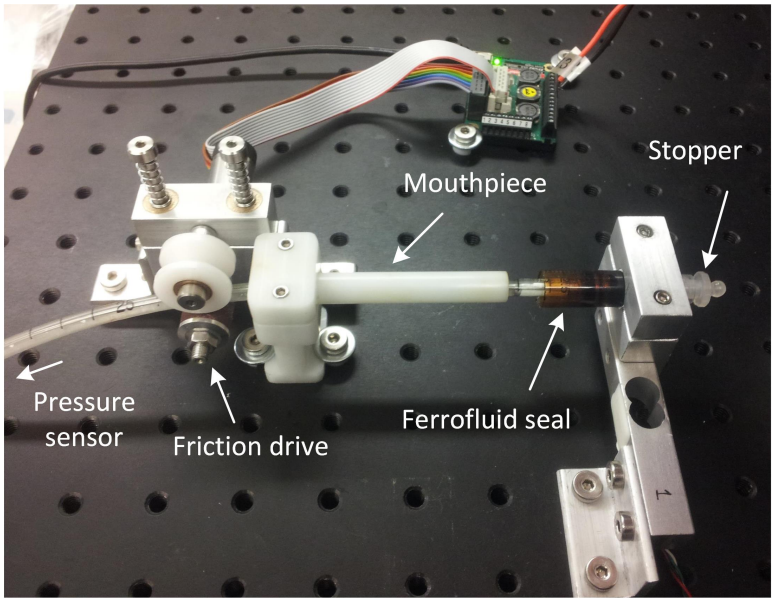

Figure 6-16: Setup to test the friction of a ferrofluid seal. The pressure sensor is not shown in the figure.

Figure 6-16 shows the setup to test the friction of the ferrofluid seal. A syringe barrel is mounted on a load cell as seen on the right side of the picture. The syringe end is closed with a stopper. The magnetic plunger is inserted into the barrel, and the ferrofluid seals the gap between them magnetic plunger and the barrel. For simplicity, the barrel is filled with air instead of water. This avoids issues of the

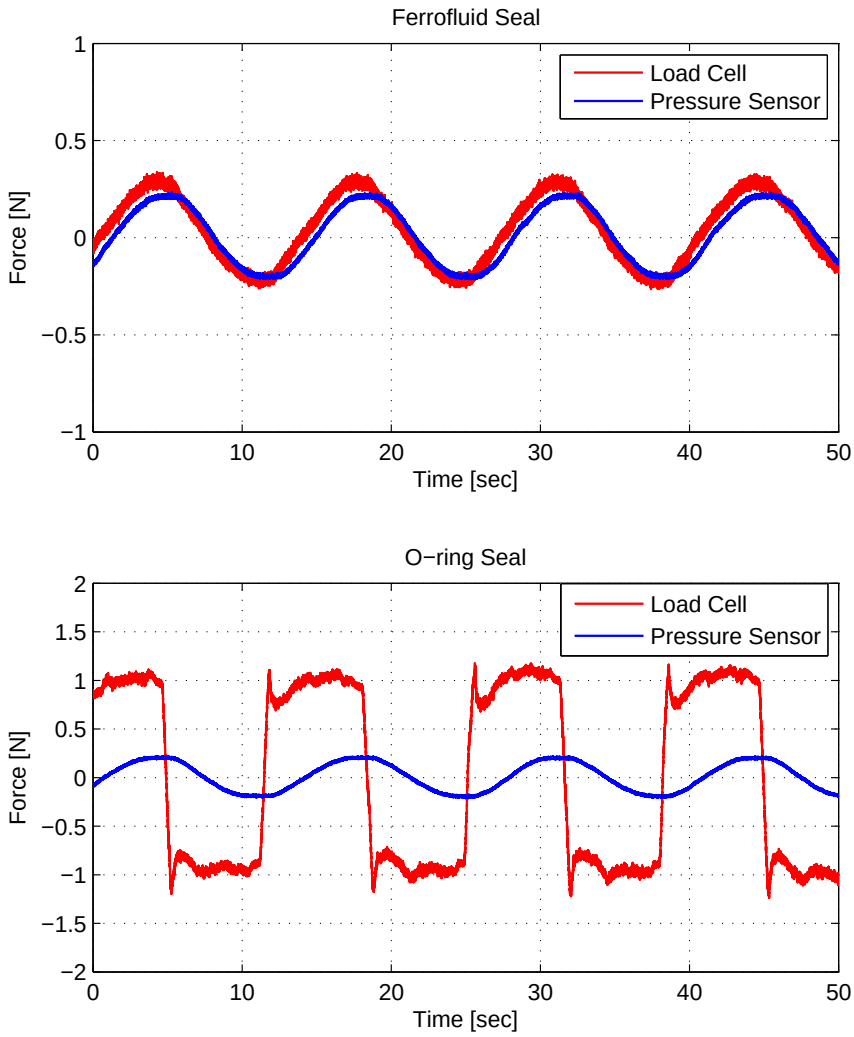

Figure 6-17: Sinusoidal beougienage with the ferrofluid seal (top) and the O-ring seal (bottom).

ferrofluid compatibility with water. The friction drive modulates the displacement of the catheter sinusoidally with a peak amplitude of ±5 mm, with the mouthpiece supporting the catheter in the lateral direction. The pushing force is estimated with a pressure sensor connected to the other end of the catheter, and compared to the load cell measurement for verification.

The top of Figure 6-17 shows the experimental results with the ferrofluid seal. The red curve is the pushing force measured with the load cell, and the blue curve is

the pushing force measured with the pressure sensor. We can see that the pressure sensor estimate matches the load cell measurement well, which implies that there is little friction loss from the ferrofluid seal. The utility of this result becomes more clear when we compare it with the O-ring seal test result, which is shown in the bottom of Figure 6-17. The same setup is used for the O-ring seal test, except the piston seal is replaced with O-rings. In this case, the pressure sensor measures a sinusoidal force profile according to the sinusoidal displacement of the catheter, but the load cell measurement takes a step change when the catheter changes the direction of motion, which is a typical characteristic of a friction force. Notice that each step starts with a sharp peak due to the static friction. In theory, a fluid seal has zero friction although it could generate a viscous drag force, which is negligible in this contest since velocities are very low. There is about 0.5 second of time delay in the pressure sensor measurement, which is presumably because of the compressibility of the air in the piston and catheter.

6.3.2 Sealing Pressure Test

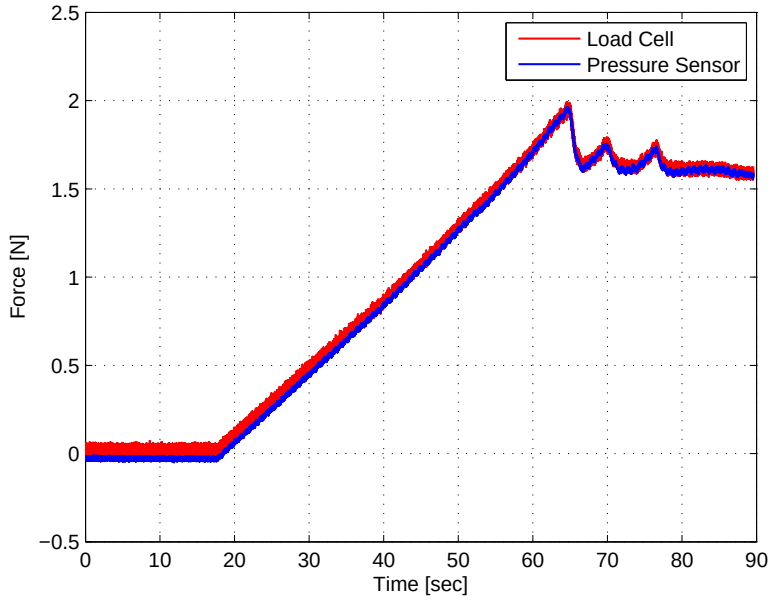

Figure 6-18: Sealing performance of the ferrofluid seal with sylinder fill of air. Note seal failure at a force of about 2 N.

The maximum sealing pressure that the ferrofluid seal can withstand is tested. The same setup as in Figure 6-17 is used but the catheter is fixed. In this case, we gradually push air into the syringe barrel. The air is pushed with a syringe pump through the catheter. Figure 6-15 shows the experimental result. The red curve is the pushing force measured with the load cell, and the blue curve is the pushing force estimated with the pressure sensor. The pushing force increases until it reaches 2 N, when the air starts to leak. After the ferrofluid seal fails, it cannot recover the maximum sealing force because some amount of ferrofluid in the gap has been squeezed out with the pressurized air. The pressure limit of such a ferrofluid seal needs to be raised to perhaps 4 times larger, so that nominal loads of 3-4 N can be sustained.

6.4 Summary

This chapter showed experimental results for the hydraulically controlled magnetic bougie system. Bougienage was performed for different gap sizes of the esophageal mock-up and the tip extension was modulated to see the advantage of hydraulic piston bougie. We also observed runaway conditions due to catheter slippage and due to syringe plunger compliance. Also, a preliminary test result on a ferrofluid piston seal was discussed, in comparison with the O-ring seal.

Chapter 7

Conclusions and Suggestions for Future Work

In this thesis, we have designed, prototyped, and tested a bougienage system to correct long-gap esophageal atresia: hydraulically controlled magnetic bougienage. The key idea is to employ two permanent magnets to stretch esophageal pouches, thereby stimulating them to grow. In order to allow control of the magnetic forces, we implemented a hydraulic piston mechanism. With this piston, the bougie can apply a tension to the esophageal pouch in a controllable manner. The piston mechanism also enables estimation of the stretching force while the bougienage is being performed.

The thesis started by explaining some background knowledge on esophageal atresia and some prior art of the correction methods. Next, we started the design process from Chapter 2 by clarifying the requirements for the device. In Chapter 3, we developed the strategy for magnetic bougienage step by step, and generated a variety of design concepts to accomplish the proposed strategy. Among the generated concepts, we decided to adopt the concept of magnetic bougienage with a hydraulic piston mechanism, in which an O-ring is used for the piston seal. Chapter 4 focused on design details of the module and components to build a prototype bougienage system. Some fabrication details were discussed as well.

In the second half of the thesis, we focused on the experimental demonstration of the prototype bougienage system. Chapter 5 explained how the test bench was built

for the demonstration, and how the modules and components prepared through the design process were integrated on the test bench. We used surgical rubber tubing as a mock-up of esophageal pouch for the bench test. We also instrumented the force on the proximal and distal components. Bougienage is performed on the mock-up with different sizes of gap in Chapter 6. The experimental results showed that our bougienage system was able to apply a desired bougienage force to the esophageal mock-up in a controllable manner. Also, we were able to estimate the bougie tip force from an external pressure sensor measurement, which reliably estimated the mock-up tension when the O-ring friction was compensated with dither. Failure modes via runaway were also investigated.

We developed the prototype bougienage system and successfully demonstrated the proposed concept on a test bench. Within the time constrains of this thesis, we were not able to refine it to the level of the final product, with which surgeons can perform bougienage operation to the real babies with long-gap esophageal atresia. The current prototype has some limitations, for example the catheter's slippage in the friction drive and the static friction of the O-ring seal in the bougie, as well as syringe plunger compliance. In future research, the friction drive could be replaced with a leadscrew mechanism to feed the catheter manually while making sure of the catheter engagement. This would give the surgeon more direct control. The O-ring seal could be replaced either with a rolling diaphragm seal or ferrofluid seal to resolve the friction issue while not sacrificing the sealing pressure. We also found some future research topics that can complement the proposed bougienage system. For example, developing a real-time magnetic source localizing system can help the surgeons to simultaneously check the position of the bougies while performing the bougienage. Such a system also can reduce the amount of X-ray exposure, which surgeons are relying on to check the progress of the procedure. We close the thesis by listing the suggestions for future research as below.

Biomechanics of esophagus

In this thesis, we have used a simple spring model for analysis of the esophageal pouch under bougienage. However, the actual esophageal wall is a muti-layered

stucture and the constitutive law of each layer is surely not simple elastic [5]. Studying the esophageal atresia in terms of biomechanics will be an interesting topic for future research. Also, the esophageal tissue grows under tension, whereas the surgical rubber tubing we have used as the mock-up of course does not grow. Applying the study of tissue growth under a controllable mechanical stimulus [13] to the esophageal atresia research will be another interesting topic.

Piston seal with a rolling diaphragm

We struggled to deal with the O-ring friction, and solved this using dither to average out the friction. However, it is better to tackle the friction issue fundamentally instead of compensating it afterwards. The requirement for any new seal design is to have as small friction as possible and to have reasonably high sealing pressure limits. A rolling diaphragm seal is a candidate for such a piston seal, which we have discussed in Section 3.2.1.

Piston seal with a ferrofluid

Ferrofluid is another candidate for the piston seal, which can in principle generates zero static friction. As shown in Section 6.3, a ferrofluid seal significantly reduces the friction, although the sealing pressure is not satisfactory in that prototype. However, ferrofluid can be a good option for the seal, because the required sealing pressure is not too high in this application, while less friction is important for the accurate measurement of the bougienage force. The current bougie design requires a sealing pressure of 50 kPa for the tip force of 4 N. The experimental result in Section 6.3.2 shows that the ferrofluid seal can reliably withstand the pushing force up to 1.5 N, which pressurizes the air by 19 kPa.

There are some additional issues on the ferrofluid idea. As shown in Figure 6-15, the ferrofluid wets the inner surface of the polypropylene barrel, which decreases the surface tension of the fluid seal. Tuteja et al. [26, 27] studied oleophobic surfaces, which can be an option for the future design. Also, *Continuum Electromechanics* written by Prof. James Melcher [15] provides thorough background on analyzing the motion of a ferromagnetic fluid under a magnetic field.

Also, we need to find a medically compatible ferrofluid in case of any leakage into the esophagus.

Magnetic sourse localization

In current surgical practice the gap between the two esophageal pouches is measured with X-ray imaging. It would be helpful to have a real-time magnetic source localizing system so that surgeons can measure the gap size simultaneously while performing the bougienage, and also check the posture of the bougie. Since we are using permanent magnets, we can in principle measure the magnetic dipole field with an array of sensors outside of the body and estimate the position and orientation of the bougie. A paper written by Model and Trahms [16] gives a good mathematical background on inverse problems for magnetic source localization.

Bougie design for the distal pouch

We have not discussed much about the bougie design for the distal pouch. The esophageal pouch in the stomach side is more cramped than the proximal pouch, which requires smaller size of bougies. We can place the same bougie but scaled down, or place a permanent magnet without a piston mechanism. Alternatively, as suggested by Dr. Kim, we might place a large permanent magnet outside of the body, for example on the back of the patient, to perform bougienage for the proximal pouch only.

Friction drive

The friction drive slipped when too much tension or compression was applied to the catheter. We found that the slip happened due to the material yielding on the catheter. That is, the catheter surface tears away from the drive wheel, despite the sandpaper surface. For the next prototype, we can design a new friction drive such that the driving wheel contacts with the catheter in a wider area to reduce the stress on catheter. Alternatively, we can design the feeding device using a manual leadscrew, so that surgeons and nurses can easily adjust the length of the catheter fed by hand.

Barrel fabrication

The barrel of the prototype bougie is fabricated with an off-the-shelf syringe as discussed in Section 4.1.1. For the future prototype, electroforming can be a good candidate to fabricate the barrel as discussed in Section 3.2.2. This fabrication method can make a thinner metal structure plated with a non-reactive metal, for example gold and platimum. A downside of such the fabricated metal barrel is that the walls are opaque.

I hope these suggestions, as well as this thesis, will be helpful for future researchers to carry on this project further, and therefore babies with long-gap esophageal atresia can have the disorder corrected in a less-invasive manner.

Bibliography

[1] H. Azar, A. R. Chrispin, and D. J. Waterston. Esophageal replacement with transverse colon infants and children. *Journal of Pediatric Surgery*, 6(1):3–9, February 1971.

[2] W. Dähnert. *Radiology Review Manual*. Lippincott, Williams, and Wilkins, Philadelphia, PA, 6th edition, 2007.

[3] J. E. Foker, T. C. Kendall, K. Catton, and K. M. Khan. A flexible approach to achieve a true primary repair for all infants with esophageal atresia. *Seminars in Pediatric Surgery*, 14:8–15, February 2005.

[4] J. E. Foker, B. C. Linden, E. M. Boyle, and C. Marquardt. Development of a true primary repair for the full spectrum of esophageal atresia. *Annals of Surgery*, 226(4):533–543, October 1997.

[5] H. Gregersen. *Biomechanics of the Gastrointestinal Tract*. Springer, 2003.

[6] W. Hardy Hendren and J. Richard Hale. Esophageal atresia treated by electromagnetic bougienage and subsequent repair. *Journal of Pediatric Surgery*, 11(5):713–722, October 1976.

[7] H. A. Haus and J. R. Melcher. *Electromagnetic Fields and Energy*. Prentice Hall, 1989.

[8] W. H. Hendren and J. R. Hale. Electromagnetic bougienage to lengthen esophageal segments in congenital esophageal atresia. *New England Journal of Medicine*, 293(9):428–432, 1975.

[9] R. Howard and N.A. Myers. Esophageal atresia: A technique for elongating the upper pouch. *Surgery*, 58(4):725–727, 1965.

[10] R. Jamshidi, J. T. Stephenson, J. G. Clay, K. O. Pichakron, and M. R. Harrison. Magnamosis: magnetic compression anastomosis with comparison to suture and staple techniques. *Journal of Pediatric Surgery*, 44(1):222–228, January 2009.

[11] R. W. Jennings. Esophageal atresia. `http://www.childrenshospital.org/health-topics/conditions/e/esophageal-atresia`, 2011.

[12] E. G. Loewen, R. S. Wiley, and G. Portas. Large diffraction grating ruling engine with nanometer digital control system. *Proc. SPIE*, 0815:88–95, 1987.

[13] T. Mammoto and D. E. Ingber. Mechanical control of tissue and organ development. *Development*, 137(9):1407–1420, May 2010.

[14] D. Meeker. Finite Element Method Magnetic (FEMM). `http://www.femm.info/wiki/HomePage`.

[15] J. R. Melcher. *Continuum Electromechanics*. The MIT Press, Cambridge, MA, 1st edition, June 1981.

[16] R. Model and L. Trahms. An inverse problem of magnetic source localization. *Numerical Algorithms*, 5(12):603–610, December 1993.

[17] D. B. Montgomery and R. J. Weggel. Magnetic forces for medical applications. *Journal of Applied Physics*, 40(3):1039–1041, March 1969.

[18] A. Oehlerking, J. D. Meredith, I. C. Smith, P. M. Nadeau, T. Gomez, Z. A. Trimble, D. P. Mooney, and D. L. Trumper. A hydraulically controlled nonoperative magnetic treatment for long gap esophageal atresia. *Journal of Medical Devices*, 5(2):027511, June 2011.

[19] D. W. Oxtoby, H. P. Gillis, and N. H. Nachtrieb. *Principles of Modern Chemistry*. Thomson Learning, 5th edition, 2002.

[20] C. Palmer and E. Loewen. *Diffraction Grating Handbook*. Newport Corporation, 6th edition, January 2005.

[21] Apple Rubber Products. Seal Design Guide. `http://www.applerubber.com/src/pdf/seal-design-guide.pdf`.

[22] F. Rehbein and N. Schweder. Reconstruction of the esophagus without colon transplantation in cases of atresia. *Journal of Pediatric Surgery*, 6(6):746–752, December 1971.

[23] R. E. Rosensweig. Magnetic fluids. *Annual Review of Fluid Mechanics*, 19(1):437–461, 1987.

[24] M. Takayasu, D.B. Montgomery, and J.V. Minervini. Characterization of bougienage electromagnetic forces. *IEEE Transactions on Applied Superconductivity*, 18(2):891–895, 2008.

[25] M. Takayasu, D. B. Montomery, and J. V. Minervini. Magnetic forces of electromagnetic bougienage. RR Series RR-07-2, MIT PSFC, 2008.

[26] A. Tuteja, W. Choi, M. Ma, J. M. Mabry, S. A. Mazzella, G. C. Rutledge, G. H. McKinley, and R. E. Cohen. Designing superoleophobic surfaces. *Science*, 318(5856):1618–1622, December 2007.

[27] A. Tuteja, W. Choi, J. M. Mabry, G. H. McKinley, and R. E. Cohen. Robust omniphobic surfaces. *Proceedings of the National Academy of Sciences*, November 2008.

[28] A. M. Vogel, E. Y. Yang, and S. J. Fishman. Hydrostatic stretch-induced growth facilitating primary anastomosis in long-gap esophageal atresia. *Journal of Pediatric Surgery*, 41(6):1170–1172, June 2006.

[29] D. Vokoun, M. Beleggia, L. Heller, and P. Sittner. Magnetostatic interactions and forces between cylindrical permanent magnets. *Journal of Magnetism and Magnetic Materials*, 321(22):3758–3763, November 2009.

[30] R. H. Walter. Diffraction grating apparatus, October 1967. U.S. No. 3344526.

[31] F. M. White. *Fluid Mechanics*. McGraw-Hill, 5th edition, 2003.

[32] M. Zaritzky, R. Ben, G. I. Zylberg, and B. Yampolsky. Magnetic compression anastomosis as a nonsurgical treatment for esophageal atresia. *Pediatric Radiology*, 39(9):945–949, September 2009.